UNIVERSITY OF SOUTHAMPTON

FACULTY OF NATURAL AND ENVIRONMENTAL SCIENCES

Ocean and Earth Science

2016/2017

Volume 1 of 1

Unifying theories for global benthic biomass distribution: the relative importance of water column and topographic drivers

by

Matteo Charlie Ichino

Thesis for the degree of Doctor of Philosophy

November 2016

UNIVERSITY OF SOUTHAMPTON

ABSTRACT

FACULTY OF NATURAL AND ENVIRONMENTAL SCIENCES

Thesis for the degree of Doctor of Philosophy

UNIFYING THEORIES FOR GLOBAL BENTHIC BIOMASS DISTRIBUTION: THE RELATIVE IMPORTANCE OF WATER COLUMN AND TOPOGRAPHIC DRIVERS

Matteo Charlie Ichino

Most benthic fauna in the deep sea relies on the flux of organic carbon synthesised in the surface ocean as a source of food. Particulate organic carbon, derived from primary and secondary production, sinks through the water column and some of this is remineralised; therefore, vertical food input to the benthos decreases as depth increases. This results in a reduction of biomass along the depth gradient, which can be observed across the full benthic size spectrum. Nevertheless, unexpectedly large benthic standing stocks have been observed, generally associated with topographic features such as seamounts and trenches. At these sites, biomass can be higher than what would be expected under normal conditions of vertical flux and attenuation of organic carbon. Lateral fluxes of organic particles are believed to sustain the growth of excess biomass in these areas, which could not be sustained by vertical fluxes alone. In this thesis, I show how the synergy of hydrodynamic and gravitational processes can explain the distribution of benthic communities around three types of topographic features in the deep sea. In fact, a positive effect of increasing slope and relative elevation on biomass (a more hydrodynamic scenario) can be reduced or reversed when the slopes are steeper (a more gravitational scenario). Furthermore, a small effect of the interaction between current direction and seafloor morphology is detected, suggesting an asymmetric distribution of particular organic matter settling around topographic features. Using knowledge from these processes, a global model for benthic biomass distribution is built that more fully considers seafloor morphology in comparison to earlier global seafloor biomass models. This model also improves the resolution of an existing seafloor biomass model by 120 times. The promising results highlight that the effect of seafloor morphology on benthic biomass can be detected at global scale. Nevertheless, the small number of data points and the related limited ranges in the variables covered by the dataset greatly reduce the model's predictive power. While this thesis focuses on a relatively remote portion of the planet's biome, its scope is much wider. Global benthic biomass has been forecasted to decrease by up to 5% under climate change scenarios with some areas declining nearly 50%. Therefore, accurate estimates of carbon stocks and fluxes through the benthic community, and their spatial variability, are needed to improve models of human impact.

Table of Contents

List of Tables

List of Figures

DECLARATION OF AUTHORSHIP

I, Matteo Charlie Ichino .....

declare that this thesis and the work presented in it are my own and has been generated by me as the result of my own original research.

Unifying theories for global benthic biomass distribution: the relative importance of water column and topographic drivers.....

.....

I confirm that:

1. This work was done wholly or mainly while in candidature for a research degree at this University;
2. Where any part of this thesis has previously been submitted for a degree or any other qualification at this University or any other institution, this has been clearly stated;
3. Where I have consulted the published work of others, this is always clearly attributed;
4. Where I have quoted from the work of others, the source is always given. With the exception of such quotations, this thesis is entirely my own work;
5. I have acknowledged all main sources of help;
6. Where the thesis is based on work done by myself jointly with others, I have made clear exactly what was done by others and what I have contributed myself;
7. Parts of this work have been published as:

Ichino, M. C., M. R. Clark, J. C. Drazen, A. Jamieson, D. O. B. Jones, A. P. Martin, A. A. Rowden, T. M. Shank, P. H. Yancey and H. A. Ruhl (2015). "The distribution of benthic biomass in hadal trenches: A modelling approach to investigate the effect of vertical and lateral organic matter transport to the seafloor." Deep Sea Research I 100: 21-33.

Signed: .....

Date: 08/07/017.....

Acknowledgements

First, I would like to thank my PhD supervisors, who have guided me through the many challenges encountered in these four years. Thanks to Henry Ruhl, for helping finding alternative ways to move forward, when the initial plans for the PhD could not be pursued. Thanks to Alan Jamieson, for his support, friendly advice and example: building fish traps the day after losing Nereus was the best way to move on. Thanks to Dan Jones, for his technical support, his advice on modelling, and his way of challenging my work in a productive way. Thanks also to my Panel Chair, Duncan Purdie, for his patience and guidance

A relevant part of the past four years was spent having useful discussions with the wide research community at NOCS. In particular, thanks to Brian Bett, for his useful statistical advises, to Adrian Martin and Andy Yool, for introducing me to computer modelling, to Kat Roberts, for her priceless help with codes and big data, and to Kirsty Morris, for being supportive and patient, and for having provided me with part of the dataset that I used in Chapter 4.

Chapter 3 would have never existed if Jim Barry and Lonny Lundsten had not kindly hosted me for a month at the Monterey Bay Aquarium and Research Institute. I would like to thank them both, along with the whole MBARI staff, for sharing with me their knowledge on image annotation, and for their useful comments on my research.

I would also like to thank the PIs of the Hadal Ecosystem Studies group for inviting me to join the (unfortunately unlucky) expedition to the Kermadec Trench, and for guiding me through the hurdles of publishing my first article as first author. In addition, thanks to IMarEST for providing part of the funding that was needed to support my research.

During the course of the past four years I took part in two research expeditions, so I would like to thank the crew and scientific staff of JC085 (2013) and TN309 (2014). I would have very much enjoyed my time at sea with you, if it had not been for other factors outside your control.

I would like to thank Valentina Guarasci, for having thought me that, sometimes, it is better to stop listening, and in general, for putting me back on track.

Probably I spent most of my last four years in office 496/20, so I would like to thank the amazing PhD students that I found there when I started, the ones that passed through, and the ones that will keep the post for the next few years. So thanks to Claudia, Grant, Charlie, Laetitia, Noelie, Simone, and in particular to Jen (for all her help, from baking to coding) and to Paris (for being an example, even if I was not looking at you).

Finally, thanks to my family...for being my family.

Definitions and Abbreviations

a = rate of change between low and high transport efficiency

ACI = Aspect-current interaction

AESA = Autonomous Ecological Surveying of the Abyss

Arc = Arctic Ocean

Atl = Atlantic Ocean

AUV = Autonomous Underwater Vehicle

B = Burial (% y^{-1})

BPI = Bathymetric Position Index

c = 50% transport efficiency threshold.

D = depth

dSD = standard deviation of current direction

EF = export flux

G = global

GAM = Generalised Additive Model

gC = grams of carbon

GCV = Generalised Cross Validation

g_{ww} =grams of wet weight

In = Indian Ocean

LTM = Lateral Transport Model

m = meters

mab = meters above bottom

MAR = Mid-Atlantic Ridge

MBARI = Monterey Bay Aquarium Research Institute

mgC = milligrams of carbon

MTE = Metabolic Theory of Ecology

NEMO = Nucleus for European Modelling of the Ocean

Pac = Pacific Ocean

PAP = Porcupine Abyssal Plain

Sou = Southern Ocean

POC = Particulate Organic Carbon

ROMS = Regional Ocean Model System

ROV = Remotely Operated Vehicle

S = Slope

T = Temperature

VARS = Video Annotation and Reference System

Y

ΔS = Slope difference

ρ = Spearman rank coefficient

τ = transport efficiency (%)

Chapter 1: Introduction

1.1 Oceanographic variables control benthic biomass distribution at global scale.

1.1.1 Primary production at the surface

The ocean seafloor constitutes more than 70% of the Earth's surface, and most of it (> 90%) lies deeper than the continental shelves (>300 m depth) (Watling et al. 2013). This makes the deep sea the largest biome of the planet. Life on the deep seafloor is known to be diverse (Woolley et al. 2016), but in general its abundance is believed to be limited by food availability. The largest proportion of food for seafloor communities comes from the organic carbon fixed in the euphotic zone (Falkowski et al. 1998), which is then exported below the mixed layer (Giering et al. 2014) and sinks towards the sea floor as Particulate Organic Carbon (POC) (Lutz et al. 2007). Benthic standing stock distribution follows patterns (at ocean basin scale) similar to those of surface primary production. Because of currents, the particles that reach the ocean seafloor can come from surface waters that are hundreds of kilometres apart (Siegel et. al 2008). This has only a small effect on areas with homogeneous production at the surface, but it can otherwise induce significant spatial differences between the surface production and the seafloor deposition (Siegel et. al 2008). Benthic biomass and abundance are higher in temperate regions, such as the Porcupine Abyssal Plain (PAP), than at sites overlaid by oligotrophic gyres (Thurston et al. 1998). Furthermore, the community composition also changes along similar gradients: larger size classes dominate at temperate sites, and smaller size classes progressively increase in dominance at sites that have less primary production at the surface (Galeron et al. 2000).

1.1.2 Depth

The fraction of surface organic carbon that reaches the seafloor depends on the sinking speed of the particles, and their rate of remineralisation through the water column (Martin et al. 1987, Bendtsen et al. 2002). This results in a reduction of flux as depth increases, and, consequently, in a decrease of meio-, macro-, megafauna and fish biomass with depth (Rex et al. 2006). The standing stock of smaller size classes (meiofauna and bacteria) decrease less with depth than that of larger fauna, therefore shallow communities are usually dominated by megafauna, while deeper communities are dominated by macro and meiofauna (Rex et al. 2016).

1.1.3 Temperature

While surface primary production and depth influence benthic standing stocks by affecting the delivery of food to the benthic communities, *in-situ* water temperature affects the individual's metabolic rate. At higher temperatures, metabolic rates are higher, resulting in higher consumption rates at equal body size (Brown et al. 2004). In the surface ocean, temperature changes with season, mostly affecting the yearly cycles of reproduction (Urzua et al. 2012). Instead, temperature below the mixed layer decreases gradually with depth and is relatively constant through time. Temperature fluctuations affect areas interested by vertical movements of water masses, such as canyons (Canals et al. 2009, James et al. 2012). Nevertheless, the effects of temperature fluctuations on benthic communities in these areas are hard to understand fully, as they are confounded by other stresses such as changes in current intensity and direction or food input.

Furthermore, temperature can have a strong effect in deep marginal seas, which generally represent end points of the thermal range either at the low end (e.g. Weddell Sea ~-0.7 °C, Linse et al. 2007) or at the high end (e.g. Mediterranean Sea ~14 °C, Tecchio et al. 2011), and therefore present extreme thermodynamic conditions (Clarke and Fraser 2004).

1.1.4 Use of models to estimate seafloor biomass

There is an interest in improving our understanding of biomass distribution in the deep sea, as this would also improve our understanding of the Earth's energetic and climatic systems (Yool et al. 2017), aiding the management of natural resources (Schlacher et al. 2013). Biomass modelling can help towards these goals by allowing estimation of biomass distribution in areas that have not been sampled yet. The best attempt, to date, at predicting extant stocks distribution is by Wei et al. (2010). They have predicted the distribution of four benthic assemblages (bacteria, meio-, macro- and megafauna) at global scale and at 1° of spatial resolution, using a Random Forests (RF) algorithm.

Their model estimated benthic biomass collected as part of The Census of Marine Life (CoML) using 39 metrics linked to the synthesis of organic carbon at the sea surface and its delivery at the ocean seafloor through the water column. These included

- primary productivity variables (decadal mean and standard deviation of net primary production, chlorophyll concentration, sea surface temperature, photosynthetic available irradiance, mixed layer depth, particle backscatter, phytoplankton growth and carbon concentration)

- water column processes (decadal mean of water-column integrated total carbon and nitrogen, detrital carbon and nitrogen, phytoplankton and zooplankton, and export flux of detrital carbon and nitrogen)
- bottom water properties (annual mean and seasonal standard deviation of bottom water temperature, salinity, oxygen, nitrate, phosphate and silicate concentrations)
- ocean depth.

The RF algorithm recursively partitioned the response variable (standing stock) into binary splits based on a single predictor, eventually creating 1000 different possible models (trees). In each of the models, only 1/3 of the predictors was used; furthermore, 2/3 of the standing stock data were used for constructing the modes and 1/3 was used to test them. Results of the model suggested that the most important predictors for benthic standing stocks are the ones related to primary productivity, which alone explained 63-80.3% of the biomass distribution.

From a spatial point of view, predicted biomass was highest on polar and temperate shelves, and in subtropical coastal areas (1.3-2.5 g C m^{-2}). Total biomass was lowest in the abyssal plains (30-80 mg C m^{-2}), but locally it increased under upwelling areas (i.e. at the equatorial divergence). For the largest ocean areas the model outputs varied by less than 10% among model runs), and the highest levels of uncertainty were associated with the highest predictions.

The whole-community global standing stock predicted by Wei et al. (2010) was 110.3±48.2 MT of living carbon biomass with a contribution of 31.4%, 12.9%, 50.7% and 5% for bacteria, meio-, macro- and megafauna respectively. Finally, the RF model left 19% to 36% of the observed variance unexplained; grain size, bioturbation, oxygen demand and high frequency temporal variability of the other predictors were suggested by the authors as predictors that could be included in future models to improve the predictions.

Overall, the authors of this study were able to provide maps of global biomass distribution, which can be used as baseline for impact studies, or as null hypothesis for ecological studies. While being valuable, these predictions miss the biomass variability introduced by sub-degree environmental patterns, as they are based on large-scale processes at the surface and to the assumption of vertical input of food from the surface to the seafloor

1.2 Lateral advection of food could cause deviations from the predicted biomass at sub-degree resolution.

Many studies have found local deviations of the measured standing stocks from the predictions, generally in relation to the presence of topographic features such as trenches (Danovaro et al.

2002, Jamieson et al. 2010), seamounts (Genin et al. 1986, Thresher et al. 2011, Zeppilli et al. 2013) and hills (Morris et al. 2016). These outliers in global biomass distribution are thought to arise as a consequence of the lateral advection of food, rather than its vertical flux from the sea surface, either as a result of currents (Genin et al. 1986), and of gravitational lateral sediment transport (Ichino et al. 2015).

1.2.1 Slope

Gravitational transport is the downslope movement of sediment towards deeper areas. This process is well documented in relation to abrupt, mass transport events such as earthquakes, which can cause resuspension of sediments (Itou et. al 2000), and turbidity currents (Meiburg and Kneller 2010, Liu et al. 2012). Nevertheless, there is evidence suggesting that downslope transport could take place also in smaller events for the POC, redistributing the food particles towards deep areas. Such redistribution has been suggested as reason for the unexpectedly high biomass found in hadal (Danovaro et al. 2002) and non-hadal trenches (Tselepides and Lampadariou 2004), in relation to generally accepted trends of decreasing biomass with increasing depth. Similarly, high nematode biomass has been found at the bottom of seamount flanks (Zeppilli et al. 2014) suggesting that some POC could sink downslope from the topographic feature towards the abyssal plain. Possible mechanisms causing this transport could be the interaction of internal tides with seafloor topography (Turnewitsch et al. 2013, Turnewitsch et al. 2014), as well as other processes such as the downslope movement of dense water masses (Ivanov et al. 2004).

1.2.2 Exposure

Standing stocks also appear to be higher than expected in some elevated areas such as the top of underwater seamounts. Abundance of corals has been recorded on elevated areas, probably benefitting from acceleration of water flow and other current conditions (Genin et. al 1986); similarly, seamounts support a high diversity of fish (Lundsten et al. 2009b), filter feeders (Roberts and Hirshfield, 2004) and other benthic invertebrates (Samadi et al. 2006). In addition, infauna seems to be able to recolonise the sediments at the top of a seamount at a faster rate than in other deep sea locations with unenriched sediments (Levin and Dibacco 1995). Among the reasons suggested for these patterns are the effect that the abrupt seamount topography can have on currents (White and Mohn 2004, Vandorpe et. al 2016, Turnewitsch et. al 2016), and the interaction with water column processes such as particle sinking and vertical migration of plankton (Genin 2004).

Furthermore, currents could also play a role in determining small scale patterns of food redistribution. The speed and direction of background currents can change when they encounter topographic features such as ridges and seamounts (Turnewitsch et al. 2004, Ilicak et al. 2011). Computer modelling work has suggested that currents generally tend to accelerate over the top of a ridge, to enter a turbulent flow state on the downstream side (Ilicak et al. 2011). Furthermore, current speeds exceeding 7 cm s^{-1} at 1 meter above bottom (mab) are believed to cause resuspension of phytodetritus from the seafloor (Lampitt and Burnham 1983). This could result in increased flux of organic matter in areas of abrupt topography such as the steep flanks of seamounts (McClain and Lundsten 2014) or continental slopes (Jones et al. 2013), and asymmetric food redistribution around seamount-like features (Turnewitsch et al. 2004).

1.3 Thesis summary.

The aim of this PhD thesis is to investigate the benthic standing stock associated with three deep sea topographic features of different size, including trenches (Chapter 2), seamounts (Chapter 3) and a hill (Chapter 4), testing the hypothesis that its distribution is affected by seafloor morphology; this framework is then used to investigate the global distribution of benthic biomass (Chapter 5). Implicitly, benthic biomass distribution is considered here as a proxy for POC supply; in fact, there is a direct relationship between the energy available (flux of organic carbon) and the quantity of biomass that can live in an area, as suggested by the Metabolic Theory of Ecology (MTE). This states that, at the individual level, metabolic rate is a negative function of body size and a positive function of body temperature (Brown et al. 2004, Clarke and Fraser 2004). These simple trends at the individual level are believed to influence many large scale ecological processes such as life history (i.e. development, reproduction and mortality), population dynamics (i.e. phytoplankton blooms and predator-prey relationships), and ultimately ecosystem processes (i.e. total biomass in relation to temperature and food availability) (Brown et al. 2004).

Throughout the thesis, the distribution of biomass around topographic features is analysed keeping in mind a spectrum between two potential mechanistic scenarios for the lateral advection of particulate organic matter. In a purely gravity dominated scenario some portion of vertically sinking Particulate Organic Carbon (POC) is expected to be transported downslope and towards deeper areas. This would result, as an example, in lower-than-expected biomass at the top and on the steep flanks of a seamount, and higher-than-expected biomass at the base of it. In a purely hydrodynamics dominated scenario the presence of particular current patterns may result in increased food availability through higher quantities of POC being entrained by currents over the higher elevations (Figure 1-1). Furthermore, the two scenarios could have different effects on different feeding groups such as suspension feeders, filter feeders and deposit feeders.

These two scenarios are ideal extremes of a continuous of intermediate situations: sediment redistribution is hardly ever controlled by only one of the two processes, which instead interact with different strengths depending on the characteristics of the local topography. The gravity-dominated scenario could be more relevant in steeper areas, while hydrodynamics could have a stronger effect in areas with strong currents. In particular, as current speed over the seafloor increases, also flux of organic particles is expected to increase. Nevertheless, at higher current speeds, phytodetritus can be re-suspended and removed (Lampitt and Burnham 1983), with a negative effect on biomass. Furthermore, this effect could also change with slope steepness, therefore the interaction between gravity and hydrodynamics is likely to generate complex patterns of biomass distribution (Figure 1-1).

Looking at topographic features of varying size and shape (from large trenches to small abyssal hills) could allow investigating the middle ground between the two extreme scenarios, ultimately improving our understanding of biomass distribution in the deep sea.

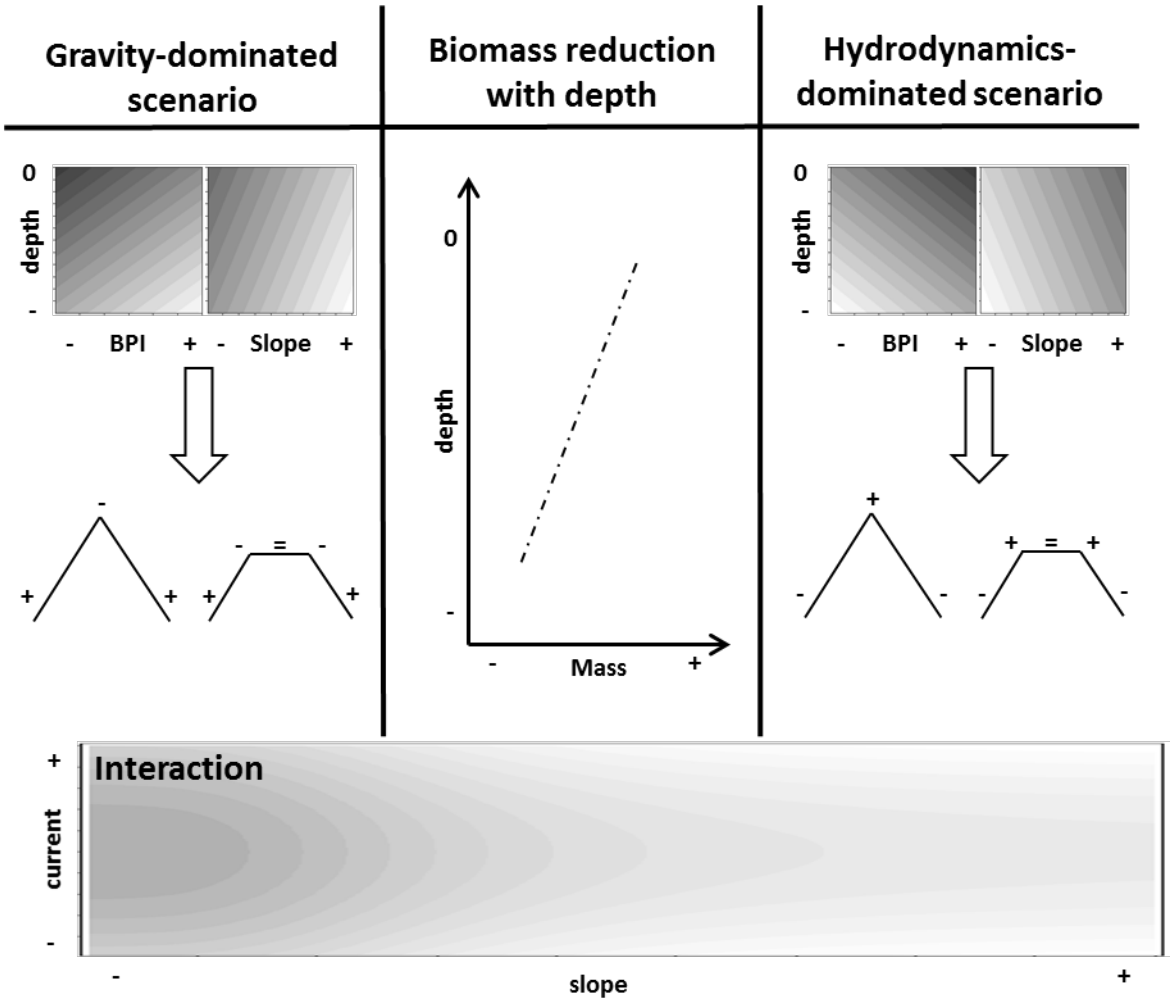

Figure 1-1: Schematic representation of the ideal extreme scenarios of sediment's lateral advection. In the central panel, the dashed trend line schematically represents the decrease of benthic biomass with depth, which can be expected because of Particulate Organic Carbon (POC) remineralisation and no lateral fluxes of organic matter. On the two side panels are schematic representations of how the biomass-depth trend could change around seamounts if two different lateral transport processes are taken into account. In a gravity-dominated scenario (left panel), biomass is transported laterally along slopes towards deeper depths because of gravity. Biomass (represented in grey scale, with black being high biomass) would therefore show a smaller than expected decrease with depth or even reversal of the biomass reduction with depth, it would decrease towards elevated areas (positive Bathymetric Position Index, BPI) and towards steeper slopes. Below the grey heat-maps, the profile of a seamount and of a guyot are represented, in order to show how biomass would be expected to vary over a topographic feature. Biomass would be lower than expected at the top of seamounts (-), it would not change on the flat top of guyots (=), and would be higher than expected at the bottom of seamount flanks (+). On the contrary, in a hydrodynamic-dominated scenario (right panel), POC flux could be higher at the top of the seamount, because of higher current speeds and other hydrodynamic processes. This would result in a more drastic decrease of biomass with depth, and an increase of biomass with BPI and slope. Biomass would be higher than expected at the top of seamounts (+), as expected on the flat top of guyots (=), and lower than expected at the bottom of seamount flanks (-). The two scenarios represented here are at the extremes of what actually is a continuum of intermediate cases where the two processes interact with different strength. Furthermore, benthic animals with different feeding strategies (filter feeders, suspension feeders and deposit feeders) would be affected differently by the scenarios of sediment redistribution. In the bottom panel, a possible interaction of slopes (x axis) and currents (y axis) in determining biomass (grey scale, with high biomass in darker shade) is represented.

1.3.1 Summary of research chapters

Chapter 2: Redistribution of particulate organic matter at large underwater topographic features. The effect on biomass distribution around a hadal trench.

The first topographic feature investigated is a hadal trench. A numerical model is developed to estimate transport of POC down the trench flanks towards the deepest parts of the axis in relation to parameters related to transport (Lateral Transport Model – LTM). The model is applied to the Kermadec Trench, north of New Zealand. Model results support the hypothesis that biomass increases with increasing depth in hadal trenches because of gravitational downslope transport. Furthermore, particular relevance is given to trench morphology, as the model predicts different patterns of biomass distribution for different parts of the Kermadec Trench.

Chapter 3: Seamount morphology, not depth, controls biomass distribution at two locations in the northeast Pacific.

Gravitational and hydrodynamic dominated redistribution of POC around large seamounts are considered in relation to the distribution of megafauna biomass at Taney and Davidson seamounts, in the northeast Pacific. Slope steepness, relative elevation and interaction of the topographic features with background currents are used as predictors in a multiple linear regression and a Generalised Additive Model (GAM) to describe the distribution of biomass recorded with Remotely Operated Vehicles' (ROV) surveys. Biomass is focussed towards the top of the features, and its distribution changes in relation to the orientation of the slope with respect to the background current; furthermore, it increases with slope steepness, at low gradients, and it decreases when slopes exceed 15°.

Chapter 4: Slope, relative elevation and currents help explaining the distribution of biomass on a small abyssal hill.

The same two scenarios of POC redistribution considered as extreme cases in Chapter 3, the hydrodynamic and gravitational POC transport, are used as a reference to investigate the factors controlling distribution of megafauna biomass around a smaller topographic feature: an abyssal hill of ~ 300 m elevation. A small size feature acts here as a natural experiment: the effect of depth change is virtually insignificant and therefore the effect of other metrics related to topography can be addressed. Seafloor morphology explains a small but significant portion of the observed variation in biomass, measured in two separate photographic surveys. Furthermore, the asymmetric distribution of biomass around the feature suggests that organic particles are distributed asymmetrically around small topographic features, possibly in correlation to local current patterns.

Chapter 5: A global predictive model for biomass distribution, based on the effect of seafloor morphology.

The benthic biomass of meio-, macro-, megafauna and fish assemblages is investigated globally in relation to the morphology of the seafloor. While the dataset used was not collected with an interest in investigating the relationship between biomass and topographic features, some of the trends detected in the local case studies arise also at global scale, such as the positive effects on biomass of slope. Overall, depth, export flux and temperature remain the most important factors in determining biomass distribution globally; nevertheless, the fact that significant links between biomass and topography metrics can be detected in a dataset that was not purposely collected suggests that great improvements can be made in this field, to understand standing stocks distribution in the deep sea better. This analysis results in global biomass predictions at the finest resolution yet available (30 arc-seconds).

Chapter 2: Lateral redistribution of sediments at large underwater topographic features. The effect on biomass distribution around a hadal trench[1].

2.1 Abstract

Most of our knowledge about deep-sea habitats is limited to bathyal (200-3000 m) and abyssal depths (3000-6000 m), while relatively little is known about the hadal zone (6000-11000 m). The basic paradigm for the distribution of deep seafloor biomass suggests that the reduction in biomass and average body size of benthic animals along depth gradients is mainly related to surface productivity and remineralisation of sinking particulate organic carbon with depth. However, there is evidence that this pattern is somewhat reversed in hadal trenches by the funnelling of organically enriched sediments, which would result in increased food availability along the axis of the trenches and towards their deeper regions. Therefore, despite the extreme hydrostatic pressure and remoteness from the pelagic food supply, it is hypothesised that biomass can increase with depth in hadal trenches. A numerical model of downwards lateral sediment transport along the seafloor as a function of slope has been developed, using the Kermadec Trench, near New Zealand, as a test environment. Local topography (at a scale of tens of kilometres) and trench shape can be used to provide useful estimates of local accumulation of food and, therefore, patterns of benthic biomass. Orientation and steepness of local slopes are the drivers of organic sediment accumulation in the model, which result in higher biomass along the axis of the trench, especially in the deepest spots, and lower biomass on the slopes, from which most sediment escapes laterally towards deeper areas. The model outputs for the Kermadec Trench are in agreement with observations suggesting the occurrence of a funnelling effect and substantial spatial variability in biomass inside a trench. Further trench surveys will be needed to determine the degree to which seafloor currents are important compared with the gravity-driven transport modelled here. These outputs can also benefit future hadal investigations by highlighting areas of potential biological interest, on which to focus sampling effort.

[1] This chapter was published as: Ichino, M. C., M. R. Clark, J. C. Drazen, A. Jamieson, D. O. B. Jones, A. P. Martin, A. A. Rowden, T. M. Shank, P. H. Yancey and H. A. Ruhl (2015). "The distribution of benthic biomass in hadal trenches: A modelling approach to investigate the effect of vertical and lateral organic matter transport to the seafloor." Deep Sea Research I 100: 21-33. Only minor changes have been made, for consistency in style with the rest of the thesis.

Comprehensive exploration of hadal trenches will, in turn, provide datasets for improving the model parameters and increasing predictive power.

2.2 Introduction

2.2.1 The effect of organic matter input on benthic biomass in the deep-sea.

The main structuring factor for benthic diversity and biomass in the deep sea is believed to be food availability (Rex and Etter, 2010; Rex et al. 2006) while depth related hydrostatic pressure is likely a limiting factor for some fauna (Laxson et al. 2011; Yancey et al. 2014). Studies of the effects of food availability on deep-sea life typically rely on inferring relationships between measures of benthic biomass and organic matter. Organic matter is mostly synthesised in the euphotic zone, and subsequently exported by gravity to deeper waters. The export mainly takes place through three processes: 1) the vertical sinking of particulate organic carbon (POC, or marine snow), produced through photosynthesis in the euphotic zone (e.g. Sweetman and Witte, 2008); 2) the delivery of dissolved organic material through currents and other water movements (Bendtsen et al. 2002); and 3) the local transfer of large lumps of organic matter through sinking of animal carcasses (Higgs et al. 2014; Lebrato et al. 2012; Smith and Baco, 2003). Furthermore, inorganic carbon can be fixed through chemosynthesis both on the seafloor (Olu et al. 1997) and in the water column (Middelburg 2011). As particulate organic matter sinks to the seafloor, it is gradually re-mineralised (Martin et al. 1987; Suess 1980) and POC fluxes decrease exponentially with depth; therefore, deeper parts of the ocean generally support lower levels of benthic biomass (Rex et al. 2006).

Food availability in the deep sea also varies spatially with latitude (Honjo et al. 2008) and distance from shore (Johnson et al. 2007), and temporally, via seasonality (Fabiano et al. 2001), inter-annual climate variation (Smith et al. 2013), upwelling of nutrient-rich waters (McGillicuddy et al. 1998) and natural iron fertilization (Venables et al. 2007). Benthic biomass is higher, and dominated by larger size classes, in areas of the deep-sea overlain by temperate waters than in those overlain by tropical seas (Galeron et al. 2000; Thurston et al. 1998). Similarly, temporal reductions in food supply have also been observed to relate to smaller body sizes (Ruhl et al. 2008) and lower biomass (Ruhl et al. 2014).

Bathymetric characteristics may play an additional role in driving regional and local scale patterns in food availability. In areas of complex hydrodynamic activity, such as the summit of seamounts, the community structure can be dominated by suspension feeders and their predators, resulting in a biomass that is higher than might be expected from vertical fluxes alone (Rowden et al.

2010a; Thresher et al. 2011). These observations suggest that, in these areas, input of organic matter through lateral advection, rather than vertical deposition of marine snow, may be the most important factor in determining standing stock (Clark et al. 2010; Duineveld et al. 2004).

2.2.2 Patterns of benthic biomass in hadal trenches.

Hadal trenches are the deepest parts of the ocean. They are formed at subduction zones of oceanic plates, and they can extend to depths approaching 11,000 m (Gardner et al. 2014). While they make up a relatively small part of the ocean seafloor area (~1-2 %), they account for 45% of the oceanic depth range (Jamieson et al. 2010). Hadal trenches are usually shaped as long and narrow valleys, and often run parallel to coastlines (e.g., Peru-Chile and Japan Trenches) or an island arc (e.g. Philippine and Aleutian Trenches). They are among the least studied habitats on the planet, and the factors that control the distribution and variation of their communities over time are poorly understood (Jamieson et al. 2010).

For more than 60 years, hadal explorations have mostly used grabs and trawls (Belyaev, 1989; Vinogradova et al. 1993), and these have only provided a qualitative description of the hadal ecosystem (Belyaev, 1989). Existing data suggest that hadal macro- and megafauna communities are dominated by beard worms (Family Sibligonidae), spoon worms (Order Echiuroidea), sea cucumbers (Order Holothuroidea) and pericarid crustaceans (Order Isopoda and Amphipoda). Other taxa, such as tunicates, cirripeds, bryozoans and sponges, are rarely collected in hadal samples. Furthermore, evidence from hadal explorations (Wolff, 1961), as well as from research on osmolytes (Kelly and Yancey, 1999; Yancey et al. 2014), suggests that fish cannot live deeper than ~8200 m (Jamieson and Yancey, 2012; Yancey et al. 2014). Depth appears also to limit the distribution of decapod crustaceans: these have been found in the Kermadec, Mariana and Japan trenches (Jamieson et al. 2009) down to a maximum depth of 7703 m.

The general trends of decreasing biomass with increasing depth observed at bathyal and abyssal depths (Rex et al. 2006) are reduced and, in some cases, reversed in hadal trenches, where biomass appears to increase with greater depth (Danovaro et al. 2002; Wolff, 1970). This pattern can be spatially variable within a trench, as suggested by research in the Puerto Rico Trench where contrasting trends with depth occur in different areas (George and Higgins, 1979; Richardson et al. 1995; Tietjen et al. 1989), likely related to trench topography. The typical V-shape cross section of trenches may act as a funnel, and could convey the sediments laterally towards the axis (Itoh et al. 2011; Itou et al. 2000), and perhaps even along the axis towards the deepest points. More recent investigations, using benthic oxygen flux data, support the theory of

higher deposition along the trench axis, as higher bacterial respiration has been recorded in trench sediments than in the surrounding abyssal plain (Glud et al. 2013).

In this chapter, I describe a modelling tool that could improve our understanding of benthic biomass in hadal trenches by accounting for the lateral transport of organic matter. The model is applied to the Kermadec Trench and the results can be used to make testable predictions about the relative distribution of benthic biomass within trenches, which can be ground-truthed, by future trench surveys. Moreover, any differences between model predictions and ground-truthed estimates could help constrain the degree to which other factors, such as movements along depth contours, need to be taken into account.

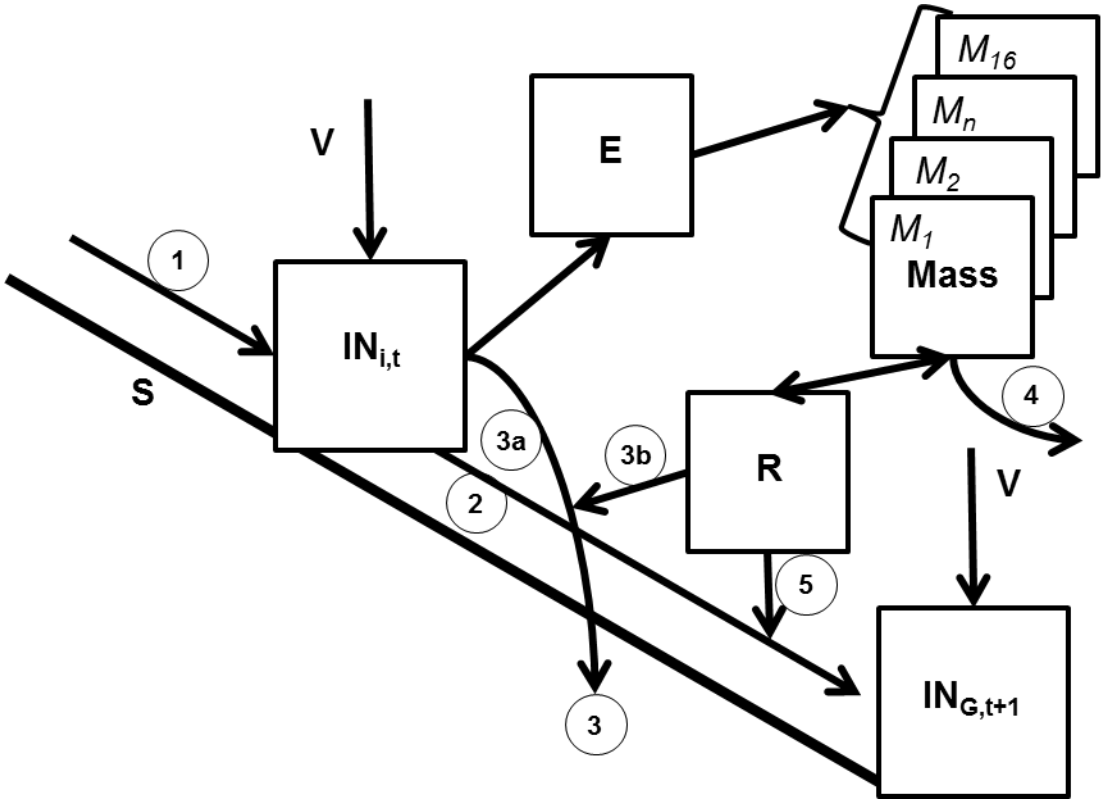

Figure 2-1: Schematic diagram of the Lateral Transport Model (LTM). S = seafloor slope. V = vertical input of organic matter, obtained from Lutz et al. (2007) in this model application. 1 = lateral input of organic matter from shallower cells. $IN_{i,t}$ = total input flux in cell 'i' at time 't' (Equation 2-4). 2 = lateral output flux towards deeper cells (G), which depends on slope steepness (Equation 2-5). 3 = burial, or flux of organic matter into the sediment, including flux from the input material (3a) and from the local stock of organic sediment R (3b). This includes also the respiration from small size classes which are not modelled explicitly. Burial depends on the parameter B, which is the yearly burial rate (Equation 2-3). E = flux of organic matter available for consumption by benthic fauna (Equation 2-3). Mass = benthic biomass stock from 16 size classes (from M1 to M16) comprising macro- and megafauna (Equation 2-8). R = stock of organic matter resulting from mortality and defecation of benthic biomass (Mass) (Equation 2-9). 4 = loss of organic matter through respiration towards the water column. 5 = flux of dead and defecated material towards deeper cells, depending on slope steepness. $IN_{G,t+1}$ = total input flux in the deeper cells (G) at time 't+1' (Equation 2-4). The model took 40 time-steps to reach equilibrium.

2.3 Materials and Methods

2.3.1 Modelling approach.

I developed a numerical model (Lateral Transport Model, LTM) to estimate the biomass of preselected benthic size classes in hadal trenches, as a function of both vertical and lateral down-slope transport of organic matter to the seafloor (Figure 2-1). The model, written with the R language (R core team, 2012), has physical and biological compartments. In the physical compartment, fluxes of organic matter between cells are calculated through matrix operations. In the biological compartment, a system of allometrically based differential equations (Kelly-Gerreyn et al. 2014) is used to calculate the biomass of 16 macro- and megafauna size classes utilizing the local organic detritus pool, which is fed by vertical and lateral POC fluxes. The size classes span from 0.12 g to 3.83 kg, and the nominal mass (geometric mean weight) of each class is double the previous one. Each cell receives a constant (i.e. equilibrium) vertical input of POC at each time step Lutz et al. (2007), as well as lateral fluxes from the neighbouring cells, determined by the slope. The organic detritus pool in each cell is used as food by the fauna and, using a size-based mortality rate, the organic matter is returned to the detrital pool and becomes available for lateral downslope transport.

The model relies on two input datasets: a 2D matrix of vertical input of POC (g C m^{-2} y^{-1}) converted to grams of wet weight, g_{ww}, by multiplying by a factor of 4, and a 2D matrix of the bathymetry of the area, which in this particular application is the Kermadec Trench, north-east of New Zealand. No error or variability estimate is provided in the source data (Lutz et al. 2007), nevertheless in figure 4 of the original publication it can be seen that the Kermadec area has low 'seasonal variability index' (net primary production standard deviation / net primary production average). The bathymetric map used was obtained from GEBCO 30'' via the method "Resample (Data Management)" available through the software ArcGIS 10 (ESRI, 2010); the new resolution of the map was 6' and the resampling type was "BILINEAR". The model is based on three key assumptions: 1) the lateral movements of sediment are controlled by gravity, or are approximated by gravity driven movement of particles down slope. 2) The POC has two sinks: one is physical, and is referred to as burial rate (B); the other is biological and accounts for energy loss through respiration (accounted for in the biological equations). 3) Scaling in the processes of growth, respiration, and mortality are determined by allometric relationships with body size (Kelly-Gerreyn et al. 2014). The effect of temperature on metabolic rates is not taken into account as this parameter is believed to be relatively constant (1-1.5 °C) throughout the trench (Blankenship et al. 2006; Jamieson et al. 2011).

For the purpose of this modelling exercise, tectonic or chemosynthetic mechanisms have not been taken into account, as they are poorly known and thus difficult to quantify. From a geophysical point of view, hadal trenches are areas where oceanic crust is recycled in the Earth's mantle. This gives rise to extrusion of material and other tectonic events that could lead to extreme sediment fluxes in trenches (Itou et al. 2000). Geophysical activity such as the formation of hydrothermal vents or methane deposits could also influence animal community in the trench through processes of chemosynthesis supplementing available food supplies. There is insufficient information, however, to parameterise these influences in our model. Furthermore, the tectonic influences may be temporally rare and chemosynthetic inputs may be rather localised compared to the scale of the model.

2.3.2 Slope calculations.

G is defined as the four cells surrounding i (the central cell of a moving window) in the four main directions (North, East, South and West): G = {N,E,S,W}.

Firstly, all slopes (S) between cells of the study area are calculated. In the general case of the slope between cell G and cell i, the slope is calculated as follows:

Equation 2-1

$$S_i^G = {}^2/_\pi \, arctan \frac{d_G - d_i}{cell}$$

where:

- d_G = depth of cell G, a negative value measured in meters
- d_i = depth of cell i, a negative value measured in meters
- cell = the resolution, or the width of the cell (~11130 m at 6' resolution), and
- 2/π = a factor to convert radians to a value between -1 and 1

The result is a value that spans between -1 (when G is deeper and the slope is vertical) and 1 (when i is deeper and the slope is vertical), 0 being a flat seafloor.

The relative slope in each particular direction is then defined as

Equation 2-2

$$\gamma_i^G = \frac{|S_i^G(1 - D_i^G)|}{\Sigma_G |S_i^G(1 - D_i^G)|}$$

where:

- S_i^G = the slope between cell G and cell i measured in degrees(Equation 2-1), and
- D_i^G = a dummy variable which is 0 if the slope is negative (i.e. downslope flux), and 1 if the slope is positive (i.e. no downslope flux)

Relative slope values are used for subdividing the lateral transport of sediment from one cell among the surrounding ones, as a proportion of the slope in each direction. If the four slopes going out of a certain cell are equal, the flux is equally divided between the directions. Similarly, if only some (or one) of the slopes are positive, the flux is directed in those (or that) directions.

2.3.3 Organic matter transport.

The flux of bioavailable organic matter (E) that, in each cell (i) at any time-step (t), is available as food for the benthic community is defined as

Equation 2-3

$$E_{i,t} = (IN_{i,t} - OUT.1_{i,t}) \cdot (1 - B)$$

where:

- $IN_{i,t}$ = the total input of organic matter in the cell (Equation 2-4, vector 1 in Figure 2-1)
- $OUT.1_{i,t}$ = the fraction of input flux that is transported laterally out of cell I as a consequence of slope steepness (Equation 2-5, vector 2 in Figure 2-1), and
- B = burial rate, measured in $\%\cdot y^{-1}$, including also the ingestion from other smaller size classes such as meiofauna and protozoa (vector 3 in Figure 2-1).

There are three fluxes of organic matter to i: 1) the vertical POC flux from the surface (V in Figure 2-1) ; 2) the lateral transport of POC from surrounding cells (vector 3 in Figure 2-1); and 3) the dead organic matter generated by the fauna in the surrounding cells (vector 5 in Figure 2-1). These three sources are combined as follows to obtain the input and output:

Equation 2-4

$$IN_{i,t} = V_{i,t} + OUT.1_{G,t-1} + OUT.2_{G,t-1}$$

Equation 2-5

$$OUT.1_{i,t} = (\gamma_i^G \cdot IN_{i,t} \cdot \tau_{S_i^G})$$

Equation 2-6

$$OUT.2_{i,t} = \Sigma_G(\gamma_i^G \cdot {}^{R_{i,t}}/_{T} \cdot \tau_{S_i^G})$$

where:

- $V_{i,t}$ = vertical input of POC (vector V in Figure 2-1), from Lutz et al. (2007)
- γ_i^G = the factor determining the possible directions (Equation 2-2)
- $IN_{i,t}$ = the input flux (Equation 2-4, vector V in Figure 2-1)
- τ_{Si}^G= the transport efficiency value determined by the slope between i and G (Equation 2-82-7)
- $OUT.1_{i,t}$ = the flux of biological detritus that is transported laterally as a consequence of slope steepness (vector 2 in Figure 2-1)
- $R_{i,t}$ = the stock of sediment (biological detritus) present in the cell i at the time step t resulting from mortality and defecation (Equation 2-9), and
- T = 100 days, residence time of organic sediments. This value was chosen to match the estimated maximum speed of lateral movement (100 m/day).
- $OUT.2_{i,t}$ = flux of dead and defecated material towards deeper cells (vector 5 in Figure 2-1)

2.3.4 Lateral transport efficiency.

An efficiency term (τ) limits the downslope fluxes of organic matter (OUT.1 and OUT.2). In the trenches, the hydrodynamic forcing from currents and tides also likely plays a role in transporting and funnelling POC. However, I expect that gravitational forcing is likely to capture organic matter distribution patterns to a first approximation, and there is very little information on hydrodynamically driven POC fluxes in trenches or (Schmidt and Siegel, 2011). Therefore, at this stage, I limited model complexity to slope-driven fluxes.

The efficiency of lateral down-slope transport was expected to follow a logistic function (Bernhardt and Schultz, 2010; Bernhardt et al. 2012): low at gradual seafloor slopes and rapidly increasing at mid slopes until reaching 100% efficiency. This efficiency is described by the following equation:

Equation 2-7

$$\tau = \frac{max \cdot (S \cdot 90)^a}{c^a + (S \cdot 90)^a}$$

where:

- max = maximum efficiency of down-slope transport. This parameter is set to 1, which results in down-slope transport of all available organic matter
- a = a parameter that controls how quickly the efficiency changes from low to high
- S = the slope between the cells (Equation 2-1), and
- c = the slope (°) at which τ is 50% of max

The values of a and c affect the shape of the logistic curve in the following way: c affects the slope steepness at which τ is 50%, while a affects how fast τ changes with S at small slopes.

2.3.5 The biomass model.

A simple model based on allometry (Kelly-Gerreyn et al. 2014) has been implemented in the LTM in order to estimate the benthic community biomass in each cell of the trench bathymetry. The model follows accepted allometric theory: biological processes such as ingestion, respiration, mortality and growth follow constant relationships with body weight across a broad spectrum of size classes. Furthermore, this model is considered relatively versatile, and has been successfully applied to three locations that differ in physical, chemical and biological characteristics: the Faroe-Shetland Channel in the north-east Atlantic, the Fladen Ground in the North Sea and the Oman Margin in the Arabian Sea (Kelly-Gerreyn et al. 2014). In this wide range of locations and conditions, the biological model provides a statistically similar and robust description of the data at each site, with only trivial changes to the parameters; therefore, I use a parameters-set that gave the best fit to the three above locations simultaneously, assuming that it would yield comparatively useful approximations for the hadal zone.

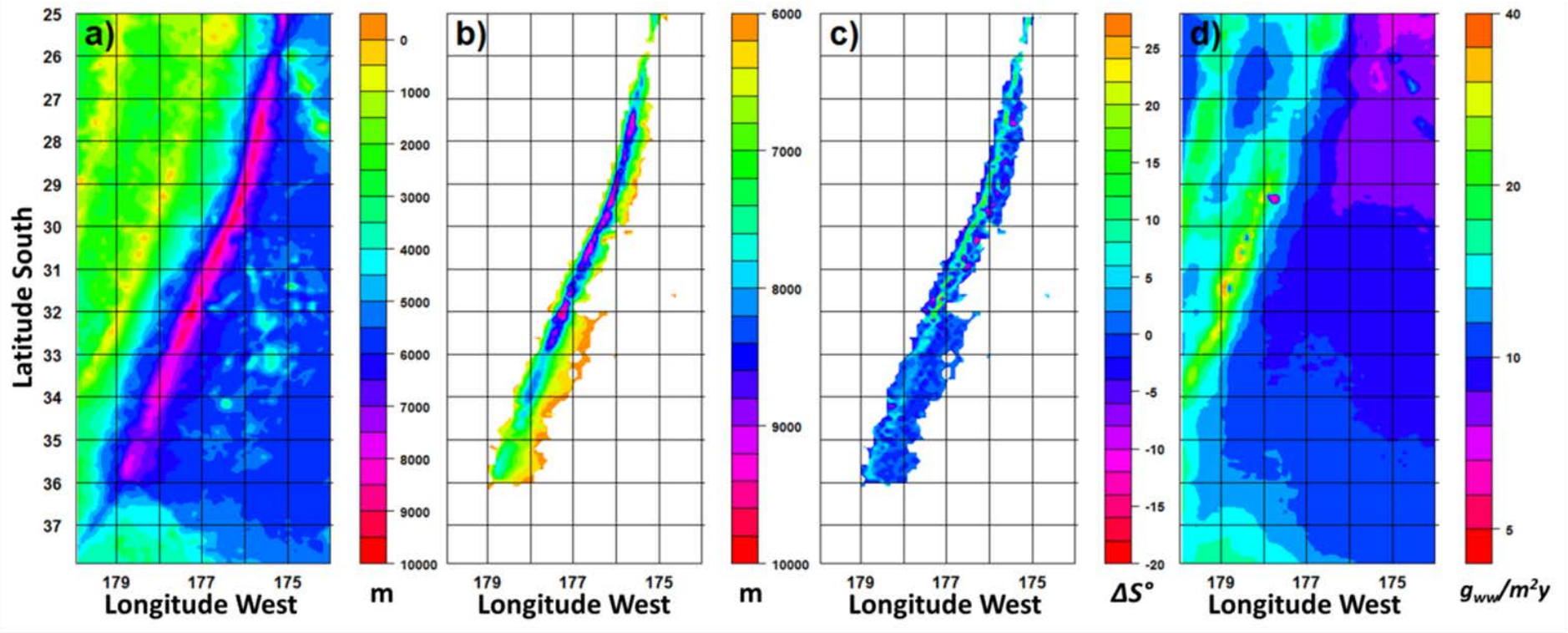

Figure 2-2: Geographic domain of the model. Panel A: bathymetric map of the Kermadec Trench region, on which the Lateral Transport Model (LTM) has been run. Panel B: the hadal area (> 6000 m depth) of the Kermadec Trench, isolated from the regional bathymetry. This map highlights the deep 'holes' found in the central and northern part of the trench, and the shape of the trench, which is wide in the southern part, and narrow in the northern part. Panel C: slope difference (ΔS°) in the hadal area of the Kermadec Trench. This variable is calculated as the sum of incoming (positive) and outgoing (negative) slopes for each cell. As a result ΔS° is negative for the cells from which there mostly is export of organic matter, it is positive for the cells that mostly receive input of organic matter, and it is 0 for the cells that have similar inputs and outputs of organic matter. The deepest parts of the trench, located north of 32° S, are the areas with highest ΔS° values, while the southern parts of the trench, being wider and with more gentle slopes, have ΔS° values closer to 0. Panel D: vertical input of POC at the seafloor, estimated by Lutz et al. (2007) for the Kermadec region, and multiplied by a factor of 4 to convert it from gC m^{-2} y^{-1} to g_{ww} m^{-2} y^{-1}.

In my application of the biological model, 16 size classes of hadal benthic macro- and megafauna ranged from 0.12 g to 3.83 kg, with doubling mass increments between size classes. This range has been chosen to represent a wide range of the possible contributors to the benthic biomass, both from the macro- and megafauna, and includes the size class of the largest fish collected in the Kermadec Trench area (cusk eel *Spectrunculus sp*., ~3 kg) (Jamieson, personal communication), allowing for the presence of potentially rare large animals. In this model the benthic community 'grows' on a common detrital food pool (simulating a single trophic level), and performs the key processes of ingestion, respiration and mortality. This results in competitive interactions for the available resources based on the allometric relationships, while predation is not explicitly accounted for in this model (Kelly-Gerreyn et al. 2014). While this is a simplified representation of ecosystem function, it should provide a general snapshot of a particular benthic community from the point of view of the relationships between body size, biomass and abundance.

In the LTM, processes scale with mean body mass, following basic allometric theory: after standardizing for the biomass of the animal, the rate of the processes decreases when the body weight increases (Griesbach et al. 1982; Peters, 1983). As a result, the temporal change of the value of biomass per size class is determined as

Equation 2-8

$$\frac{dMass_n}{dt} = (1 - r_n) \cdot a \cdot g_n \cdot R_{i,t} \cdot Mass_n - m_n \cdot Mass_n^2$$

Where:

- $Mass_n$ = benthic biomass of the n^{th} size class
- r = respiration coefficient equal to $0.61 \cdot Mn^{0.0046}$
- a = assimilation coefficient equal to 0.21
- g_n = ingestion coefficient equal to $1.76 \cdot Mn^{-0.13}$
- $R_{i,t}$ = detritus (Equation 2-9)
- m = mortality equal to $0.0009 \cdot Mn^{-0.40}$
- n = size class number, and
- Mn = nominal mass (geometric mean weight) of each size class (from 0.93 g to $3.06 \cdot 10^3$ g).

Note that respiration rate was given by $r_n a g_n$ and so it decreased with Mn.

With this biomass model, it is possible to estimate the mortality that occurs in each size class, which is then added to the detritus pool as an input. Therefore, the temporal change of the detritus pool resulting from the mortality and defecation of the animals is calculated as

Equation 2-9

$$\frac{dR_{i,t}}{dt} = E_{i,t-1} - \Sigma_n a \cdot g_n \cdot R_{i,t} \cdot Mass_n + m_n \cdot Mass_n^2$$

2.3.6 Tuneable parameters, sensitivity analysis and evaluation.

I ran the LTM using the bathymetry of the Kermadec Trench area (between 25° and 38° S, and 174° W and 180° W, Figure 2-2), as this trench is among the better studied hadal areas of the ocean, focus of current research and characterised by intermediate levels of surface primary production (Longhurst et al. 1995). The Kermadec trench has a relatively simple shape, being straight with a relatively constant slope gradient along the axis, with saddles separating increasingly deep basins towards the deepest point (~10047 m). The western slope (fore arc) is steeper than the eastern slope. The southern end of the trench is ~ 160 km from the nearest land mass (New Zealand), and therefore likely to receive low fluxes of terrigenous materials relative to high levels of organic matter that have been observed in other trenches (e.g., Peru-Chile Trench, Danovaro et al. (2003)).

In order to explore the sensitivity of the LTM to variations of two independent variables, burial rate (B, Section 2.3.3, Equation 2-3) and transport efficiency (τ, and ultimately a and c, Section 2.3.4, Equation 2-7), I ran the model to equilibrium in five modes to provide examples of how these parameters relate to each other. Firstly keeping τ constant (a = 3, c = 6°) and varying the value of B (4.5, 9 and 18% y^{-1}, covering the range of organic sediment burial suggested by Reimers et al. (1992) for a wide depth interval). Secondly, with B = 9% y^{-1}, I varied the threshold of τ (c = 3°, c = 6° and c = 12°), chosen as representative of the range of slopes present in the hadal trench (from 0° to 16°). Variability of the 'a' parameter was not tested to avoid overcomplicating the results; nevertheless, future investigations should address this as well, as it is an important parameter describing the transport efficiency variability with slope. The differences between the runs are measured by the response of four variables to variations of slope difference (ΔS): lateral organic matter input (Equation 2-4), buried organic matter, amount of organic matter available for ingestion (Equation 2-3) and resulting benthic biomass (Equation 2-8). These results are interpreted using two-way parametric ANOVA: main effects are ΔS (three levels) and the model scenario (either c or B, three levels each). Two-way parametric ANOVA is also used to interpret the effect of model scenario (either c or B, three levels each) by depth (shallow or deep) and topography (southern or northern part of the axis) on the modelled benthic biomass. In all the

ANOVA tests, the interactions between main effects are considered as well. All the analyses are done with the computer program R (R core team, 2014).

2.4 Results

2.4.1 Slope analysis.

The mean slope in the hadal area of the Kermadec Trench (Figure 2-2b) is 0.2° and the maximum is 16°. For the purpose of organic matter redistribution, the difference between incoming and outgoing slopes (one from each direction G) for each cell determines whether the organic matter is mostly exported from the cell (local maxima in the bathymetry, such as the summit of underwater hills and seamounts, with negative slope difference values) or imported (local minima in the bathymetry); this is referred to as slope difference (ΔS). The frequency distribution of ΔS° is normal, with a mean of 0°, ranging between -19.5° and 27.6° (Figure 2-3).

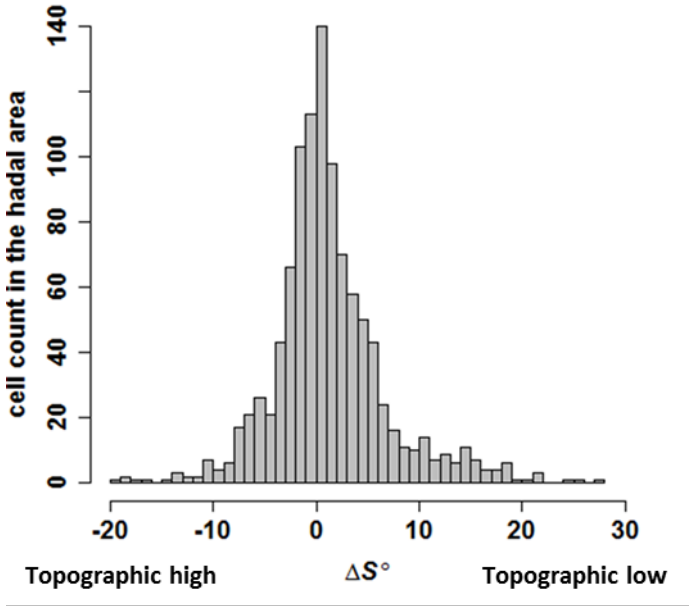

Figure 2-3: Slope difference (ΔS°) cell counts in the hadal area of Kermadec Trench. The slope difference is the net quantification of the amount of slopes towards and from each cell; therefore it is negative in the local maxima (hills and seamounts) and positive in the local minima (bottom of depressions). The frequency distribution is centred on cells with slope difference of 0°, therefore cells with equal inputs and outputs. These can be flat, or sloping.

Table 2-1: F values and statistical significance obtained from testing the effect of ΔS and model scenario on four outputs of the LTM, through eight ANOVA tests. A) The level of slope difference (ΔS = negative, zero or positive) always has a statistically significant effect on the model outputs when lateral transport efficiency threshold is held constant (c = 6°), while the level of burial rate (B = 4.5, 9, 18 % y^{-1}) does not appear to significantly affect the lateral sediment input. Only for the model output 'sediment burial' there is

significant interaction between ΔS and B. B) When the burial rate is held constant (B = 9 % y^{-1}), all four model outputs are affected significantly by an interaction of ΔS (ΔS = negative, zero or positive) and level of lateral transport efficiency threshold (c = 3°, 6°, 12°). The degrees of freedom of the residuals are 3114 for each test. Significance codes used: 0 '***' 0.001 '**' 0.01 '*' 0.05.

A)	***ΔS* (d.f. = 2)**	**Level of *B* (d.f. = 2)**	**Interaction (d.f. = 4)**
Lateral sediment input	1208.6 ***	0.0	0.0
Sediment burial	768.5***	5286.2***	109.8***
Mass of available food	987.7***	7.4***	0.2
Biomass	508.2***	3.6*	0.0
B)	***ΔS* (d.f. = 2)**	**Level of *c* (d.f. = 2)**	**Interaction (d.f. = 4)**
Lateral sediment input	691.9***	665.1***	215.4***
Sediment burial	699.1***	20.4***	221.9***
Mass of available food	699.1***	20.4***	221.9***
Biomass	483.4***	1.4	127.6***

The LTM is run under five scenarios, where the varying parameters are burial rate (or uptake inefficiency) (B = 4.5, 9 and 18% y^{-1}), and downslope transport efficiency (50% efficiency (c) at 3°, 6° or 12° of steepness. Lateral organic matter inputs, burial of organic matter and available organic matter from which the benthic fauna depended, all have a positive relationship with the main effect ΔS (three levels: negative, zero and positive); although the model outputs change only marginally when varying B, they are strongly affected by variations of c.

2.4.2 Slope and levels of lateral sediment input, burial, available sediment and benthic biomass.

Lateral organic matter input (Figure 2-4, Table 2-1 and Table 2-2): Lateral organic matter input increases with ΔS when c is held constant while there is no main effect from B. When B is held constant, there is interaction between c and ΔS in determining the increasing trend of lateral organic matter input; as a consequence lateral organic matter input increases more strongly from areas with negative ΔS to areas with positive ΔS when the transport efficiency is high (c = 3°), rather than when it is low (c = 12°).

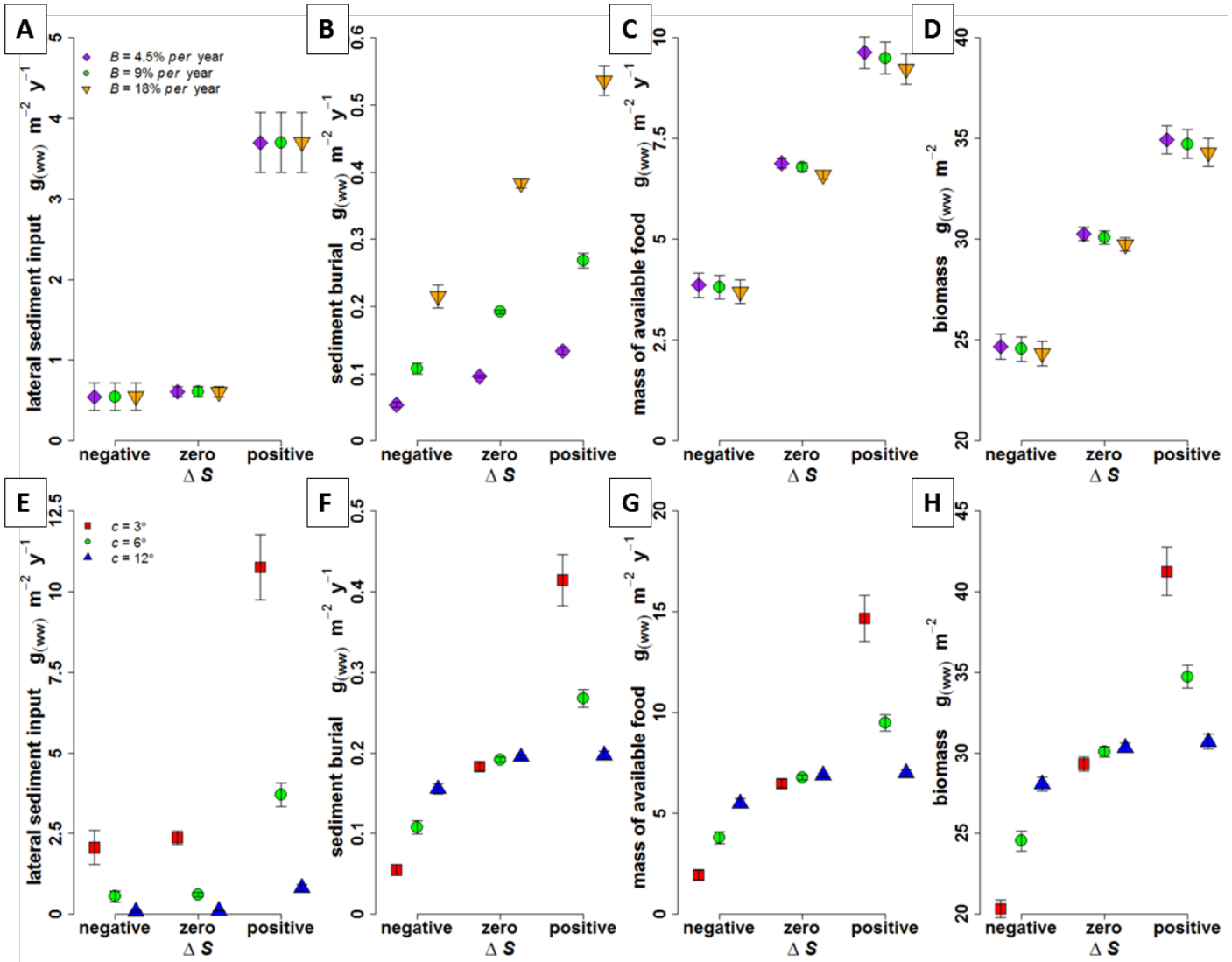
A
B
C
D
E
F
G
H
B = 4.5% per year
B = 9% per year
B = 18% per year
c = 3°
c = 6°
c = 12°
lateral sediment input g(ww) m−2 y−1
sediment burial g(ww) m−2 y−1
mass of available food g(ww) m−2 y−1
biomass g(ww) m−2
negative
zero
positive
Δ S

Figure 2-4: Variation of four modelled response variables with the slope difference (ΔS) in the hadal area of the Kermadec trench. Error bars show 95% confidence intervals. The first row of plots (A to D) summarises the results from model runs in which the burial rate (B) varies between 4.5% and 18% y^{-1}. The second row of plots (from E to H) summarises the results from model runs in which the transport efficiency threshold (c) varies between 3° and 12°. A) and E) lateral input in each cell; B) and F) burial of sediment, C) and G) sediment available for ingestion, D) and H) benthic biomass. The responses are measured in five different model settings represented with different symbols and colours. All the response variables have a positive relationship with ΔS. When B is modified, the response variables show only small variations, while large variations of the response are recorded when c is changed

Table 2-2: LTM output summary: means and standard deviations of four model outputs under 5 sets of model parameters of varying burial rate (B) and transport efficiency threshold (c), in relation to slope difference

	Slope difference			**Slope difference**		
	negative	**zero**	**positive**	**negative**	**zero**	**positive**
B = 4 ; *c* = 6	0.5 (0.1)	0.6 (-)	3.7 (0.2)	0.1 (-)	0.1 (-)	0.1 (-)
B = 9 ; *c* = 6	0.5 (0.1)	0.6 (-)	3.7 (0.2)	0.1 (-)	0.2 (-)	0.3 (-)
B = 18 ; *c* = 6	0.5 (0.1)	0.6 (-)	3.7 (0.2)	0.2 (-)	0.4 (-)	0.5 (-)
B = 9 ; *c* = 3	2.1 (0.3)	2.4 (0.1)	10.8 (0.5)	0.1 (-)	0.2 (-)	0.4 (-)
B = 9 ; *c* = 12	0.1 (-)	0.1 (-)	0.8 (0.1)	0.2 (-)	0.2 (-)	0.2 (-)
B = 4 ; *c* = 6	3.9 (0.2)	6.9 (0.1)	9.6 (0.2)	26.7 (0.3)	30.3 (0.2)	34.9 (0.4)
B = 9 ; *c* = 6	3.8 (0.1)	6.8 (0.1)	9.5 (0.2)	24.6 (0.3)	30.1 (0.2)	34.7 (0.4)
B = 18 ; *c*= 6	3.7 (0.2)	6.6 (0.1)	9.2 (0.2)	24.3 (0.3)	29.7 (0.2)	34.3 (0.3)
B = 9 ; *c* = 3	1.9 (0.1)	6.5 (0.1)	14.7 (0.6)	20.3 (0.3)	29.3 (0.2)	41.3 (0.8)
B = 9 ; *c* = 12	5.5 (0.1)	6.9 (0.1)	7.0 (0.1)	28.1 (0.2)	30.3 (0.2)	30.7 (0.2)

Table 2-3: The slope (k), y-intercept (l) and x-intercept (m) of the linear regression of animal density ($y = \log_{10}(\text{ind. } m^{-2})$) against the size range of benthic animals ($x = \log_{10}(\text{g ind.}^{-1})$) obtained under five different model scenarios of varying burial rate (B)and transport efficiency threshold (c). The regressions are calculated for areas of the trench with net sediment output (negative ΔS), equal inputs and outputs of sediment (zero ΔS) and net sediment input (positive ΔS). All the regressions have negative slope as the number of individuals per meter squared decreases when the nominal size of the individual increases. Furthermore, the negative y-intercepts (l) suggest that animals heavier than 1 g are always present in abundances lower than 1 ind.m^{-2}.The x-intercept (m) gives the nominal size of the animals that, at each level of food input, reach a density of 1 ind.m^{-2}.The steepness of the regressions does not change between areas with different ΔS, nor between different model runs, suggesting that the density ratios between size classes remain constant notwithstanding the different levels of food availability. On the contrary, the height of the linear regression (i.e. x-and y-intercepts) changes with model run and ΔS, resulting in higher biomass and density in areas of higher food availability (i.e. positive ΔS)

$\log_{10}(\text{ind.}\cdot m^{-2}) = k\cdot\log_{10}(g\cdot\text{ind.}^{-1}) + l$	**Negative ΔS**			**Zero ΔS**			**Positive ΔS**		
Model run	**k**	**l**	**M**	**k**	**l**	**m**	**k**	**l**	**m**
***B* = 4 ; *c* = 6**	-0.733	-0.381	0.3018	-0.736	-0.252	0.4544	-0.737	-0.179	0.5716
***B* = 9 ; *c* = 6**	-0.733	-0.387	0.2960	-0.736	-0.255	0.4499	-0.737	-0.181	0.5675
***B* = 18 ; *c* = 6**	-0.735	-0.303	0.3873	-0.736	-0.262	0.4405	-0.737	-0.188	0.5550
***B* = 9 ; *c* = 3**	-0.722	-0.557	0.1693	-0.736	-0.265	2.2945	-0.737	-0.086	0.7651
***B* = 9 ; *c* = 12**	-0.735	-0.303	0.3873	-0.736	-0.252	0.4544	-0.736	-0.249	0.4591

Burial of sediment (Figure 2-4, Table 2-1 and Table 2-2): With constant c = 6°, the amount of annually buried organic matter per cell is positively affected by an interaction of ΔS and B. Similarly, ΔS and c have an interacting effect on the amount of annually buried organic matter per cell when B is held constant.

Mass of available food (Figure 2-4, Table 2-1 and Table 2-2): When c is held constant, both B and ΔS (main effects) have a significant effect on the amount of available food in each cell: this increased with ΔS, and decreased with the level of B. When B is held constant, ΔS and c have an interacting effect on the mass of available food. Therefore, in cells with negative ΔS, available food is highest under low c conditions and lowest under high c conditions, while the scenario is reversed in cells with positive ΔS.

Biomass of fauna (Figure 2-4and Figure 2-5, Table 2-1 and Table 2-2): the biomass of benthic fauna in the hadal area of the Kermadec Trench significantly increases with ΔS when c is held constant, and there is also a small but significant positive effect from the increase of B. When B is held constant, ΔS and c have an interacting positive effect on benthic biomass.

The relationships between benthic biomass, slope difference and parameter sets are used to derive maps of expected benthic biomass in the Kermadec Trench area (Figure 2-5). Two characteristics stand out from these plots; the first is the relative similarity between a), b) and c), which suggests that variations of B have a small effect on biomass; by contrast the large differences between d) b) and e) suggest the relative importance of transport efficiency threshold (c) in determining the distribution of biomass. Substantial differences in spatial heterogeneity of biomass are also apparent between the differing transport efficiency thresholds: at low levels of transport efficiency (Figure 2-5e) predicted biomass decreases gradually northwards, possibly as a consequence of lower POC input towards the more oligotrophic (tropical) parts of the trench. When the transport efficiency is higher (Figure 2-5d), predicted biomass is higher along the axis and lower along slopes of the trench.

Higher levels of food availability, estimated to occur at the local minima of the bathymetry, affect the total benthic biomass estimate but not the relative abundance of the size classes (Table 2-3). Density increases consistently across size classes when food availability increases, and this could be quantified by taking as reference point the density of 1 ind·m^{-2}: with higher food input, bigger individuals could reach this reference density. This allows suggesting that the community composition changes with food availability, as the presence of larger size classes is supported by higher food availability.

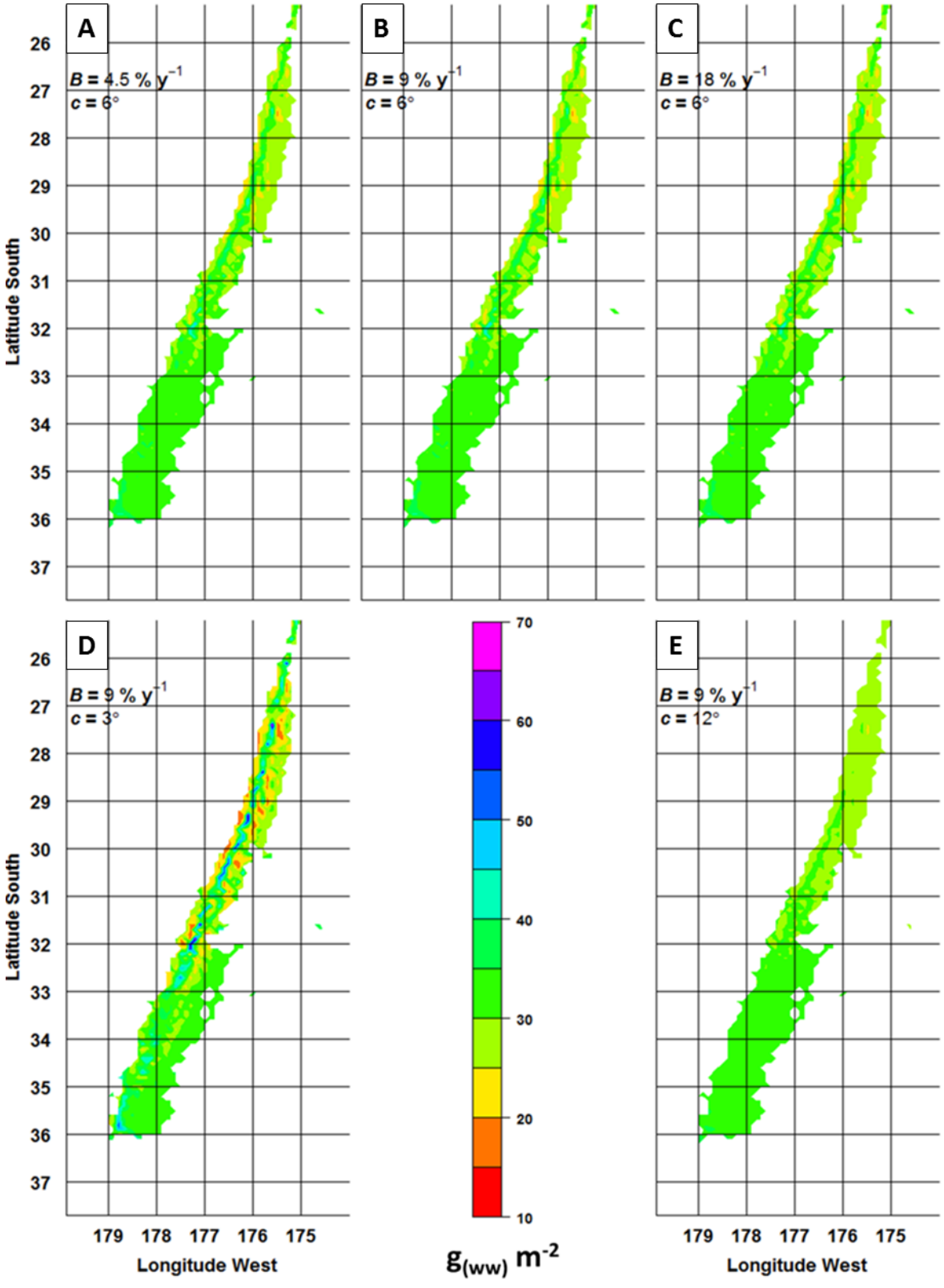

Figure 2-5: Maps of the distribution of benthic biomass (g_{ww} m^{-2}) in the hadal area of the Kermadec Trench (the model was run also on the blank parts of these mats, around the trench, but results are not shown here, to highlight the variability of biomass within the trench). The five maps show results from five runs of the Lateral Transport Model (LTM) under five combinations of burial rate (B) and transport efficiency threshold (c). In the top three maps c is held constant (6°), while B is increased from 4.5 % y^{-1} to 9% y^{-1} and 18 % y^{-1}. In the two bottom maps, B is held constant at 9% y^{-1},

while c is changed from low slope values (3°) to high slope values (12°). Two characteristics stand out from these maps; the first is the relative similarity between map A, map B and map C, which suggest that B has a small effect on benthic biomass; by contrast the differences between map D, map B, and map E, suggest the high importance of transport efficiency threshold in determining the distribution of benthic biomass.

Table 2-4: F values and statistical significance obtained from testing with two ANOVAs the effect of depth and model scenario on the benthic biomass estimated through the LTM. When transport efficiency is constant (c = 6°) the depth factor (shallow vs. deep) causes a significant increase of benthic biomass, while there is no effect from changing the level of burial rate (B = 4.5, 9, 18 % y^{-1}). When the burial rate is held constant (B = 9 % y^{-1}), depth factor and transport efficiency threshold (c = 3°, 6°, 12°) have an interacting effect on the modelled benthic biomass. This increases with increasing depth under high and intermediate levels of transport efficiency, while it decreases with depth when the transport efficiency is low (c = 12°). The degrees of freedom of the residuals are 357 for each test. Significance codes used: 0 '***' 0.001 '**' 0.01 '*' 0.05.

	Depth factor (d.f. = 1)	**Model scenario (d.f. = 2)**	**Interaction (d.f. = 2)**
Varying *B*, constant *c*	59.0554***	0.7349	0.0031
Varying *c*, constant *B*	34.726***	93.553***	16.822***

2.4.3 Trench depth, shape and axis topography.

Benthic biomass increases with depth under all model scenarios, apart from the one with low transport efficiency (Figure 2-6 and Table 2-4). When c is held constant (Figure 2-6a) the modelled biomass is positively affected by increasing depth, while there is no effect from the level of B. When B is held constant (Figure 2-6), transport efficiency and depth interval interactively affect the variation of biomass: the response is similar between levels of c up to 8500 m, while in the deepest parts of the trench biomass increases more strongly with high transport efficiency values.

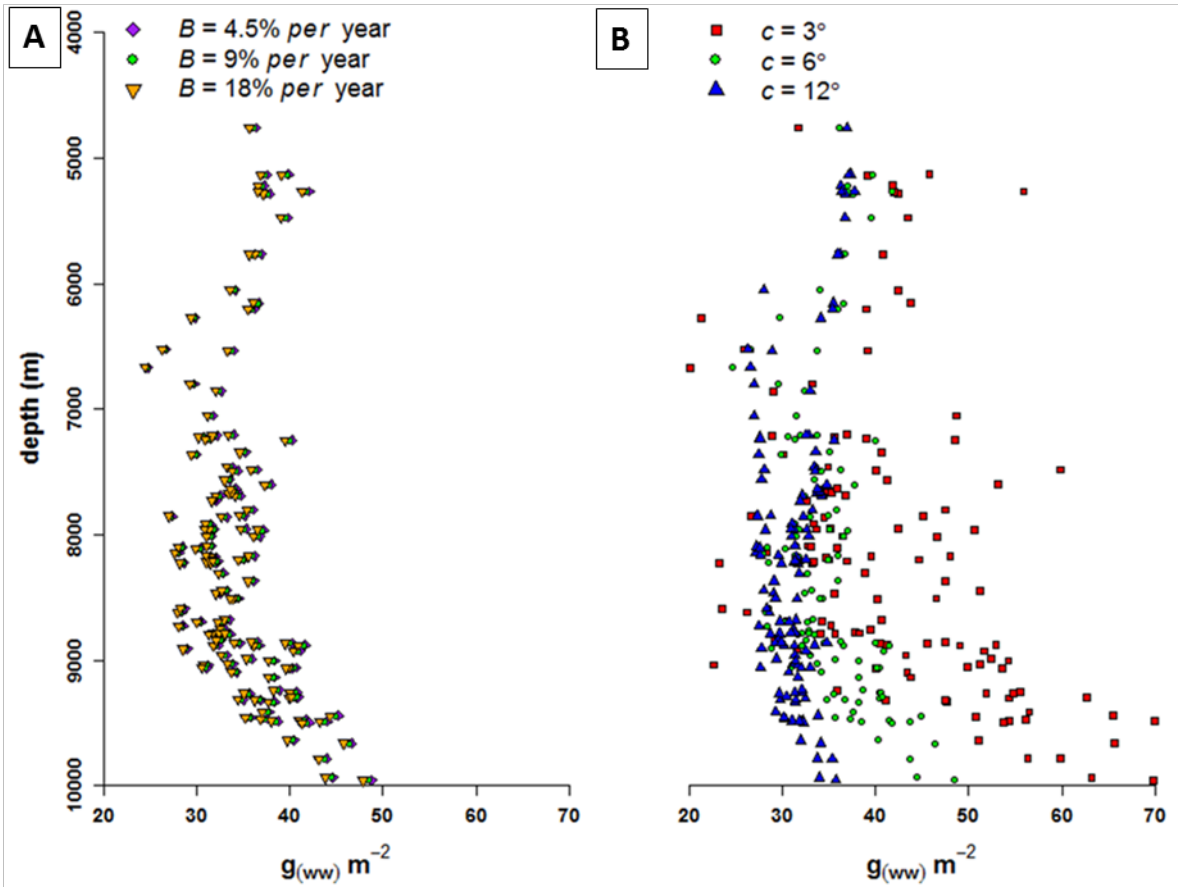

Figure 2-6: The increase of benthic biomass (g_{ww} m^{-2}) with depth along the axis of the Kermadec Trench. The benthic biomass was predicted through five runs of the LTM, with different levels of burial rate (B, panel A) and transport efficiency threshold (c, panel B) represented with different symbols and colours. The benthic biomass increase with depth is small in the shallow part of the trench (down to 8500 m) and stronger in the deep part of the trench (deeper than 8500 m). The response differs between model runs only between different levels of c, while different levels of B do not result in significantly different outputs.

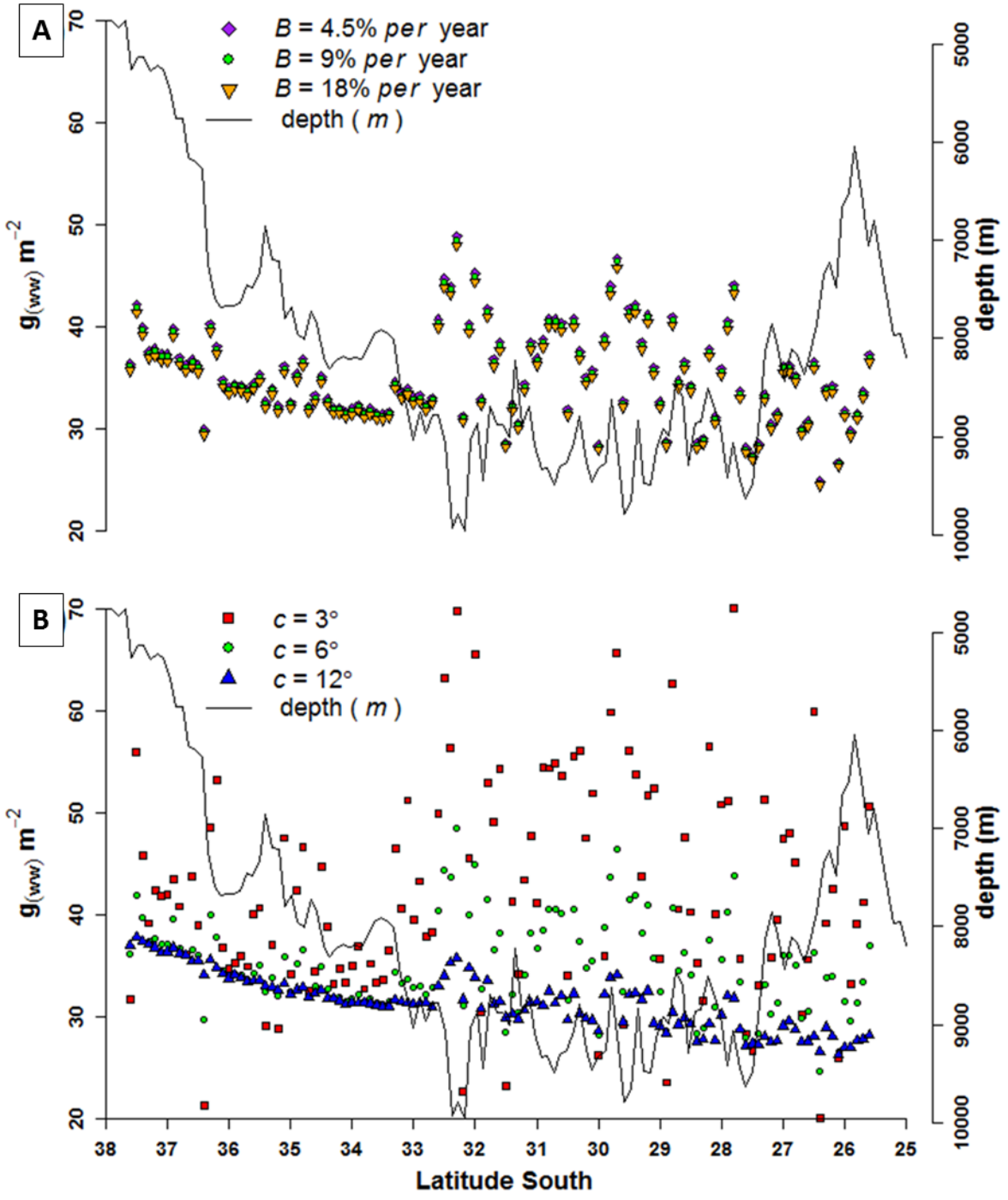

Figure 2-7: Benthic biomass along the axis of the Kermadec Trench, under 5 different sets of parameters. Depth profile along the axis of the trench is superimposed to both panels and measured on the right-hand-side y axis. From the south, the depth increases up to ~8500 m, after which it fluctuates around this value, before decreasing towards the north. Panel A: benthic biomass along the axis of the Kermadec Trench, as predicted from the LTM keeping transport efficiency threshold constant (c = 6°) and varying burial rate (B = 4.5, 9 and 18% y^{-1}). Panel B: Benthic biomass along the axis of the Kermadec Trench, as predicted from the LTM keeping burial rate constant (B = 9% y^{-1}) and varying transport efficiency threshold (c = 3, 6 and 12°). The benthic biomass is low and less variable in the southern part of the trench, where the depth increases, and then it becomes highly variable in the central and northern areas of the axis, where the trench is narrower with steeper slopes (Figure 2-2).

Together with depth, trench topography plays a role in determining benthic biomass patterns in the model. Depth increases along the axis of the Kermadec Trench, from south to the centre of the trench, until reaching ~8500 m (Figure 2-7). In the southern part of the axis the modelled benthic biomass is relatively low and it decreases towards the mid part of the axis under all model conditions (Figure 2-7a and Figure 2-7b, Table 2-5). Such behaviour changes in the central and northern parts of the axis where the biomass is much more variable. When B varies and c is constant (Figure 2-7a), the biomass does not change significantly along the axis between the northern and southern areas. However, when c varies and B is kept constant (Figure 2-7b) the two main effects (position along the axis and transport efficiency threshold) interact resulting in a higher difference in the modelled biomass between the northern and southern parts of the axis.

Table 2-5: Panel A: mean and standard deviation of benthic biomass (g_{ww} m^{-2}) in the southern and northern part of the Kermadec Trench axis, measured under five LTM scenarios with different levels of sediment burial rate (B) and the transport efficiency threshold (c). Panel B: F values and statistical significance obtained from testing with two ANOVAs the effect of location (north vs. south) and model scenario on the benthic biomass estimated through the LTM. When transport efficiency is constant (c = 6°) benthic biomass does not change significantly with location nor with burial rate (B = 4.5, 9, 18 % y^{-1}). When burial rate is constant (B = 9 % y^{-1}) benthic biomass is affected interactively by location and transport efficiency threshold (c = 3°, 6°, 12°). When the transport efficiency is high (3°) benthic biomass increases from south to north, while when transport efficiency is low (12°) benthic biomass decreases from south to north. The degrees of freedom of the residuals are 357 for each test. Significance codes used: 0 '***' 0.001 '**' 0.01 '*' 0.05.

A)	**south**	**north**	**t-test (p-value)**
B = 4 % y^{-1}; *c* = 6°	34.6 (0.4)	35.5 (0.6)	-1.22 (0.2265)
B = 9 % y^{-1}; *c* = 6°	34.4 (0.4)	35.3 (0.6)	-1.22 (0.2259)
B = 18 % y^{-1}; *c* = 6°	34.0 (0.4)	34.9 (0.6)	-1.22 (0.2246)
B = 9 % y^{-1}; *c* = 3°	38.7 (1.0)	44.4 (1.4)	-3.37 (0.0010)***
B = 9 % y^{-1}; *c* = 12°	33.5 (0.3)	30.1 (0.3)	6.30 (3.919e-13)***
B)	**location (d.f. = 1)**	**model scenario (d.f. = 2)**	**Interaction (d.f. = 2)**
Varying *B*, constant *c*	2.9043	0.6357	0.0001
Varying *c*, constant *B*	2.0825	84.9628***	13.6145***

Overall, slope and topography affected the accumulation of organic sediment (and biomass) resulting in patterns that would not have been expected if only the vertical flux of organic carbon from the ocean surface was taken into account (Figure 2-8). Under high levels of lateral transport, efficiency up to twice as much biomass was found in areas with positive ΔS° than would be expected in the absence of lateral transport, and up to half as much biomass in areas with negative ΔS°. Furthermore, the process of lateral transport caused biomass levels in areas of net sediment input (deepest holes along the axis, especially in the central and northern parts) to be between two and four times higher than in areas of net sediment output.

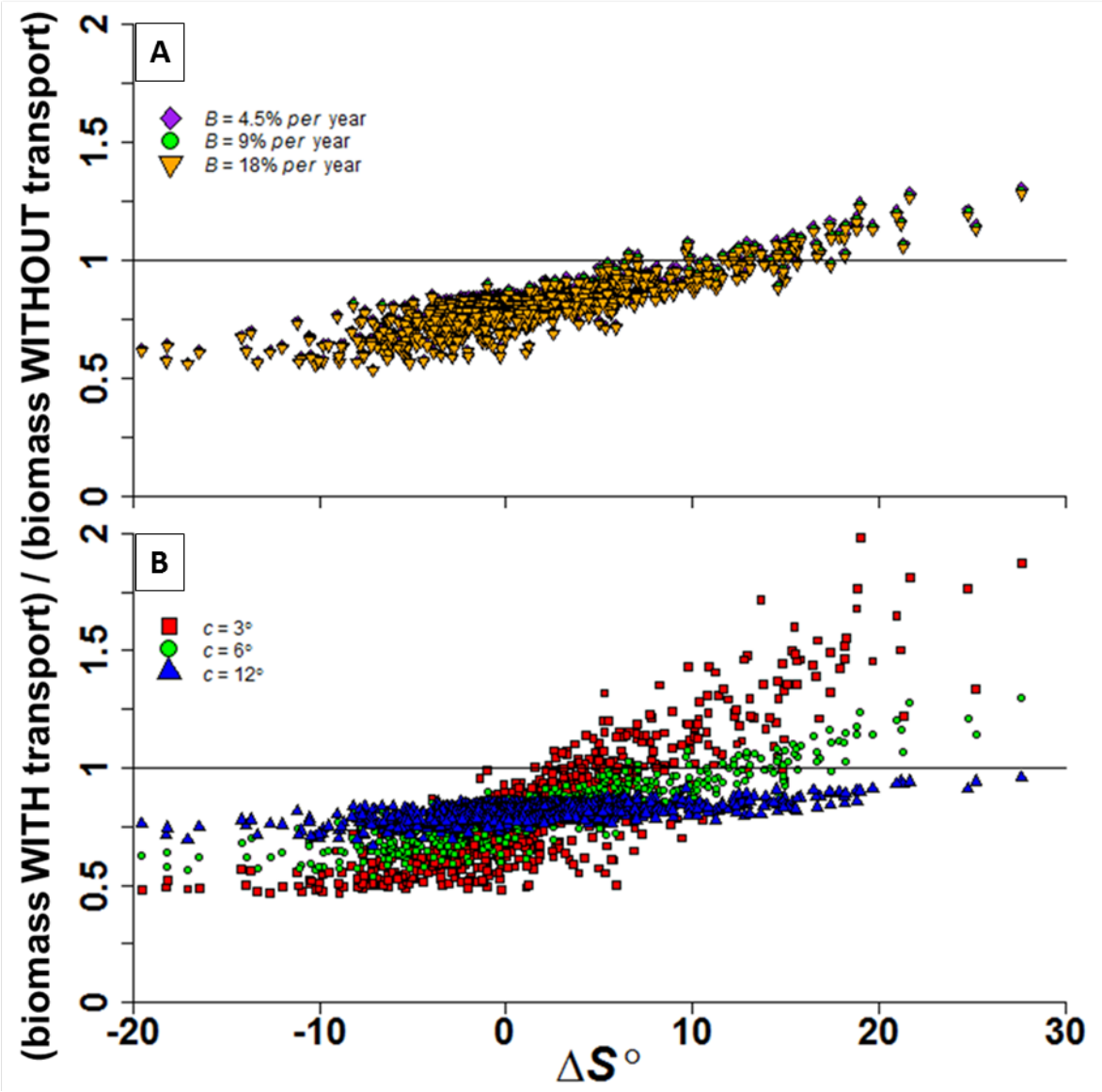

Figure 2-8: The figure shows the change in modelled benthic biomass in the hadal area of the Kermadec Trench when introducing lateral transport, in relation to local topography (slope difference, ΔS°). The presence of lateral downslope transport results in higher benthic biomass levels than what would be expected in the absence of this process. A value of y = 1 means "no change". Panel a) shows three model runs with varying burial rate (B), and panel b) shows three model runs with varying transport efficiency (c). The increase in expected benthic biomass is highest under high transport efficiency conditions, reaching a maximum increase factor of ~2

2.5 Discussion

I have presented a model that estimates biomass of benthic fauna because of vertical and lateral organic matter inputs. The results provide testable hypotheses for elucidating the potential

effects of local topography on benthic biomass distribution in trench environments. To my knowledge, this is the first such model for deep-sea habitats, and I believe that it can be used to improve our understanding of benthic ecology in relation to topography.

In this framework, the effect of local topography (ΔS) on biomass, and its consequent spatial distribution, results to be mostly dependent on transport efficiency (c), while burial rate of organic sediment (B) does not appear to have a strong effect. The relative insensitivity of the model to changes in the burial rate suggests that constraining the residence time of sediments, which appears to be highly variable and dependent on sediment type (Mayor et al. 2012), would only slightly improve the accuracy of model predictions. In areas of negative ΔS (hills or high areas) the biomass is higher under high c scenarios (low transport efficiency), while this pattern is reversed in areas of positive ΔS (depressions, or the trench axis). Future attempts to fully evaluate this model should therefore be aimed at measuring the benthic biomass in areas with a wide range of ΔS, as this would help determine a more accurate value for c. The current application of the model is intended only to provide general trends between benthic biomass and ΔS, depth and trench shape, and uses the Kermadec Trench as an example area. Model outputs include maps of the expected biomass distribution for this area of interest. Such maps can be used for survey planning as they provide an overview of the biomass patterns theoretically induced by local topography.

In the Kermadec Trench, under all sets of parameters, the model predicts an accumulation of organic matter and benthic biomass along the axis of the trench, and depletion on the surrounding slopes. The benthic biomass levels are predicted to be up to twice as high than with no lateral transport in the central and northern parts of the trench, where the axis reaches greater depths, and the trench is narrower with steeper slopes. In the southern part of the trench the slopes are gentler; therefore, the biomass is predicted to change only marginally between the slopes and the axis. This prediction is opposed to what would be expected because of the surface primary production and vertical POC flux. As the trench runs in a south-north direction from temperate to sub-tropical regions, it receives a gradient of POC flux decreasing from south to north. This gradient, which is likely to have a strong effect on the ecology at the ocean surface, may not translate to areas within the trench where lateral fluxes become important. The response of benthic biomass to ΔS does not change when it is standardised by the vertical flux (V), suggesting that ΔS, rather than vertical sediment input, drives the biomass distribution in the model. In case of extremely low lateral transport efficiency (c = 12°) the benthic biomass across the whole hadal area is lower than it would be in the absence of lateral transport. This result suggests an interaction between lateral transport and burial rate that results in lower fluxes of biologically available sediment (E).

Accumulation of organic sediments and biomass along the axis of the trench can be similar to that found along the axis of submarine canyons, where organic matter and benthic biomass levels are generally higher than on the surrounding slopes (Vetter and Dayton, 1998). Strong currents along the axis of canyons (up to 1.9 m s^{-1} in the Scripps Canyon) generally are suggested as a reason for large organic matter fluxes through the axes (Inman et al. 1976). There is no evidence that trenches experience the kind of intense cascading currents seen closer to shore at shallower depths (e.g., Canals et al. (2006)), and hence gravitational transport may provide a useful first approximation in trenches, even without suggesting a mechanism for the transport. The few empirical measurements from hadal trenches suggest that typical current speeds for these regions are low (about 1 cm s^{-1} in Puerto Rico trench (Schmidt and Siegel, 2011), and 16.2 mm s-1 ± 8.5 in the Kermadec Trench (Jamieson et al. 2013). Currents recorded in the Mariana Trench were null for most of the time, and the maximum speed at the deepest station was 8.1 cm s^{-1} directed along the axis of the trench (Taira et al. 2004)). Furthermore, the effect on sediment redistribution due to water mass movements around deep-sea topographic features is complex (Turnewitsch et al. 2013), and would need to be addressed with a significantly more complex modelling approach.

Even though the effective sinking speed is limited by the time step interval, grid spacing, slope and transfer efficiency applied, the model results are insensitive to variations in time step and grid spacing because the model is run to equilibrium, as confirmed by a sensitivity analysis. In the future, better understanding of effective speed and slope transport may allow for improvement in this aspect of our model framework.

Table 2-6: Comparison of literature data with ΔS° predictions through the GEBCO 6’ bathymetry.

Reference	Site name	Trench name	Lat	Long	Depth (m)	GEBCO Depth (m)	ΔS°	Meiofauna		Bacteria
								Abundance no./10cm^2	Biomass µgC/10 cm^2	Respiration
Tietjen et al. 1989		Puerto-Rico	19° 08.7' N	66° 14.3' W	7460	7394	-2.37	44 (± 10)	3.8 (± 1.6)	
Tietjen et al. 1989		Puerto-Rico	19° 35.7' N	66° 11.2' W	8189	8373	4.30	96 (± 15)	14.3 (± 5.1)	
Danovaro et al. 2002	B1	Atacama	23° 30.5' S	70° 42.8' W	1050	2359	3.78	550 (± 186)	1053 (± 140)	
Danovaro et al. 2002	B4	Atacama	23° 46.6' S	70° 34.4' W	1140	1733	6.74	672 (± 350)	578 (± 239)	
Danovaro et al. 2002	C7	Atacama	23° 15.0' S	70° 40.0' W	1355	2324	0.26	639 (± 425)	723 (± 534)	
Danovaro et al. 2002	A1	Atacama	23° 15.0' S	71° 21.0' W	7800	7592	13.03	6378 (± 3061)	824 (± 348)	
Glud et al. 2013	Reference	Mariana	10° 50.8' N	142° 33.8' E	5982	6531	1.75			Low
Glud et al. 2013	Challenger Deep	Mariana	11° 22.1' N	142° 25.8' E	10813	9494	6.38			High

High-frequency fluid dynamics may have an important effect on sediment distribution above the trenches, as suggested by research in north-western Pacific trenches (Turnewitsch et al. 2014); areas with high internal tides intensity have sediment deposition that is lower than expected, possibly as a consequence of particle break-down and consequent re-suspension or lower sinking rate. In addition, abrupt events such as earthquakes (Itou et al. 2000) can induce extreme levels of sediment and associated organic matter transport in hadal trenches. Cyclones could have similar effects in trenches that are close to landmasses, as they increase the input of terrestrial organic materials in the water column, which can then be transported to depth (George and Higgins, 1979). While no attempt was made to take either of these into account in the LTM, their existence is acknowledged.

Distance from land is, potentially, another relevant factor in determining the amount of lateral sediment fluxes to a trench. High meiofauna abundance in the Puerto-Rico and Atacama trenches have been attributed to inputs of terrestrial organic materials (Danovaro et al. 2002; Tietjen et al. 1989). Similarly, abundance, species richness, and diversity appear to be higher in the New Britain Trench, rather than in the Mariana Trench, possibly because of higher allochthones food input (Gallo et al. 2015). Furthermore, distance from land has been found to influence the meiofauna abundance and community composition in Mediterranean non-hadal trenches off the Greek coast (Tselepides and Lampadariou, 2004). A factor accounting for distance from shore could probably improve model interpretations when comparing multiple trenches.

ΔS could be an effective indicator of organic sediment matter accumulation from lateral transport in the Kermadec Trench, and could explain some of the benthic biomass patterns found in other hadal trenches. Meiofauna biomass and abundance in the Puerto-Rico Trench, recorded by Tietjen et al. (1989), were higher at the deep station (8189 m) than at the shallow station (7394 m). With a simple slope analysis for these two areas through the GEBCO bathymetry it can be seen that the deep station is in an area of net organic matter input, having positive ΔS, while the shallow station is an area of net organic matter output (Table 2-6). Therefore, according to the presented model, the two stations would have different organic matter input rates, which could explain the different levels of observed meiofauna biomass and abundance (Tietjen et al. 1989). In the same trench, George and Higgins (1979) investigated the macrofauna biomass and abundance at Brownson (8800 m) and Gillis Deep (7600 m) sites, finding that both were higher at the shallower station. They suggested that this was caused by the input of plant debris through a submarine canyon at Gillis Deep, something that cannot be confirmed with this model framework yet, as the station location data is not precise enough. In the Peru-Chile trench there are meiofauna hotspots at a depth of 7800 m supported by high concentrations of nutritionally rich organic matter (Danovaro et al. 2002). This site has a higher ΔS° value than the other sites

examined by Danovaro et al. (2002) (Table 2-6). More recently, Glud et al. (2013) suggested elevated rates of organic matter inputs as the cause of higher concentration of microbial cells and higher oxygen consumption at Challenger Deep in the Mariana Trench, when compared to a site on the neighbouring abyssal plain (Reference site). In addition, in this case the ΔS° estimated through the GEBCO bathymetry is higher for the suggested high-deposition site (Table 2-6). Glud et al. (2013) also found that bacterial respiration in the deepest point of the Mariana Trench was about twice that on the adjacent abyssal plain. For the Kermadec Trench was found a similar result, as the modelled biomass in the areas of highest input, under high transport conditions (B = 9 % y^{-1}, c = 3°) can be up to two times higher than with no transport. Furthermore, under almost all model scenarios the local minima in the trench bathymetry were found to have higher biomass levels than would be expected without transport.

There are few quantitative data of benthic fauna biomass/abundance currently available for the Kermadec Trench and these data are mainly from sampling expeditions in the 1950s (Belyaev, 1989). These data are insufficient to fully validate the model. Nevertheless, Belyaev (1989) noted that of the two trawl stations of the Vityaz expedition, benthic biomass was estimated to be slightly higher at the deepest site (0.06 g m^{-2} at ~10,000 m compared with 0.04 g m^{-2} at ~9000 m). These values are low compared to the ones estimated by the LTM, possibly because of undersampling by the trawl gear (Gage and Bett, 2005). Belyaev (1989) also reported the estimates of benthic fauna abundance from two types of trawl samples recovered by the Galathea expedition from the Kermadec Trench: abundance was highest at the deepest site (2100 ind. m^{-2} at ~8200 m, compared with 63 to 1100 ind. m^{-2} at shallower hadal depth sites). The biomass increase with depth, predicted by my model is generally consistent with these very limited data, and suggests that lateral transports of organic matter could explain the distribution pattern of benthic fauna in the Kermadec Trench.

2.6 Conclusions

Here I developed a model that estimates the hadal benthic biomass as a function of vertical and lateral organic matter inputs, providing a broad-scale understanding of the potential effects of local topography on biomass distribution, and a quantitative theoretical framework to guide future sampling of trenches. Future developments of this model should include a detailed analysis of transport efficiency in relation to slope steepness. This would help constraining the a and c parameters (Equation 2-7).

Since early hadal exploration, unexpectedly high biomass levels found in some deep locations have suggested that benthic biomass might increase with depth in the trenches instead of

decreasing as along other depth gradients. Lateral transport of food, and accumulation at depth, could be driving these trends.

Presented outputs would allow, in the presence of a comprehensive hadal biomass dataset, constraining the lateral transport parameter (c) in the model. With this objective in mind, a survey should aim at sampling across the full depth range, and in areas with a range of estimated slope difference (ΔS), as this factor may be a key driver of food accumulation in trenches. Variations in the burial rate of organic matter only resulted in small differences in model outputs, suggesting that this factor might play a smaller role.

Trench topography appears to play a major role in determining areas of high benthic biomass: the presence of deep holes, opposed to a smooth and flat axis, is predicted to result in areas of higher biomass variability. Overall, my model suggests that the simple process of lateral downslope sediment transport can result in complex patterns of benthic biomass inside a trench.

Chapter 3: Seamount morphology, not depth, controls biomass distribution at two locations in the northeast Pacific[2].

3.1 Introduction

Seamounts are a common and prominent topographic feature of the world's seafloor; they are of ecological relevance at local scale (see Rowden et al. (2010a) for a review), and thus cumulatively also play an important ecological role at global scale, as they introduce heterogeneity. Defined as isolated elevations of more than 1000 m above the surrounding abyssal plain, they can generally be divided into guyots (or tablemounts), with a flat top, and seamounts, with a sharper, pointed, summit. Recently it has been estimated that the total number of seamounts and guyots in the ocean could exceed 10,000 units, covering an area of approximately 9,000,000 km^2 (2.43% of ocean seafloor) (Harris et al. 2014). Other estimates also including the features with a ratio of length to width greater than 2, bring the number of seamounts over 33,000 units (17,204,675 km^2) (Yesson et al. 2011).

Owing to their size, seamounts are believed to influence the direction and intensity of background oceanic currents (Genin et al. 1986, Turnewitsch et al. 2004), and to support the formation of revolving cap current regimes above them, which can be temporally stable depending on the characteristics of the impinging flow (Bashmachnikov et al. 2013). This not only can result in the retention of organic particles around the seamount (Rodgers, 1994) but, depending on the depth and feature size, can also have an effect on the mixing of ocean surface layers, influencing primary production (Falkowski et al. 1998, Turnewitsch et al. 2016). Furthermore, seamounts are generally associated with coarser sediment types in comparison to abyssal plain sites, possibly because of the removal of finer sediments by hydrodynamic action or by gravitational sediment fluxes (Tempera et al. 2012). All these physical characteristics introduce spatial discontinuity on the seafloor and in the water column relative to the surrounding seafloor. In addition, seamounts have been held to support an oasis hypothesis (Rowden et al. 2010b) which suggests that seamounts support a high diversity of fish (Lundsten et al. 2009b), filter feeders (Roberts and Hirshfield, 2004) and other benthic invertebrates (Samadi et al. 2006). Seamount morphology

[2] The video annotations for this chapter were performed by the staff at the Monterey Bay Aquarium and Research Institute (MBARI), and where provided to me by Jim Barry and Lonny Lundsten. I then converted to wet weight the measured size of the individuals.

could play an important role in determining the distribution of biomass and communities. This is supported by the high meiofauna abundance and biomass on the flanks and at the base of Condor Seamount (Zeppilli et al. 2013, Zeppilli et al. 2014), the abundance of deposit feeders at the top of Rodriguez guyot (Lundsten et al. 2009a), and by the passive filter feeding community at the top of Jasper, Davidson and Pioneer seamounts (Genin et al. 1986, Lundsten et al. 2009b). Indeed, there can be high variability of community composition and standing stocks of biomass within the same seamount, potentially because of depth, slope and terrain position (McClain et al. 2010, Chivers et al. 2013, McClain and Lundsten 2014).

To some extent, the patterns of biomass distribution and community composition introduced by seamounts can cause the benthic biomass to diverge from its widely observed reduction with depth, believed to be caused by the decrease in food availability (Rex et al. 2006). Most benthic communities depend on a rain of particulate organic carbon that sinks from the photic zone to deeper depths, which is remineralised gradually as it sinks (Lutz et al. 2002, Ruhl and Smith, 2004, Johnson et al. 2007, Ruhl et al. 2014). Therefore, since biomass generally decreases with increasing depth in each of the meio-, macro- and megafauna size classes (Rex et al. 2006), seamount tops are expected to have higher biomass than the surrounding plains, while the flanks and base would have progressively lower biomass because of the remineralisation of organic particles with depth. Furthermore, some evidence suggests that, on seamounts, food particles are trapped by current-seafloor interactions near or at the top creating more favourable conditions for benthic communities to thrive and preventing further sinking of the sediment (White and Mohn 2004). By contrast, the steep flanks of the seamount could enhance gravitational sinking of the particles, reducing and potentially inverting the trend of biomass decrease with depth (Wolff 1970, Danovaro et al. 2002). A similar gravitational process has also been suggested to be important in driving the higher biomass in the deep areas on the axis of hadal trenches when compared to the trench flanks (Ichino et al. 2015).

Table 3-1: Chapter 3 study sites

Site	Latitude N	Longitude W	Shape	Summit (m)	Base (m)	Dives (Transects)	Size measurements
Davidson	35°430’	122°43’	Seamount	1250	3530	6 (33)	305
Taney	36°45’	125°21’	Guyot	2200	4000	6 (24)	90

Here the distribution of biomass around large seamounts is studied in relation to the interacting effect of gravitational and hydrodynamic transport. If only gravity influences sediment transport (gravity-dominated scenario) some portion of vertically sinking Particulate Organic Carbon (POC) is expected to be transported laterally and deeper along the steep seamount flanks. This would result in lower-than-expected biomass at the top and on the steep flanks of the seamount, and

higher-than-expected biomass at the base of the seamount. If only currents affect sediment transport (hydrodynamics dominated scenario), the presence of particular current patterns around the seamount may result in increased food availability through higher quantities of POC being entrained by currents over the higher elevations of the seamount (Figure 1-1).

The aim of this study is to determine how the two scenarios interact, increasing the spatial variability of benthic biomass at local scales in comparison with what would be expected if depth alone was accounted for. To investigate the three-dimensional distribution of benthic communities in relation to seamount terrain, I look at the megafauna biomass estimated using Remotely Operated Vehicles' (ROV) video footage at two seamount areas in the northeast Pacific, which have been the target of intensive surveying by the Monterey Bay Aquarium Research Institute (MBARI) (Table 3-1, Figure 3-2).

3.2 Materials and methods

3.2.1 Video surveys.

Video transects of the seafloor were recorded over the course of 12 dives on two distinct topographic features: Davidson Seamount and Taney Seamounts (Table 3-1, Figure 3-2).

Davidson Seamount is located at 35°43'N 122°43'W, approximately 50 nautical miles away from the California coastline. Its summit lies at a depth of 1250 m and its base is at 3530 m. It has a volcanic origin and it is characterised by an elongated shape in the southwest-northeast direction, and a sharp summit. In this study data from six ROV survey dives and 33 transects ranging between 1300 m and 3300 m depth were used (Figure 3-2). Davidson seamount is also located 35-50 nm to the south of the Monterey Canyon.

The Taney Seamounts chain is composed of four seamounts covering a depth range between 2200 and 4000 m. They are located approximately at 36°45'N 125°21'W, ~140 nm from the coast. The chain has a volcanic origin, probably linked to the presence of a hotspot, and all the seamounts have a truncated cone shape with craters at the top; the crater is collapsed in the westernmost seamount. Also for these seamounts six ROV survey dives from the three westernmost seamounts of the chain were used, during which 24 video transects were recorded, ranging between depths of 2200 and 3300 m (Figure 3-2).

3.2.2 Biomass estimate.

Two ROVs were used for these explorations: Tiburon and Doc Rickets, both operated by the Monterey Bay Aquarium Research Institute (MBARI). They were fitted with two 640 nm red lasers placed 30 cm apart on Tiburon and 29 cm on Doc Rickets. The D5-HD video tapes, recorded with high-definition (HD) cameras, were first annotated for density and community composition by the MBARI Video Lab team using the Video Annotation and Reference System (VARS Schlining 2006, Lundsten et al. 2009a, Lundsten, et al. 2009b, McClain, et al. 2010, Duffy, et al. 2014, McClain and Lundsten 2014).

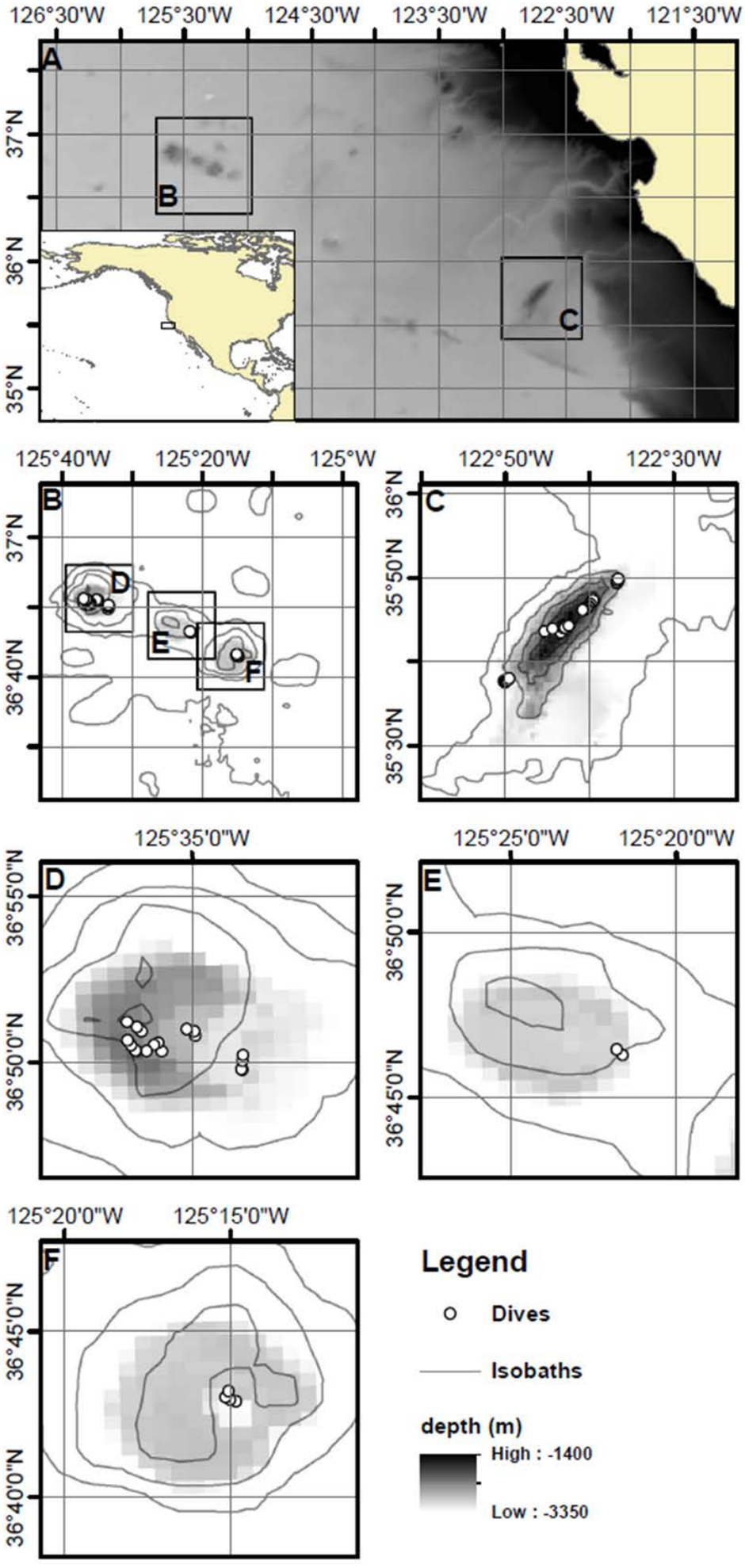
126°30'W
125°30'W
124°30'W
123°30'W
122°30'W
121°30'W
37°N
36°N
35°N
A
B
C
125°40'W
125°20'W
125°W
36°40'N
D
E
F
122°50'W
122°30'W
36°N
35°50'N
35°30'N
125°35'0"W
36°55'0"N
36°50'0"N
125°25'0"W
125°20'0"W
36°50'0"N
36°45'0"N
125°20'0"W
125°15'0"W
36°45'0"N
36°40'0"N
Legend
Dives
Isobaths
depth (m)
High : -1400
Low : -3350

Figure 3-1: Bathymetric maps of the Taney seamounts area (panel B) and Davidson seamount area (panel C), with the ROV transect locations (white dots). Zoomed views on three seamounts of the Taney chain are shown in panels D, E and F The grey scale in panels B-F represents the shipboard multibeam resampled at 740 m by 740 m. Panel A shows where the two study areas are in relation to each other and to the whole NE Pacific.

Then the lasers were used to scale the size of specimens chosen randomly from the pool of annotated individuals. Measurements of pixel dimensions of 10 or more specimens from 25 megafauna taxa were made with the VARS software (Schlining 2006) and converted to length measurements with reference to laser scalers (Figure 3-3). These were echinoderms (holothuroidea, paleopatides, pseudostichopus, psychropotes, oneirophanta, elasipodida, synallactes, peniagone, ophiuroidea, asteroidea, pterasteridae, brisingida, ophiacanthidae, astrodia, phytonaster), crustaceans (munida, glyphocrangon), molluscs (cephalopoda, gastropoda), cnidarians (hormatiidae, sicyonis, actiniaria and umbellula); for crinoidea and porifera, instead, mean values of 0.7 and 8 grams per individual respectively were used (Durden et al. 2016). The ranges of individual wet weights were estimated from the measured size distribution and empirical size/weight relationships (Durden, et al. 2016). A total of 305 specimens were measured at Davidson, while 90 specimens were measured at Taney seamounts.

The size of 33 taxa, which accounted for 80% of all the individuals encountered, could not be converted to weight. These included Foraminifera, Sipuncula (Golfingiida), Cnidaria (Anthozoa, Scleractinia, Pennatulacea, Antipatharia, Cladopathidae, Hexacorallia, Alcyonacea, Hydrozoa, Aiphonophorae, and Rhodaliidae), Mollusca (Bivalvia, Aeolidiidae, Dendronotidae, and Neoloricata), Anellida (Polychaeta, Phyllodocida, and Laetmonice), Arthropoda (Amphipoda, Paguridae, Cirripedia, Barnicle, and Mysida), Echinodermata (Paxillosida, Echinoidea, Psolus, Comatulida) and Chordata (Fish).

One of the major groups of large animals whose biomass that was not estimated is that of the erected corals, which accounts for 1.6% of all the counted individuals, and probably a larger proportion of the total biomass (as a consequence of the large size of some of these colonial organisms). Nevertheless, no evidence that the inclusion of these taxa would have changed the trends highlighted by the models was found: density of erected corals along transects at a comparable depth between the two study sites is neither significantly correlated to any of the morphology predictors, nor to current direction SD (Figure 3-11). Even though this does not account for potential differences in colony size, it suggests that including the mass of erected corals in this analysis would not have affected greatly the trends of biomass distribution around the topographic features. Future advancements in volume estimation with 3D imaging could help

improving the estimation of coral size, ultimately allowing better measurements of biomass of organisms with complex morphological geometry (Dansereau et al. 2011).

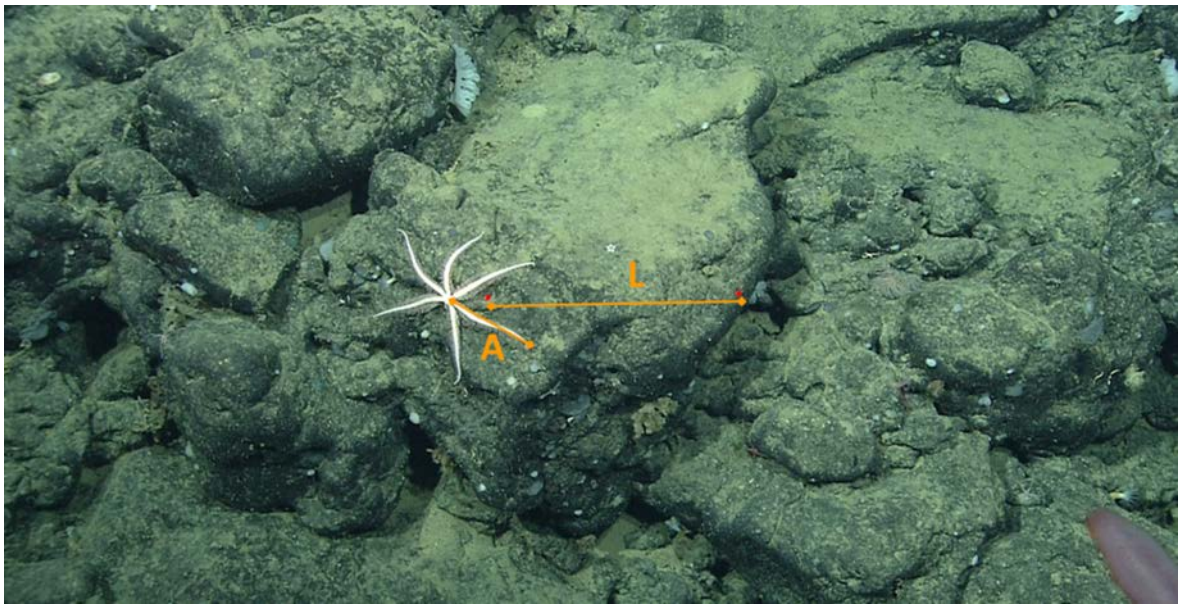

Figure 3-2: Example of animal size measurement, using the lasers shining on the seafloor as reference. A frame grab is taken from the video. On the frame grab two segments are drawn: one connecting the two lasers shining on the seafloor (L) and one along the animal body, between its frontal and distal end, or along the body part relevant for size measurement (A). The length in pixels of these two segments is then calculated using a Python program; the pixel number is converted to length in cm using a proportion between the known length (L) = 29 or 30cm depending on the ROV (Doc Rickets and Tiburon, respectively), and the unknown length (A). The frame grab used in this example comes from the Tiburon dive T1102 on a seamount of Taney's chain, and depicts the measurement of the arm/leg of a Brisingid echinoderm. Among the other visible animals, there are a pseudostichopus on the bottom-right corner, small white anemones on the vertical faces of the rocks, a sponge on the top-left corner and an *Umbellapathes* in the top-centre of the frame grab.

3.2.3 Environmental variables.

The distribution of benthic biomass over the topographic features was analysed with seven predictor variables (Table 3-2). Depth, measured in meters, was obtained from shipboard multibeam at 30 m by 30 m resolution, and resampled to a coarser resolution of 740 m by 740 m using ArcGIS 10.2 ("Resample" tool, "Data Management" toolbox). This corresponds to the resolution of the GEBCO '08 measurements for this area (BODC 2003), and was chosen as a resolution through which each transect would be fully included in a single cell of the bathymetry,

and could therefore be used as a single sampling unit. Therefore, this study investigates the effects of morphology on the scale of kilometres, while it does not investigate the effect of smaller features.

Table 3-2: List of the predictors used to estimate benthic biomass at Davidson and Taney seamounts.

	Minimum	Mean (SD)	Maximum	Notes
Depth (m)	-3342	-2404 (78)	-1420	740 m by 740 m resolution, constructed by resampling a 30 m by 30 m shipboard multibeam dataset in ArcGIS 10.2 ("Resample" tool, "Data Management" toolbox)
EF = POC export (mgC $m^{-2}y^{-1}$)	19990	29220 (1053)	35940	Export of particulate organic carbon from the mixed layer (Henson et al. 2011). This is used only in the multiple regression.
T = Temperature (°C)	1.520	1.541 (0.002)	1.566	Seabed temperature estimated at 1/4° resolution, from the World Ocean Atlas (from the NOAA National Oceanographic Data Center). This is used only in the multiple regression.
S = Slope steepness (°)	1	9 (1)	21	Slope calculated via the ArcGIS tool "Slope" in the "Spatial analyst" toolbox, on the depth layer.
BPI = Bathymetric Position Index	-318	99 (21)	419	Relative elevation with respect to the surrounding features. Calculated using the Benthic Terrain Modeller plugin for ArcGIS 10.2 on the depth layer, within a 1 cell radius (Wright et al. 2012).
ACI = Aspect-current interaction (°)	-172.70	-50 (13)	162.20	Interaction between aspect (Spatial analyst, ArcGIS 10.2) and current direction (NEMO 1/12, Madec 2008), a continuous variable defining the direction from which the current hits the slope.
dSD = Standard deviation of current direction (°)	1.809	1.812 (0.0003)	1.814	Calculated with the Yamartino method (Yamartino 1984) on a one-year current estimate obtained from NEMO 1/12.

Surface export flux (mg C $m^{-2}y^{-1}$) was obtained from a global model built on thorium-derived export measurements (Henson et al. 2011). This should account also for potential coastal/canyon induced upwelling and consequent surface primary production. On the contrary, there is no evidence to suggest that there could be input of organic carbon from Monterey Canyon to the

seamounts, through lateral transport along the seafloor, as the distance among the features is large.

Inputs from the costal/canyon-induced production. Seabed temperature estimates (°C) were obtained from the World Ocean Atlas (National Geophysical Data Center and Commerce 2009). The effect of seamount morphology on benthic biomass was the main focus of this study. Slope steepness has been calculated in R (R core team 2014) depth field using the Arc GIS tool 'Slope' in the 'Spatial analyst' toolbox, with a UTM projection.

The Bathymetric Position Index (BPI), a measure of relative elevation of an area in relation to the surrounding ones, was calculated to summarise the terrain position on the bathymetric feature using the Benthic Terrain Modeller plugin for ArcGIS 10.2 with a 1-cell radius (Wright et al. 2012). From a mathematical point of view, it is the second order derivative of the surface, with negative values in the local minima of the bathymetry, values around 0 on constant slopes, and positive values at local maxima such as the top of seamounts or ridges (Figure 3-3). Here it was calculated with a 1-cell radius, meaning that the depth of each cell is compared only to the ones immediately surrounding it.

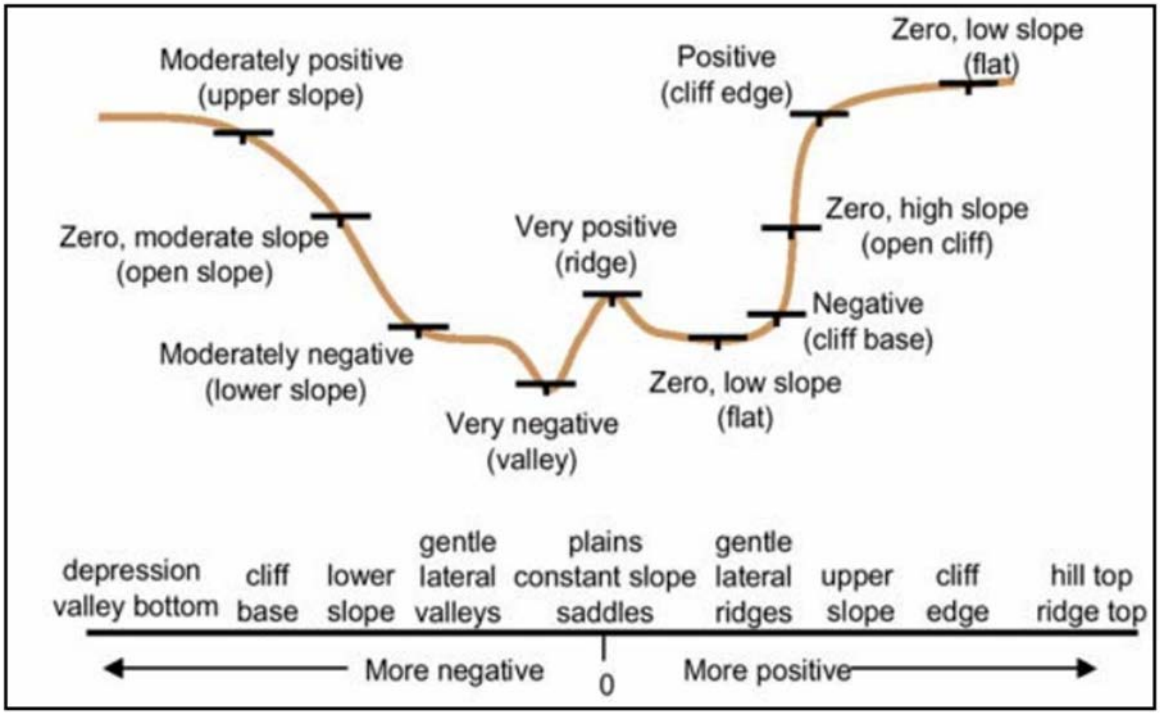

Figure 3-3: Figure 2 from Verfaillie et al, 2007. Schematic representation of how BPI varies across a range of topographic features.

Mean current direction and standard deviation were calculated with the Yamartino method (Yamartino 1984) on a one-year current estimate for the seafloor, obtained from the NEMO ocean circulation model at 1/12° (about 9 km) spatial resolution (Madec 2008). These current estimates are spatially and temporally coarse compared to what could be obtained from current meters;

nevertheless, they provide a picture of the global current patterns, and can be used as an estimate of the background current variation present in an area. In particular, to explore the interaction of current with the topography, mean current direction was combined with seafloor aspect (the direction towards which the slope faces), obtaining an aspect-current interaction value ranging between -180° and +180°; aspect-current interaction has negative values for the areas where the current comes from the left of the slope, and positive values when the current comes from the right of the slope (Figure 3-4). This metric has been calculated to detect possible asymmetric patterns of biomass distribution around the seamounts, caused by the change in direction and speed of the background current around the features. Such a process has been suggested as the cause for sediment redistribution at an abyssal hill in the northeast Atlantic (Turnewitsch et al. 2004). Applying the aspect-current interaction metric to the same northeast Atlantic hill, with the same north-flowing current, positive values of aspect current interaction correspond to the areas were the Regional Ocean Model System (ROMS, IMCS ocean modelling) used by Turnewitsch et al. (2004) predicted current backflow, and where sediment focussing was measured (Figure 3-4).

The Monterey Canyon greatly affects the ecosystem in the Monterey Bay. Through the upwelling of nutrient-rich waters, it is responsible for up to 1/3 of the primary production in the area (Kunze et al. 2002). Monterey Canyon and Davidson Seamount have similar megafauna species composition, but with different community structure (McClain et al. 2009). Evidence has shown that gravity flows in the canyon can bring large amounts of sediments from shallow depths down to more the 1200 m in a short time (<10 minutes) (Paull et al. 2003). Nevertheless, it is unlikely that such sediment transport can directly influence Davidson seamount: in fact, at a deep station in the canyon (>3000 m) the recorded mean current flow was towards NNW (Xu et al. 2002). It is more likely that the seamount is influenced by the suspended particulate matter produced thanks to the mixing of water masses above the canyon (Ryan et al. 2005), which could be transported through the south-flowing 'California Current'. Nevertheless, this input of material should be accounted for by the export flux (EF) model here (Henson et al. 2011). Among the environmental predictors used here, only depth was directly measured while all the other variables were interpolated from the depth field and from global predictions. These have different resolutions from 1° (~8800 m at the latitude of this study) for the export flux, to 740 m of the seafloor morphology metrics calculated from the shipboard 30 m by 30 m multibeam bathymetry. Local sediment deposition patterns are likely to play a more important role than vertical fluxes around topographic features, and temperature is not likely to have large fluctuations on the seafloor. Errors in the estimate of current direction and variability could be more relevant in this study, especially because current direction (1/12° resolution) is used in relation to seafloor aspect

interpolations at a finer resolution (1/120° resolution). Current direction should in this case be interpreted as the average direction of background currents.

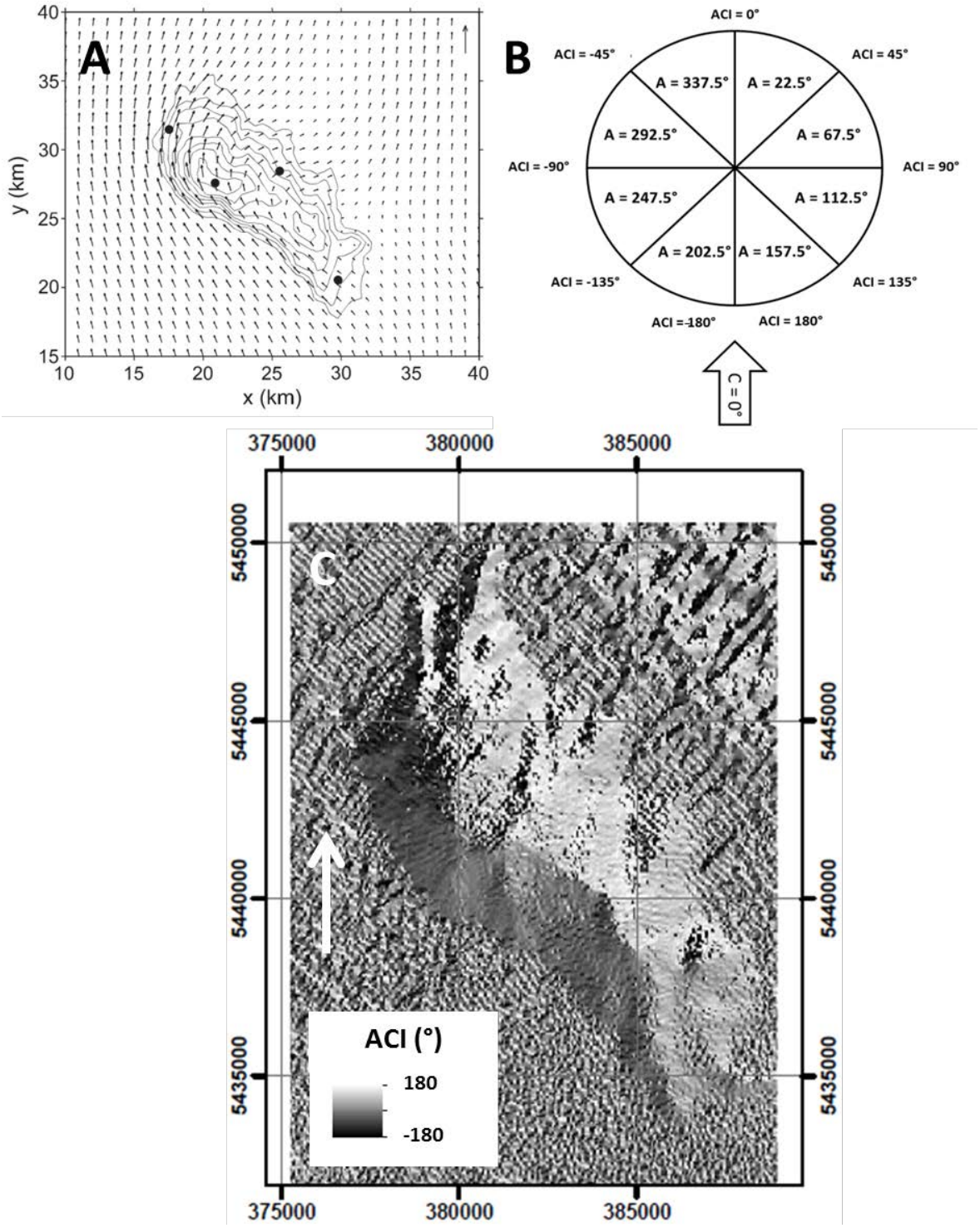

Figure 3-4: Aspect-current interaction (ACI) at a large abyssal hill, due northwest of the Porcupine Abyssal Plain (PAP) long term observatory. Panel A: figure taken from Turnewitsch et al. (2004). It represents a bathymetric map of the abyssal hill, together with the current speeds and directions (black vectors) predicted by the Regional Ocean Model System (ROMS) by applying a north-flowing current. The model predicts an asymmetric current flow pattern, with acceleration on the west flank and deceleration/reversal on the east flank. Panel B: schematic drawing of how the aspect-current interaction (ACI) predictor varies around a seamount. The circle

represents an aerial view of an idealised seamount, divided into 45° sectors of A = aspect = direction of the slope. When a north current (C = 0°) hits the seamount, it hits its parts with different angles, according to the local aspect (A). This angle is the ACI and it varies from -180°, facing the current, to -90° with the current coming from the orographic left, to 0° with the current coming from the opposite side of the feature, to 90° with the current coming from the orographic right, to 180° facing the current again. Panel C: aspect-current interaction obtained by applying the same north-flowing current used by Turnewitch et al. (2004) over the hill area (white vector). The aspect-current interaction is negative on the western flanks of the hill; here the ROMS model predicts an increase in current speed, and positive values where the ROMS model predicted a reversal of current direction and a decrease in speed. The ACI does not replicate a flow field, and does not provide information on how much background currents change with topography. It only provides a qualitative proxy for the exposure of the slope to the current, which could help recording potential asymmetric distribution of standing stocks around features.

3.2.4 Analysis.

Hypotheses were tested using correlations and statistical model fitting. All the statistical analyses were performed using R (R core team 2014). Pairwise Spearman rank correlations ('corr.test' routine from the package 'psych' (Ravelle 2015)) between untransformed biomass measurements and independent environmental variables were used as a test to highlight the cases of covariance between the model predictor variables, and as a first test of the hypotheses. Linear models between biomass and each predictor were tested using 'lm' and 'anova' routines.

Shapiro-Wilk tests were performed on the residuals of each regression to test the assumption of normality; a $\log_{10}$ transformation of the biomass measurements was used in the linear models and in all the subsequent analyses, to meet the assumption of normality of the residuals. Heteroscedasticity of the residuals was tested with Breusch-Pagan test ('bptest' routine in the 'lmtest' package (Zeileis and Hothorn 2002)). Finally, Moran's test of spatial autocorrelation was used to test for the independence of the residuals (Paradis et al. 2004).

The cumulative effect of the predictors was then investigated using multiple regressions ('lm' tested with the ANOVA routine in R, R Core Team, 2014) and Generalised Additive Models (GAMs), which allow for non-linear smoothed relationships between the predictors and biomass, with the aim of obtaining a predictive model ('gam' routine from the R package 'gam' (Hastie 2015)). The effect of depth was not included in the cumulative models, to test the hypothesis that seamount morphology can explain the distribution of benthic biomass better than depth alone. POC export from the euphotic zone (Henson et al. 2011) was instead included in the multiple regression, as the difference in surface productivity between Davidson (inshore) and Taney seamounts (offshore) could play a role in determining the overall amount of input to the study areas. The modelled patterns of biomass in relation to topography were extrapolated to the

greater study area and were then discussed in relation to the null hypothesis of biomass varying only because of depth and not in relation to terrain type position.

3.3 Results

3.3.1 Spearman rank correlations.

At Davidson seamount, all the variables are correlated among each other and with biomass, apart from BPI, which was not correlated to any other variable, and aspect-current interaction, which was negatively correlated to current direction SD (Table 3-3). At Taney seamounts, depth was negatively correlated to current direction SD and positively correlated to BPI, which was also negatively correlated to temperature (Table 3-3). The collinearity detected should not substantially affect the fit and predictive power of the comprehensive models because the 'ρ' values are below the |0.7| threshold, apart from the correlations with temperature (Dormann et al. 2013).

3.3.2 Linear models.

At Taney seamounts, biomass ranges between 1 and 2.6 $\log_{10}(g_{ww}\ m^{-2})$, while at Davidson it ranges between 0.4 and 2.3 $\log_{10}(g_{ww}\ m^{-2})$. At comparable depths (between 3500 and 2000 m) the biomass at the two study sites is not statistically different (Welch Two Sample t-test t = -1.4195, df = 32.56, p-value = 0.1653), while it is lower for the shallower part of Davidson seamount (Figure 3-5).

Among the linear models at the two locations, only the increase of biomass with increasing depth at Davidson seamount is significant (F = 27.3, d.f. = 31, R^2 = 0.3, p-value < 0.05, Shapiro-Wilk's p-value > 0.1, Breusch-Pagan's p-value > 0.5, Moran's p-value > 0.05) (Table 3-4, Figure 3-5a). For both locations the assumptions of normality, homoscedasticity and independence of the residuals are met. There is also a positive trend between slope and biomass at Davidson (Spearman rank correlation: ρ = 0.4, p-value < 0.05). All the other linear models tested are not significant.

Biomass is not correlated significantly with the variability of current direction at either of the two locations (Table 3-4, Figure 3-5e). However, biomass is negatively correlated with current direction SD when the two locations are considered together (Spearman rank correlation ρ = -0.72, p-value < 0.001).

Table 3-3: Spearman ρ values obtained from the pairwise analysis of all the variables. Highlighted in bold are the correlations with a significant p-value. On the bottom-left part of the table are the results for the Taney seamounts dataset while on the top-right are the ones for Davidson seamount. Correlations to export flux are not shown because this predictor only changes between the two areas, but not within.

Taney \ Davidson	Mass	Depth	Current direction SD	Slope	BPI	Temperature	AC Interaction
Mass		**-0.661**	**-0.653**	**0.435**	-0.181	**-0.752**	0.044
Depth	0.215		**0.695**	**-0.474**	0.326	**0.787**	0
Current direction SD	-0.38	**-0.699**		**-0.356**	0.232	**0.955**	**-0.534**
Slope	0.347	-0.141	-0.042		0.22	**-0.512**	-0.175
BPI	-0.249	**0.615**	-0.151	-0.295		0.125	-0.091
Temperature	0.015	-0.133	-0.063	-0.148	**-0.547**		-0.302
AC Interaction	-0.129	0.018	0.101	0.214	0.307	-0.089	

Table 3-4: One-way ANOVA summary

Davidson	**Spearman ρ**	**lm F (d.f.)**	**coefficient**	**lm adj. R^2**	**lm p-value**	**Residual st. error**	**Shapiro-Wilk's p-value**	**Breusch-Pagan's p-value**	**Moran's p-value**
Depth	-0.7 *	27.3 (31)	-0.0005519	0.45	< 0.05	0.3	0.1	0.8	> 0.05
Slope	0.4 *	3.373 (31)	0.02829	0.7	> 0.05	0.4	0.2	0.9	< 0.05
BPI	-0.2	1.271 (31)	-0.0006760	0.008	> 0.1	0.6	0.2	0.01	< 0.05
AC Interaction	0.04	0.1943 (31)	0.0002981	-0.03	> 0.5	0.5	0.2	0.8	< 0.05
Current Speed SD	0.05	0.5633 (31)	46.4682	-0.01	> 0.1	0.5	0.3	0.005	< 0.05
Taney	**Spearman ρ**	**lm F (d.f.))**	**coefficient**	**lm adj. R^2**	**lm p-value**	**Residual st. error**	**Shapiro-Wilk's p-value**	**Breusch-Pagan's p-value**	**Moran's p-value**
Depth	0.21	1.1 (22)	0.0002587	0.003	>0.1	0.4	0.8	0.7	>0.5
Slope	0.3	2.6 (22)	0.02742	0.07	>0.05	0.4	0.3	0.04	>0.5
BPI	-0.2	0.8 (22)	-0.0004738	-0.008	>0.1	0.4	0.5	0.8	>0.5
AC Interaction	-0.1	2.3 (22)	-0.001964	0.05	>0.05	0.4	0.4	0.2	>0.5
Current Speed SD	0.06	5.5e-05 (22)	-0.2350	-0.05	>0.5	0.4	0.6	0.4	>0.5

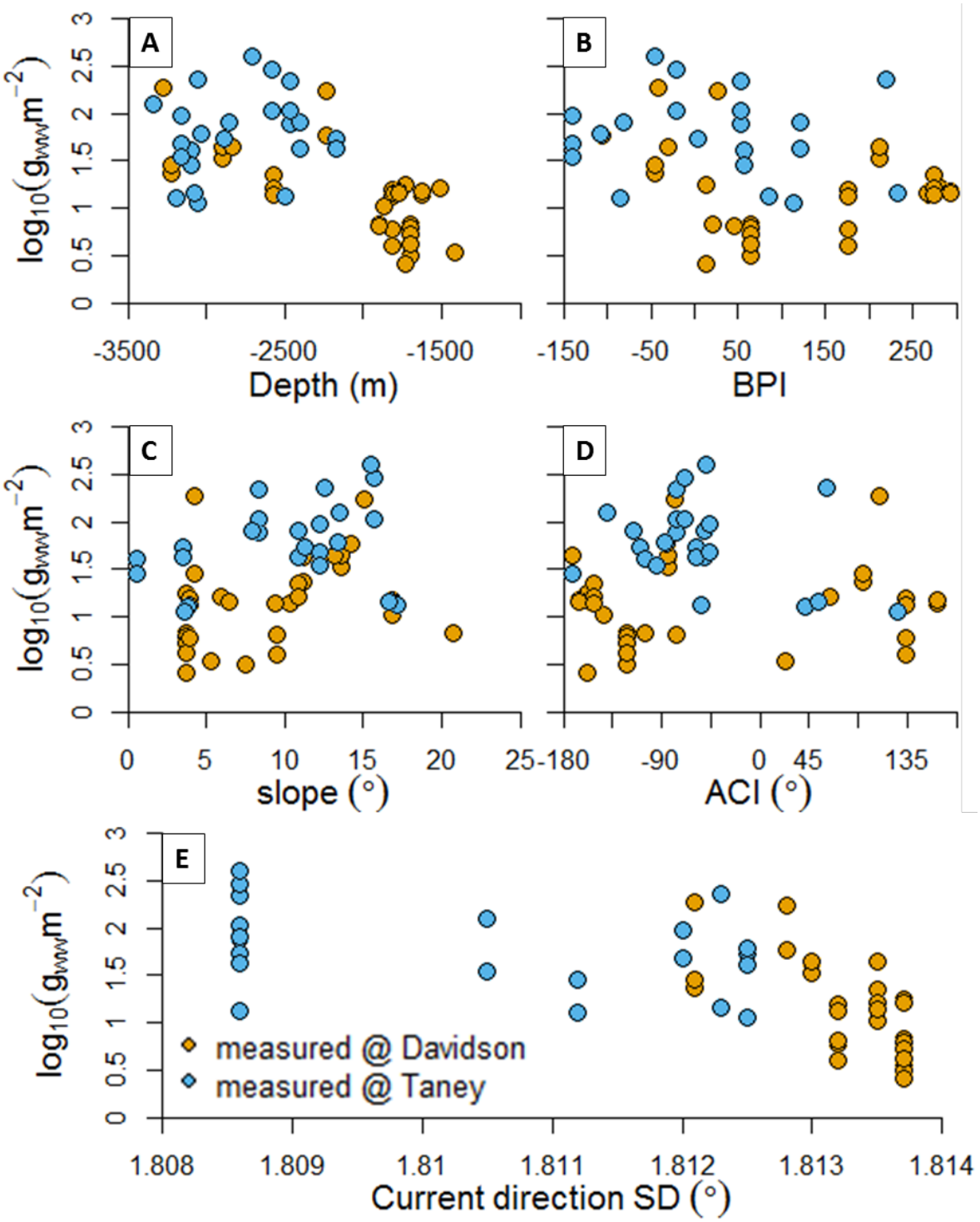

Figure 3-5: Scatterplots of biomass against five predictors: depth, Bathymetric Position Index (BPI), slope, aspect-current interaction (ACI) and standard deviation (SD) of current direction.

3.3.3 Multiple regression.

In order to jointly consider variables, a multiple linear model for the biomass distribution at the two seamounts has been tested:

$$log_{10}(mass) = EF \cdot T + dSD + S \cdot BPI \cdot ACI$$

The model includes the interacting effects of water column properties like POC export from the euphotic zone (EF) and temperature (T), as well as the interacting effects of topographic variables. Depth is not included in this model, as the aim is to see if topography metrics other than depth can explain the distribution of biomass around the seamounts. The model is significant and with relatively high R^2 values (R^2 = 0.6, Table 3-5, Figure 3-6), but none of the regression coefficients is significant. The predictors with the strongest effect are temperature (T = -0.25) and current direction SD (dSD = -0.14), possibly because they discriminate between the two locations; the lowest effect comes from the interaction between the topographic predictors (S : BPI : ACI = -0.01) (Table 3-5, Figure 3-6). The residuals are not spatially autocorrelated.

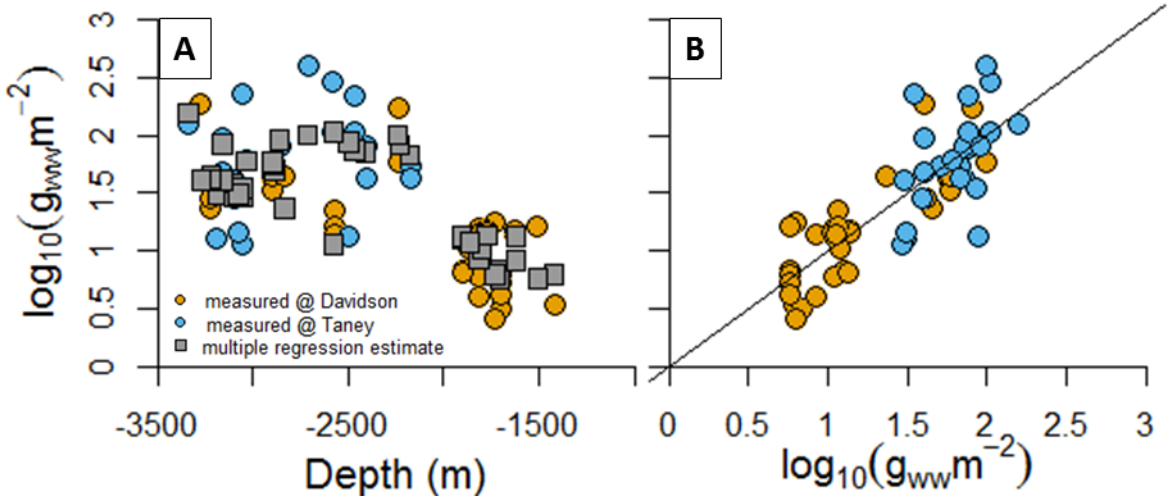

Figure 3-6: a) Biomass predictions from the multiple regressions (grey squares), in comparison to the measurements at Davidson (orange circles) and Taney seamounts (blue circles). Panel b shows the scatters of measured against predicted values from the multiple regression.

Table 3-5: Summary of the multiple regression of biomass against six environmental predictors and their interactions. Coefficients and significance are reported both for a scaled version of the model, and for a non-scaled one. In the scaled version of the models, the range of the predictors has been uniformed, and centred around 0. After scaling, the value of each coefficient represents the strength of each effect.

	Scaled	Not-scaled
Intercept	1.44235 ***	1.308e+02
Export flux	-0.04979	1.024e-03
Temperature	-0.25109	4.105
Current direction SD	-0.14393	-7.487e+01
Slope	0.04509	1.068e-02
BPI	-0.04076	6.046e-04
AC interaction	-0.09674	-3.901e-04
Export flux : temperature	-0.08643	-6.687e-04
Slope : BPI	-0.05256	-7.445e-05

	Scaled	Not-scaled
Slope : AC Interaction	-0.05651	-9.631e-05
BPI : AC Interaction	0.05268	4.817e-06
Slope : BPI : AC interaction	-0.01272	-1.599e-07
P-value	< 0.001	
Adj R^2	0.60	
F (d.f.)	8.64 (11-45)	
Residual error	0.3395	
Spatial autocorrelation	0.31	
Normality	0.3	
Homoscedasticity	0.15	

3.3.4 GAM.

In the GAM algorithm, none of the individual predictors has a significant effect on biomass, while together they explain more than 50% of the dataset's variance (Adjusted R^2 = 0.41, Deviance explained = 52.8%, GCV score = 0.21, n =57, Moran's p < 0.05, Table 3-6, Figure 3-7). The GAM results suggest some non-linear trends of biomass in relation to the predictors. To investigate these, I have applied simple linear models to subsets of the dataset. Biomass increases from 0° to 15° of slope (coeff = 0.07, p-value < 0.001, R^2 = 0.3) and decrease again towards the steeper slopes (coeff = -0.08, p-value < 0.05, R^2 = 0.8). In addition, biomass increases significantly in the range of aspect-current interaction from -180 to 0 (coeff = 0.007, p-value <0.001, R^2 = 0.25), while it does not change when the aspect-current interaction has positive values. The residuals are spatially autocorrelated (Table 3-6, Moran's p-value < 0.05).

Table 3-6: Summary table for the Generalised Additive Model (GAM). The number in parentheses under each predictor is the smoothing parameter used in the GAM.

Slope (0.2)	F BPI (0.2)	AC interaction (0.1)	n	adj. R^2	dev. exp. %	GCV score	Moran's p
0.069	0.369	0.122	57	0.412	52.8%	0.21484	0.03

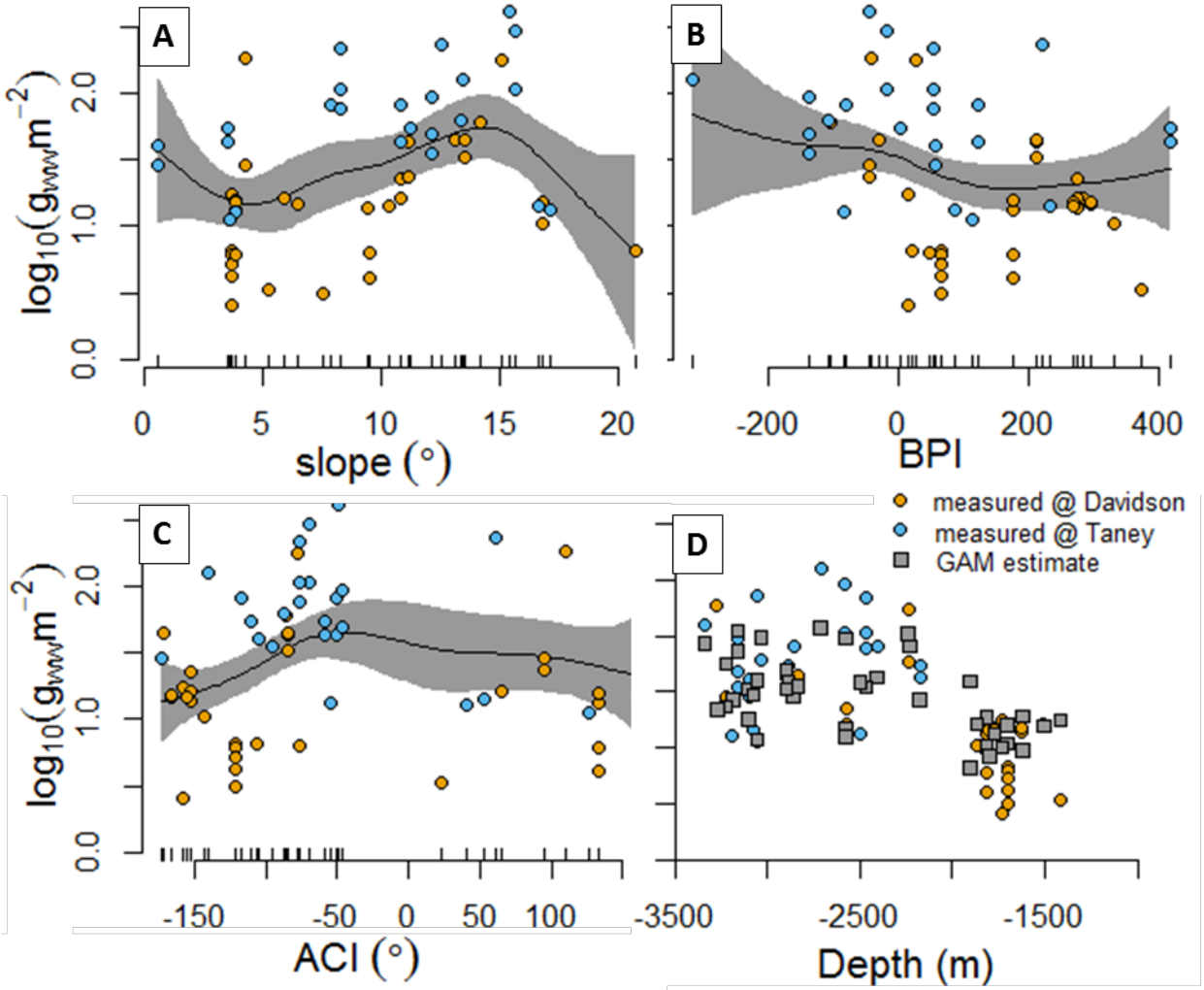

Figure 3-7: Generalised Additive Model (GAM) summary. Panels A, B and C show the smooth function predicted by the GAM (black line) together with the 95% confidence intervals (grey areas) and the measurements from the two seamount areas (orange dots for Davidson, blue dots for Taney). Panel D is a scatter of biomass against depth, with measurements from the two seamount areas (orange dots for Davidson, blue dots for Taney), and predictions from the GAM (grey squares).

3.4 Discussion

In this study, the distribution of benthic detritus-dependent megafauna around two topographic features in the northeast Pacific is analysed in relation to metrics of seafloor morphology. The distribution of standing stocks is a proxy for the availability of energy and, consequently, of the delivery of particulate organic matter. This is likely to be affected by an interaction of gravity processes, which alone would bring particulate organic carbon to deeper, flatter areas, and hydrodynamic processes, which can lead to more suspended particulate organic matter arriving at

or fluxing through exposed areas such as seamount tops and steeper slopes.

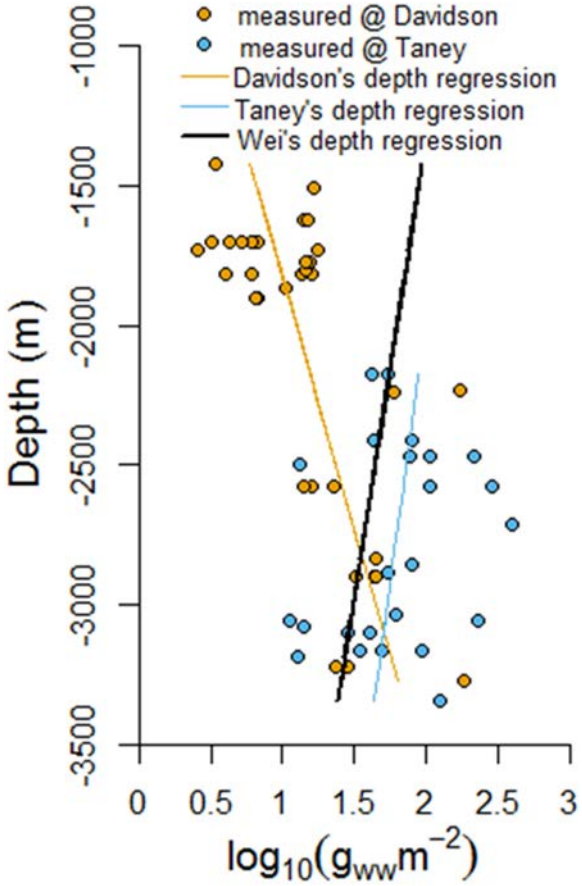

Figure 3-8: Comparison of the megafauna biomass measured at Davidson (orange circles) and Taney seamounts (blue circles) with the megafauna biomass that could be expected for the same locations using the partial regression of biomass against depth presented in Wei et al. (2010) (black line). The coloured lines are the trends of biomass with depth for Davidson (orange) and Taney (blue) seamounts.

The biomass estimate for this survey did not include 33 taxa, which accounted for 80% of all the individuals encountered. Among these were the erected corals, as the volume occupied by their large three-dimensional colonies cannot be estimated easily through simple pictures. In the future, thanks to 3D imaging, it could be possible to improve the estimation of biomass of organisms with complex morphological geometry (Dansereau et al. 2011). Currently, these taxa are not included in other biomass estimates either (i.e. Wei et al. 2010).

As shown in Figure 3-8, biomass at the Taney seamounts can be up to 1 order of magnitude higher than what would be predicted by depth regressions alone (Wei et al. 2010), while biomass at the top of Davidson is 1 order of magnitude lower than the Wei et al. (2010) estimate for the same depth. This provides an example of how seamounts can introduce substantial spatial variability in the deep sea biomass. Nevertheless, none of the simple linear models tested here, which included only one topographic variable at a time, has high predictive power (Table 3-4).

Therefore, a multiple linear model for biomass distribution was proposed to overcome the distinction between gravity and hydrodynamically dominated scenarios. In this model, metrics related to the seafloor morphology were included among the predictors, while depth was excluded.

POC export from the surface ocean and seafloor water temperature play an important role in determining benthic biomass, as they determine the overall 'energy level' for an area (Thurston et al. 1998, Portner 2002), influencing the metabolism of the individuals. A multiple regression to estimate biomass with POC flux and temperature alone is significant ($p < 0.001$, $R^2 = 0.57$), and shows an increase of biomass when export flux and temperature increase. When adding the effect of the topographic metrics the $R^2 = 0.60$; this shows that including seamount morphology in the model allows obtaining a slight increase in the accuracy of biomass prediction around topographic features. Furthermore, the multiple regression explains a higher proportion of biomass distribution than the regression with depth alone (Davidson: F = 27.31, d.f. = 31, coeff.: -0.0006, $R^2 = 0.45$, p-value < 0.05. Taney: F = 1.1, d.f. = 22, coeff.: = 0.0003, p-value > 0.1) and explains the opposite trends of biomass with depth between Davidson and Taney seamounts (Figure 3-6a).

The global-scale seafloor megafauna biomass estimates provided by Wei et al. (2010) with a Random Forest (RF) simulation on a 1 by 1 degree grid are much lower than the ones from the partial regression with depth (Figure 3-9). In addition, this highlights the positive effect that seafloor morphology can have on benthic biomass. By including seamount morphology metrics, the amount of spatial heterogeneity that can be resolved in model predictions is increased, thereby improving the fit of the model in relation to the previous 1 by 1 degree model (Wei et al. 2010). These spatial predictions are still driven mostly by large scale variables such as export flux and temperature. However, the spatial extrapolations of the multiple regression to the whole Davidson and Taney areas show the spatial variability introduced at medium scale by the seamounts, with biomass maxima in the abyssal plain around the Taney seamounts and at the south west of Davidson.

The model obtained with GAM routines does not perform as well as the multiple regression, explaining only 52.8% of the deviance of benthic biomass. On the one hand this could be because additive models, by definition, do not include the effect of interactions between predictors; on the other hand, with only 57 data points, it was not possible to include all the predictors in the GAM, and it was also necessary to manually set the smoothness of the GAM model response to avoid overfitting. Nevertheless, the GAM results are useful to show how the response of biomass

to BPI, slope and aspect-current interaction might follow non-linear trends. Larger datasets would be needed to investigate these non-linear relationships.

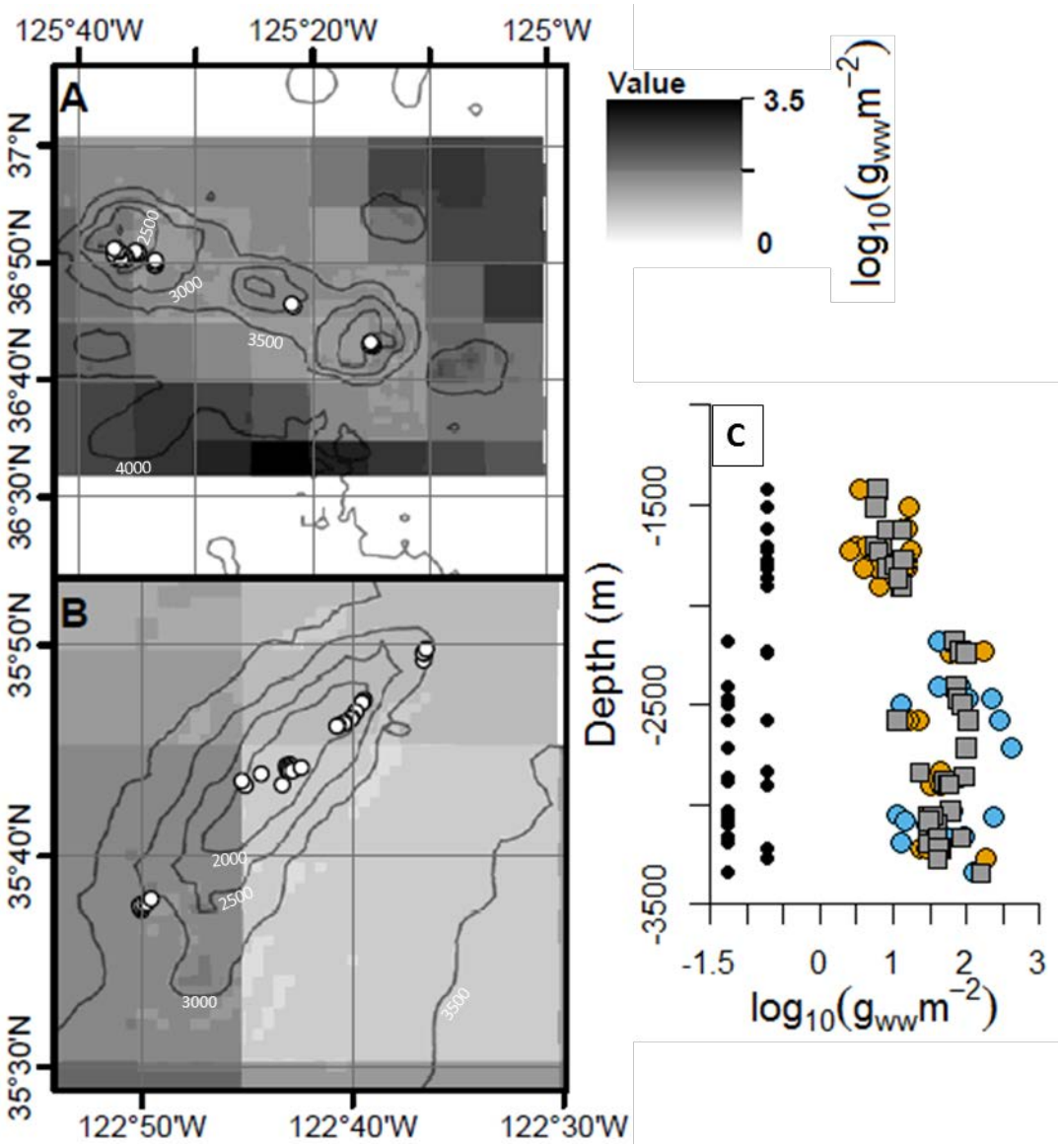

Figure 3-9: Biomass predictions for the Davidson and Taney areas, according to the multiple linear regression. On the left are the spatial predictions for Taney (a) and Davidson (b) seamounts. The estimated biomass values are shown in a scatterplot (c) on the right (grey squares) in relation to the measured values (orange for Davidson, blue for Taney) and to the prediction from the global Random Forest model presented by Wei et al. 2010 (black dots).

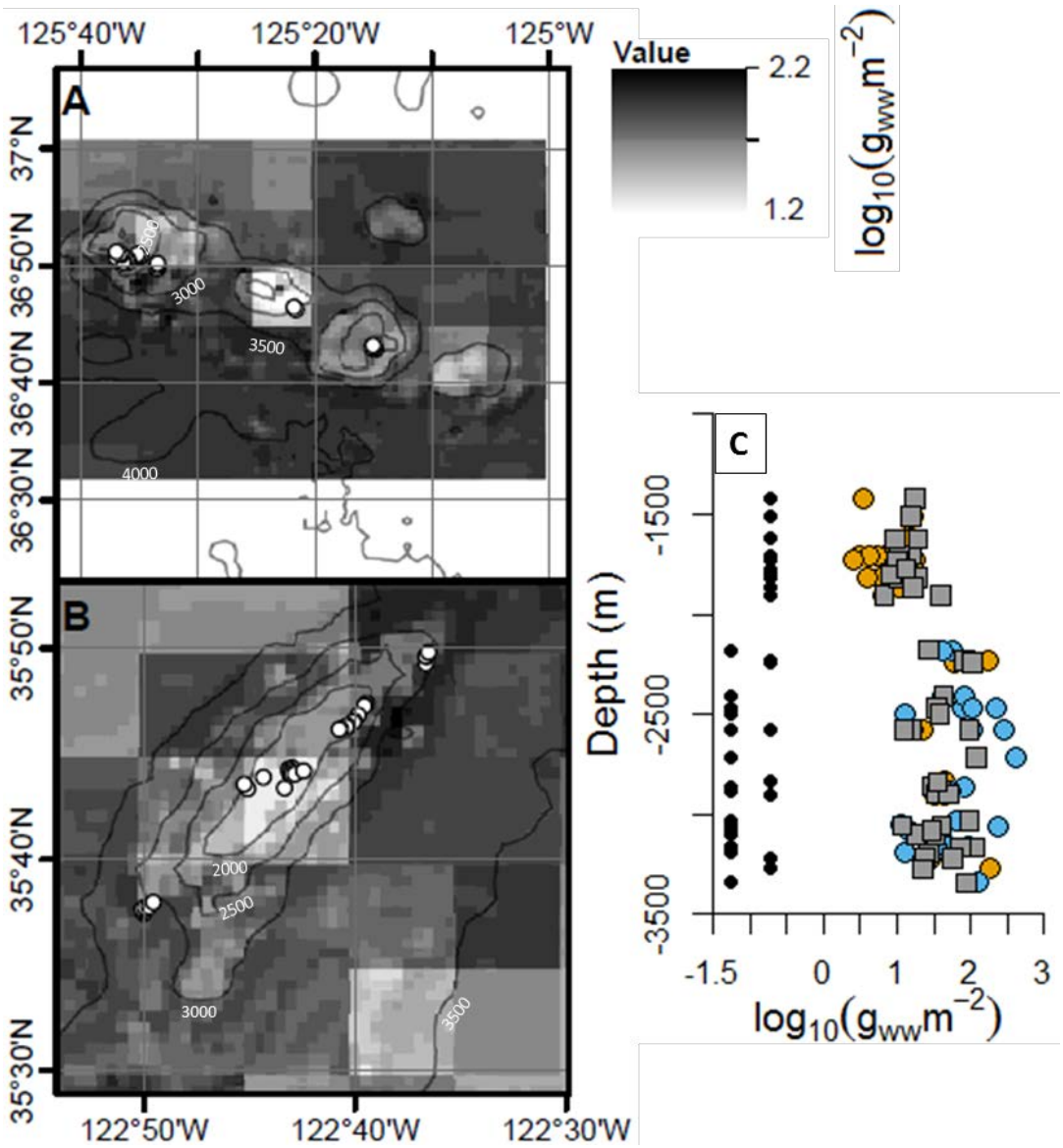

Figure 3-10: Biomass predictions for the Davidson and Taney areas, according to the Generalised Additive Model (GAM). On the left are the spatial predictions for Taney (A) and Davidson (B) seamounts. The estimated biomass values are shown in a scatterplot (C) on the right (grey squares) in relation to the measured values (orange for Davidson, blue for Taney) and the prediction from the global Random Forest model presented by Wei et al. 2010 (black dots).

The multiple regression predicts extremely high values for the abyssal plains around the seamounts (> 10^3 g_{ww} m^{-2}), which have not been surveyed, while the GAM predicts intermediate biomass values for the abyssal plain area (< 10^2 g_{ww} m^{-2}) with the extreme values localised only on the seamounts. This result, obtained including only three predictors (BPI, slope and aspect-current interaction), suggests that a better understanding of biomass distribution around topographic features and better spatial extrapolations could be obtained firstly by expanding the sampled range of the predictors. This better coverage of the local topographic variability could be

used in non-linear approaches such as Generalised Linear Models (GLM). Furthermore, including biomass surveys from abyssal plains could be used as reference values for seamount comparison (*sensu* Morris et al. 2016) (and Chapter 4).

3.5 Conclusions

The patterns of redistribution of POC around Taney and Davidson seamounts were investigated, using the distribution of megafauna biomass as proxy, recorded with ROV surveys. Results have shown that large scale variables related to oceanography features (export flux and temperature) are the strongest drivers of biomass distribution, and they differ between the two locations, but do not vary within the locations. Furthermore, the use of GAMs has highlighted that biomass increases with slope at low steepness, and it then decreases at high steepness. This suggests that slope could act as a control affecting the interaction between hydrodynamic and gravitational transport of organic carbon.

Nevertheless, constraints related to the sampling design have resulted in weak correlations. Future studies to investigate the influence of terrain types on seafloor biomass would benefit from a sampling strategy designed especially to investigate the effect of topography on benthic biomass distribution. In such study, the samples will be distributed more consistently over a wider range of the predictors. Furthermore, a future sampling effort would benefit from improved size-biomass conversion, and improved estimates of seafloor substrate/grain size distribution. This has been shown to affect community composition of all size classes from megafauna (Durden et al. 2015) to unicellular organisms (Stefanoudis et al. 2016). Furthermore, constraining the range of some topographic variables, or addressing them more explicitly, could allow better understanding of the interaction between predictors such as depth, BPI and slope. In chapter 4 I address the effect of topography on biomass distribution, in an area with a limited depth range.

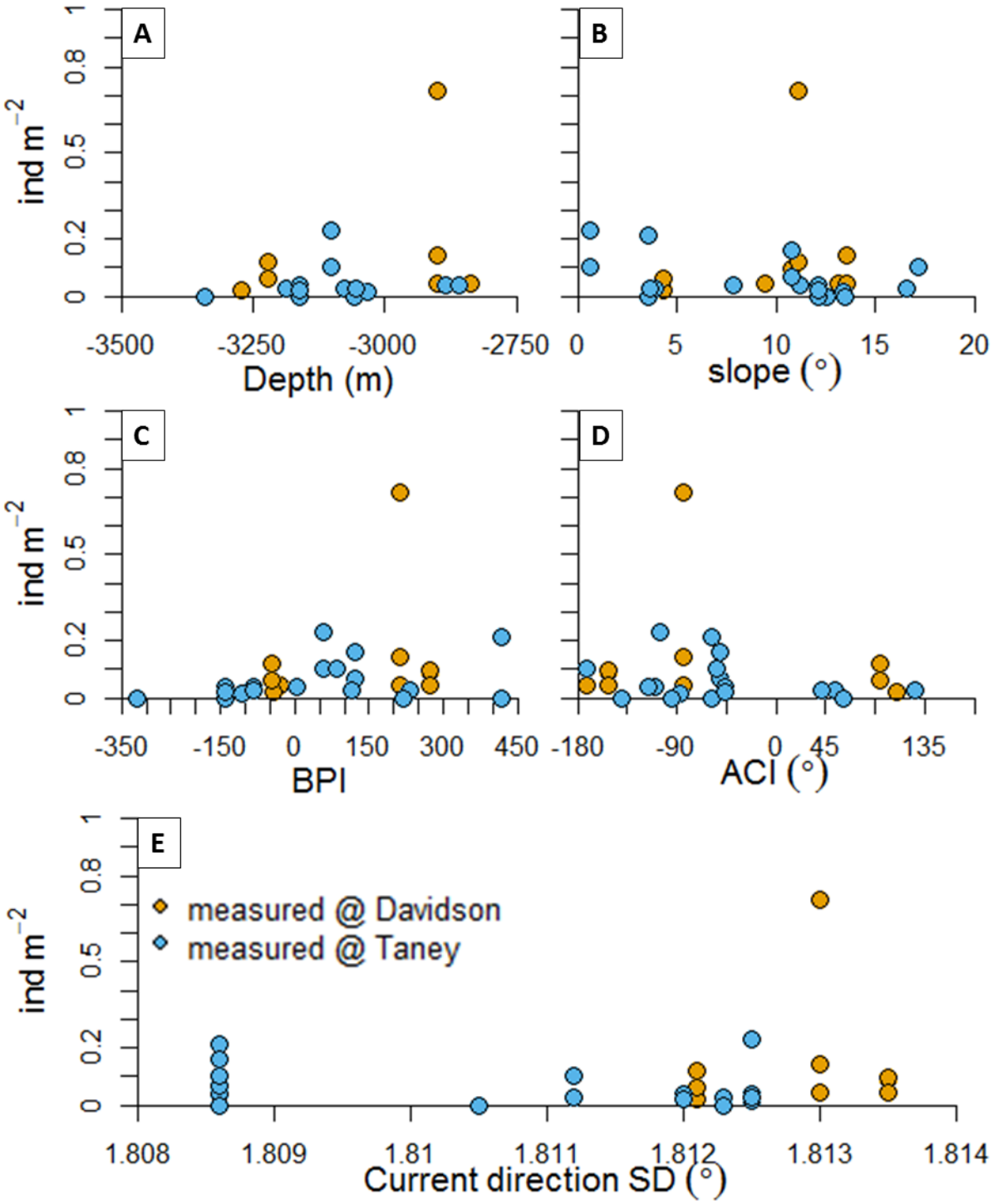

Figure 3-11: Density of erected corals for the transects with comparable depth between the two locations (orange circles for Davidson and blue circles for Taney seamounts) against five environmental predictors (Depth, Slope, Bathymetric position index (BPI), Aspect-current interaction (ACI) and standard deviation (SD) of current direction.

Chapter 4: Slope, relative elevation and currents help explain the distribution of biomass on a small abyssal hill[3].

4.1 Introduction

The Porcupine Abyssal Plain (PAP), in the northeast Atlantic between the European continental shelf and the Mid Atlantic Ridge (MAR), has been the focus of oceanographic studies since the 1980s (Billett and Rice 2001), and is now the site of a long term observatory (4850 m water depth, 49° 00' N 16° 30' W). Many ecological studies in this area have focussed on bentho-pelagic coupling, or the interaction between the ocean surface, the water column, and the benthos, recording the effect of seasonality in phytoplankton blooms on the benthic communities (Lampitt 1985, Fabiano et al. 2001, Lampitt et al. 2001, Hudson et al. 2003). The seafloor around the long-term observatory is relatively flat; nevertheless, some hills occur near it. Abyssal hills are underwater terrain features that rise less than 1000 m above the surrounding seafloor, and are likely the most common underwater topographic feature, covering an estimated 41% of the seafloor (Harris et al. 2014). Recent studies have focussed on the physical and biological characteristics of these reliefs, finding that they are linked to changes of sediment grain size where sediments are relatively coarse on hills when compared to the surrounding plain (Durden et al. 2015); this, in turn, seems to affect the morphology of agglutinating foraminifera's tests, in which sediment particles are incorporated (Stefanoudis and Gooday 2015, Stefanoudis et al. 2016). Also, hills seem to affect the deposition pattern of particulate organic matter, by influencing the direction and speed of local currents (Turnewitsch et al. 2004, Morris et al. 2016) Finally, the megafauna biomass increases by a factor of 2-3 from the abyssal plain to the top of the hill (Durden et al. 2015, Morris et al. 2016).

The physical and biological effects of elevated underwater topographic relief have mainly been studied in relation to seamounts. Currents can be deflected by the seamounts, creating revolving water mass caps over the top of seamounts (Bashmachnikov et al. 2013, Mohn et al. 2013), which are potentially associated with increased primary productivity at the sea surface (White and Mohn 2004). This increased productivity could be among the causes of the exceptionally high

[3] I did not take part in the surveys during which the data-collection for this chapter took place. The videos and pictures' annotation, individual's measurements and conversion to mass was done by Jen Durden, Kirsty Morris and Henry Ruhl. I devised and pursued the method for the statistical analysis and interpretation presented in this chapter.

biomass of filter feeders that can be found over the top of some seamounts (Genin et al. 1986, Thresher et al. 2011); nevertheless, higher than expected biomass can be found also at the bottom of the seamounts, possibly as a consequence of lateral gravitational transport of organic matter along the seamount flanks (Zeppilli et al. 2013).

In Chapter 3, possible interactions among gravitational and hydrodynamic processes were highlighted by investigating biomass distribution around large seamounts in the northeast Pacific. Nevertheless, one of the challenges related to the size of such features consists in disentangling the effect on biomass of vertical flux of organic matter and water mass characteristics (such as temperature and oxygen concentration) from the effect of sea floor morphology (slope, relative elevation and relative current direction). Abyssal hills provide a natural experimental setting in which water mass characteristics vary only slightly, as the depth range is minimal. In fact, while seafloor that extends over a large bathyal range, such as continental slopes or large seamounts, is likely to receive different amounts of vertical flux in different parts, depending on the local depth, the vertical POC flux is expected to vary only marginally across the area of an abyssal hill; similarly, also temperature, salinity and dissolved oxygen should have small variations over such a small depth range. The vertical flux of POM that reaches a 300 m hill at~4800 m depth is likely to be only about 3% more than the flux that reaches the abyssal plain (300 m deeper) (Martin et al. 1987, Lutz et al. 2007). Since the relationship between changing POC flux and biomass is approximately linear, and with a slope coefficient of ~0.6 biomass/flux (Yool et al. 2013), differences greater than ~3% between benthic biomass communities from across a single hill are likely to be influenced by seafloor morphology.

Notwithstanding the relatively small size, hills appear to be affected by hydrodynamic activity, which results in coarser sediment size and higher biomass on the hills than on the surrounding plains (Durden et al. 2015). Strong currents near the seafloor can cause resuspension of POM, as suggested by a study by Lampitt and Burnham (1983) who found that resuspension took place when currents speed exceeded 7 cm s^{-1} at 1 mab. Since hills can induce a deflection and change in speed of background currents (Turnewitsch et al. 2004, Turnewitsch et al. 2013, Turnewitsch et al. 2015), this can also result in a spatial variability of megafauna distribution

A small abyssal hill in the vicinity of the long term PAP observatory has been targeted by various extensive surveys which included a high resolution mapping with an AUV (Autosub6000) equipped with photographic cameras (Morris et al. 2016). The small topographic feature influences the distribution of phytodetritus % cover and megafauna biomass, which follow a decreasing trend from the top of the hill to the surrounding plain (Morris et al. 2016). Looking at the effect of small, common deep sea topographic features on benthic ecology improves our understanding of

habitats' heterogeneity in the deep sea. This knowledge could be useful for impact studies in areas where direct (i.e. deep sea mining) or indirect (i.e. climate change) human impact could affect the ecology of the deep sea.

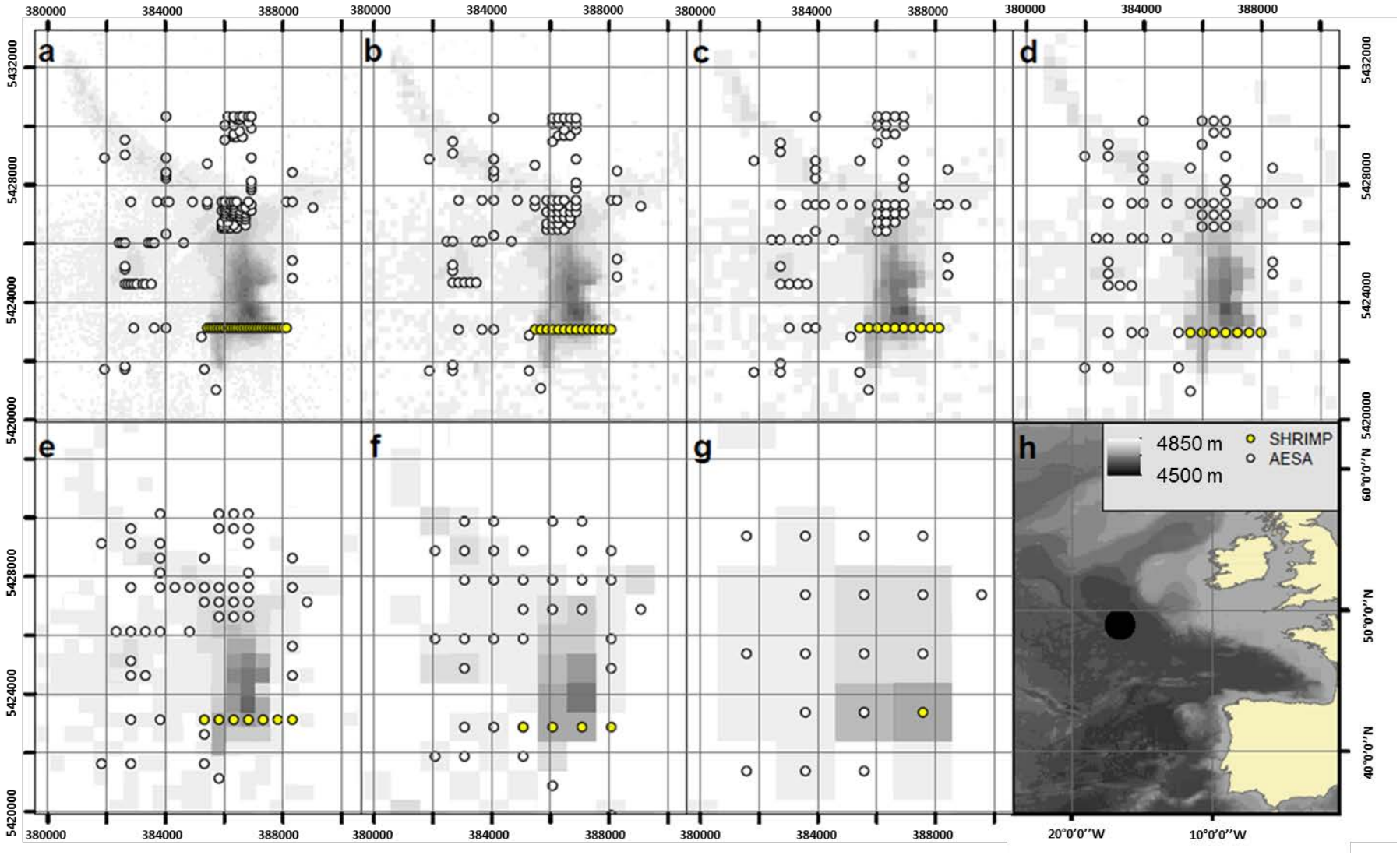
a
b
c
d
e
f
g
h
380000
384000
388000
5432000
5428000
5424000
5420000
4850 m
4500 m
SHRIMP
AESA
60°0'0''N
50°0'0''N
40°0'0''N
20°0'0''W
10°0'0''W

Figure 4-1: Study area and sampling locations at the small abyssal hill in the Porcupine Abyssal Plain (PAP).A) 100 m resolution, B) 200 m resolution, C) 300 m resolution, D) 400 m resolution, E) 500 m resolution, F) 1000 m resolution and G) 2000 m resolution. White circles are the Autosub6000 tiles, while in yellow are the Seabed High Resolution Imaging Platform (SHRIMP) images. Inset H shows the location of the study area in relation to the British Isles and the northeast Atlantic. Panels from a to g have a UTM 28N projection and the coordinates are eastings and northings. Panel H has WGS84 projection.

Here, the patterns of benthic biomass distribution around a ~300 m hill located in the PAP, in the northeast Atlantic (Figure 4-1), are investigated to test two alternative hypotheses: at the lower end of the steepness range, the benthic biomass would increase with steepness and be higher towards the top of the hill where there is likely to be increased flux of particles thanks to higher exposure to currents. On the contrary, at the higher end of the steepness range, gravitational processes are expected to remove organic carbon from the top of the hill in favour of the flatter areas surrounding it, and the megafauna community will be concentrated in these deeper parts of the topography Figure 3-1.

4.2 Materials and methods

4.2.1 Image surveys.

The abyssal hill investigated in this study is found northwest of the long term observatory of PAP Central (4850 m, 49° N, 16° 30' W). The hill rises ~300 m above the surrounding abyssal plain, and has an oblong shape with an elongated ridge protruding towards the NW (Figure 4-1). An extensive sampling effort focussed on this area in summer 2012, when fine detailed bathymetry was obtained via shipboard multibeam, and an extensive AUV imaging survey was conducted (Morris et al. 2014, Morris et al. 2016). The AUV missions were planned to follow two regular grids: one with 1000 m line spacing over the hill area and the surrounding abyssal plain and ridge to the northwest; the other with 100 m line spacing on the abyssal plain to the north of the hill, and on its northern flank. Colour pictures were taken by the AUV at 0.9 seconds intervals with a vertically-mounted Point Gray Research Inc. Grasshopper 2 camera, at a target altitude over the seafloor of 3.2 m (Morris et al. 2014, Morris et al. 2016). This produced 64,690 images, grouped in tiles of 10 pictures each, covering an area of ~14.2 m^2 each.

An additional survey transect conducted from west to east with the towed camera system 'Seabed High Resolution Imaging Platform' (SHRIMP) over the top of the hill is included in this study (Jones et al. 2009). The Imenco Camera on the SHRIMP platform produced .jpg images that were readily annotated without colour correction. In order to reduce the effects of window distortion the pixels were cropped to an image of 1200 by 1400 pixels centred on x = 241 (±167) pixels and y = 924 (±65) pixels, depending on the altitude of each individual image.

The AUV and SHRIMP surveys were used to identify the taxon and body size of each observed individual, and this information was then used to estimate individual wet weight body mass (Durden et al. 2016). The pictures and tiles from these surveys were merged at 7 spatial scales in order to understand the influence of analytical scale in the investigation of biomass around small

abyssal hills (100 m, 200 m, 300 m, 400 m, 500 m, 1000 m and 2000 m sized grid cells). At the finest scale, the effect of the topographic feature is expected to be masked by noise caused by smaller scale variability; conversely, when the resolution is too coarse, the topographic feature would be blurred into the surrounding abyssal plain and no pattern would be picked up by the analysis.

4.2.2 Environmental predictors.

The environmental predictors used in this study are summarised in Table 4-1. At ocean basin scale, surface primary productivity is the main source of organic carbon available for export to the seafloor (Lutz et al. 2002, Lutz et al. 2007). Depth is then used as a proxy for remineralisation of vertically sinking Particulate Organic Carbon (POC). Nevertheless, the study area is relatively small and therefore essentially receives its vertical flux from the same portion of ocean surface. Furthermore, depth varies by ~300 m across the study area, therefore reductions in POC flux induced by such a depth range are estimated to be only ~3% (Martin et al. 1987, Lutz et al. 2007), and are likely to have just a small effect on biomass. In fact, flux and biomass have a predicted coefficient of correlation of ~0.6 biomass/flux (Yool et al. 2013). Thus, at this local scale, other measures of seafloor morphology and environmental conditions are more suited to investigate the patterns of food input to include the effect of laterally transported POC as well. The depth measurements used were obtained from multibeam surveys, with 50 m spatial resolution, performed during expedition JC062 aboard the RRS James Cook in 2011, and were resampled at 7 levels of spatial resolution (100 m, 200 m, 300 m, 400 m, 500 m, 1000 m and 2000 m).

Table 4-1: List of the environmental predictors used to explain the distribution of benthic biomass around a small abyssal hill.

Variable	Notes
Depth	Multibeam recorded on JC062, originally at 50 m resolution, and then resampled into 7 depth rasters with decreasing spatial resolution (100 m, 200 m, 300 m, 400 m, 500 m, 1000 m and 2000 m).
Slope steepness	Obtained on ArcGIS from the depth rasters, with the “slope” tool (Spatial analyst), at the 7 levels of spatial resolution.
Bathymetric position index (BPI)	Relative elevation with respect to the surrounding seafloor, calculated at a fine (1 cell radius) and at a broad resolution (4000 m), on each of the depth rasters. This was done using the Benthic Terrain Modeller plugin for ArcGIS 10.2 (Wright, Pendleton et al. 2012).
Aspect-current interaction	Interaction between aspect and current direction to obtain a continuous variable defining the direction from which the current

hits the slope. Currents obtained from NEMO 1/12 (Madec 2008). See Figure 3-4 for a schematic description of the aspect-current interaction.

Slope is the maximum change, measured in degrees (°), between the depth value of one pixel and the ones immediately surrounding it. It is expected to enhance the lateral transport of organic carbon towards deeper depths in a gravity-dominated scenario. Here it was calculated in ArcGIS 10.2 with the Slope tool (Spatial Analyst) from the depth multibeam raster, and it ranged between 0° and 22°.

BPI is the second order derivative of the surface, and it is used to define the elevation of a pixel in relation to the surrounding ones, in a defined radius (Wilson et al. 2007): positive values are for local maxima of the bathymetry, negative values for local minima, and values around 0 for flat areas or constant slopes (Figure 3-3). In this study for each of the 7 spatial resolutions, a fine scale BPI was calculated at the smallest possible radius (1 cell radius), and a broad scale BPI with an outer radius of 4000 m (40 cells radius for the 100 m resolution, 2 cells radius for the 2000 m resolution). The Benthic Terrain Modeller (Wright et al. 2012) in ArcGIS 10.2 was used for these calculations. The resulting fine BPI ranged between -45 and 90, while the broad BPI ranged between -25 and 105.

Finally, the aspect-current interaction was calculated. This is an estimate of the average angle of incidence between the background current direction and the aspect of the seafloor. The aspect was estimated using the 'Aspect' tool (Spatial Analyst) on ArcGIS 10.2. The mean current direction over the course of one year was estimated with the Yamartino method (Yamartino 1984) from the global circulation model NEMO at 1/12° of spatial resolution (Madec 2008). The resulting aspect-current interaction has negative values when the current comes from the orographic left-hand side, 0 when it pushes away from the slope, and positive values when it comes from the right-hand side. This variable can help identify cases of asymmetric distribution of standing stocks around the hill; such spatial patterns could happen when the presence of the topographic feature causes deflections and changes of intensity of the local current, which could affect the sedimentation (Turnewitsch et al. 2004, Turnewitsch et al. 2013) (Figure 3-4 for a schematic description).

4.2.3 Analysis.

All the statistical analyses were performed using R (R core team 2014). Firstly, the dataset was tested for spatial autocorrelation using Moran's test in the R library "ape" (Paradis et al. 2004). This test was also executed on the residuals of each subsequent model.

Spearman rank correlations ("corr.test" routine from the package "psych" (Ravelle 2015)) were used to highlight the cases of covariance between the predictors, and as a first test of the hypotheses. Log_{10} transformed biomass was tested with one-way ANOVAs against each single predictor independently ("lm" and "anova" routines, from the package "stats"). The trends highlighted by the regressions were used to evaluate the two alternative hypotheses: positive trends of biomass with depth, slope and BPI would highlight the presence of more biomass in elevated areas that could potentially be more exposed to currents and, therefore, increased particulate organic matter flux. Negative trends of biomass along the same gradients would suggest that biomass is higher in less exposed, deeper areas, which could receive fluxes of organic carbon from the surrounding steeper flanks of the hill.

With the aim of obtaining predictive models, the interacting effect of slope, fine BPI, broad BPI and aspect-current interaction on log_{10} transformed biomass was investigated using multiple regressions. Furthermore generalised additive models (GAMs) were used to investigate non-linear effects of the same topographic predictors. Depth was not included in the predictive models, as the aim was to explain the biomass distribution around the hill only as a function of hill shape; the reduction of POC with depth is expected to result in minor differences of vertical flux between the top and the bottom of a small feature such as the abyssal hill investigated here. For the simple and multiple linear regressions the results of Shapiro-Wilk tests for normality of the residuals, of the Breusch–Pagan test for homoscedasticity of the residuals and of the Moran test for spatial autocorrelation of the residuals (Zeileis and Hothorn 2002) have been reported.

The patterns of biomass in relation to topography have then been extrapolated to the whole area and have been discussed in relation to the null hypothesis of biomass varying only because of depth. Each test, apart from the GAMs, has been performed at each of the 7 spatial resolutions (100 m, 200 m, 300 m, 400 m, 500 m, 1000 m and 2000 m). The GAMs could not be performed at 1000 m and 2000 m resolution for insufficient degrees of freedom at that scale.

4.3 Results

4.3.1 Spearman rank correlations.

At all resolutions apart from 1000 m, depth is positively correlated to slope and to the two scales of BPI (where shallower areas are steeper), while at 1000 m it is not correlated to slope. At all resolutions from 100 to 500 m slope is correlated to depth and to broad scale BPI, while at 1000 m it is not correlated to any other predictors, and at 2000 m it is correlated to depth only. Fine BPI is correlated to depth and broad BPI at all scales, while it is also correlated to aspect-current

interaction at 300 m resolution. Broad BPI is correlated to depth, slope and fine BPI at all resolutions apart from 1000 and 2000 m, and to aspect-current interaction at 200 and 300 m. Finally, aspect-current interaction is correlated to depth and broad BPI at 200 m and to depth, broad and fine BPI at 300 m (Table 4-2).

At 100 m, 200 m and 300 m resolutions only the significant correlation between depth and broad BPI exceeded the threshold of ρ = |0.7| suggested by Dormann et al. (2013) as an indicator for when the effect of collinearity severely distorts coefficient estimations and, therefore, predictions. Since broad BPI and depth are not used together in the multiple regressions, this correlation should not reduce the predictive power of the multiple linear models.

At larger grid scale resolutions, the |0.7| threshold is exceeded also in the correlation between depth and fine BPI, and in the correlation between fine and broad BPI. Depth and fine BPI are not used together in the multiple regression, so their collinearity does not pose a problem. Conversely, the correlation between fine and broad BPI at coarse spatial resolution is inevitable, as the two measurements tend to converge (and in fact, the correlation 'ρ' equals 1 at 2000 m resolution). Therefore, the interaction between fine and broad BPI should be disregarded at resolutions coarser than 400 m, when their coefficient of collinearity exceeds |0.7|.

Table 4-2: Strength and significance of pairwise correlations between dependent and independent variables, calculated with the Spearman rank correlation. The values reported are the Spearman rank coefficient (ρ), and highlighted in bold are statistically significant ones ($p < 0.05$). In different sections of the table are reported the correlations from different levels of spatial resolution. Asterisks highlight cases of strong collinearity.

	Biomass	**Depth**	**Slope**	**Fine BPI**	**Broad BPI**
100 m					
Biomass					
Depth	**0.197**				
Slope	0.135	**0.606**			
Fine BPI	-0.095	**0.281**	0.075		
Broad BPI	0.151	**0.918 ***	**0.538**	**0.351**	
Aspect-current interaction	0.109	0.152	0.018	0.044	0.186
200 m					
Biomass					
Depth	**0.241**				
Slope	**0.228**	**0.6**			
Fine BPI	-0.029	**0.442**	0.104		
Broad BPI	**0.208**	**0.906 ***	**0.527**	**0.524**	
Aspect-current interaction	0.072	**0.293**	0.164	0.135	**0.329**
300 m					
Biomass					
Depth	**0.281**				
Slope	0.218	**0.588**			

	Biomass	Depth	Slope	Fine BPI	Broad BPI
Fine BPI	0.046	**0.452**	-0.061		
Broad BPI	**0.228**	**0.81 ***	**0.431**	**0.655**	
Aspect-current interaction	0.031	0.153	-0.109	**0.255**	**0.293**
400 m					
Biomass					
Depth	0.179				
Slope	**0.253**	**0.548**			
Fine BPI	-0.024	**0.593**	0.077		
Broad BPI	0.165	**0.84 ***	**0.463**	**0.711 ***	
Aspect-current interaction	0.163	0.127	0.108	-0.027	0.1
500 m					
Biomass					
Depth	**0.307**				
Slope	0.204	**0.496**			
Fine BPI	0.177	**0.674**	0.026		
Broad BPI	0.207	**0.802 ***	**0.269**	**0.886 ***	
Aspect-current interaction	0.049	0.255	0.008	0.142	0.212
1000 m					
Biomass					
Depth	0.23				
Slope	0.305	0.146			
Fine BPI	0.163	**0.775 ***	-0.208		
Broad BPI	0.225	**0.835 ***	-0.1	**0.958 ***	
Aspect-current interaction	0.02	0.273	0.053	0.102	0.134
2000 m					
Biomass					
Depth	0.401				
Slope	0.122	**0.589**			
Fine BPI	0.341	**0.893 ***	0.265		
Broad BPI	0.341	**0.893 ***	0.265	**1 ***	
Aspect-current interaction	-0.103	0.057	0.154	0.079	0.079

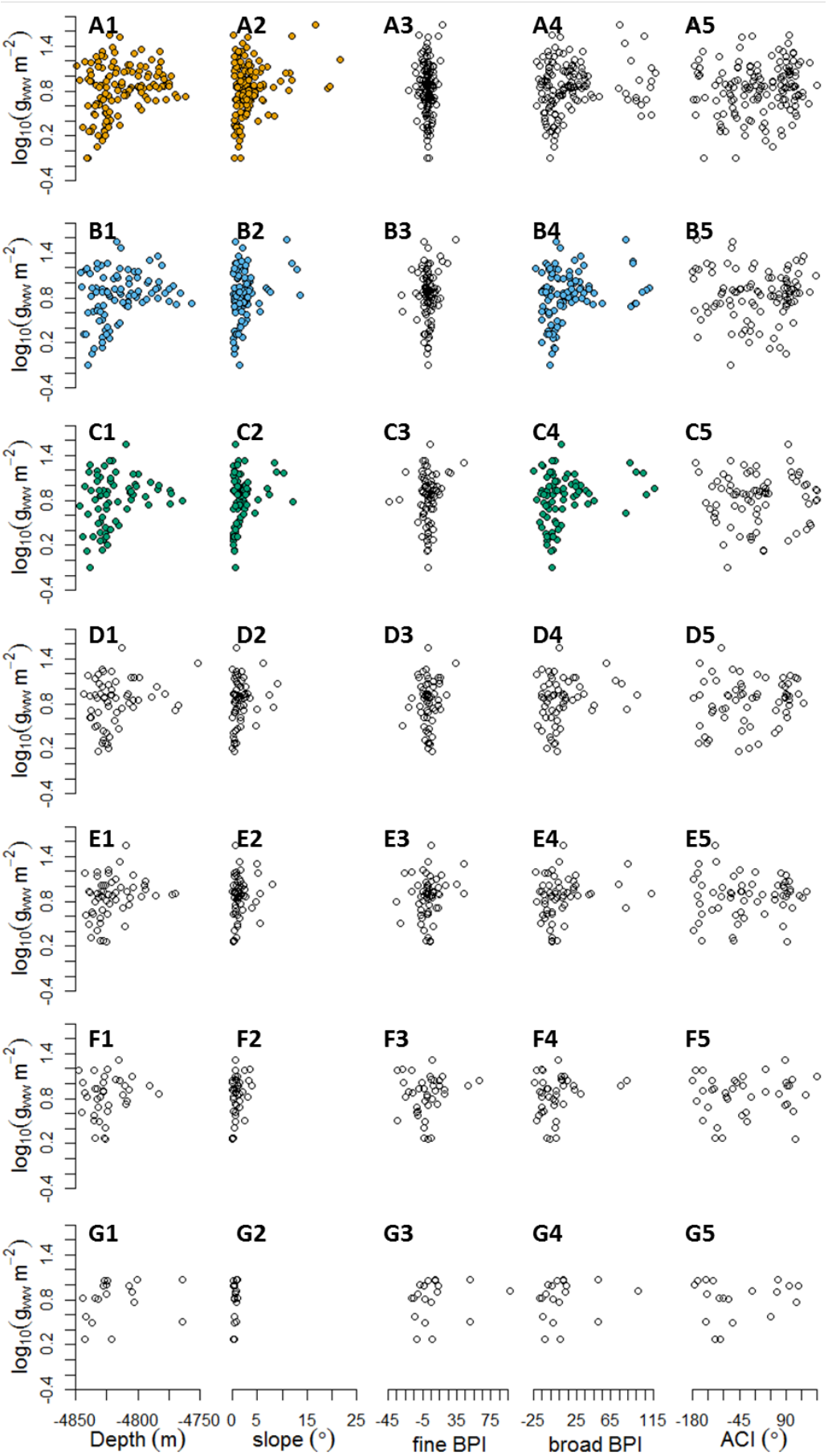

Figure 4-2: Scatter plots of megafauna biomass ($log_{10}(g_{ww}\ m^{-2})$) against 5 environmental variables (along the columns) and at 7 spatial resolutions. A = 100 m, B = 200 m, C = 300 m, D = 400 m, E = 500 m, F = 1000 m, G = 2000 m. 1 = depth (m), 2 = slope (°), 3 = fine BPI, 4

= broad BPI, 5 = aspect-current interaction (°). Significant linear regressions are highlighted with coloured circles.

4.3.2 One Way ANOVAs.

Biomass increases significantly as depth gets shallower at 100, 200 and 300 m resolution (Table 4-3, Figure 4-2); similarly, it increases significantly with slope steepness at the same levels of resolution (Table 4-4, Figure 4-2). The effect of fine BPI is never significant (Table 4-5, Figure 4-2), while biomass increases significantly with broad BPI at 200 and 300 m resolution (Table 4-6, Figure 4-2). Finally, the aspect-current interaction does not have a significant effect on biomass (Table 4-7, Figure 4-2).

Table 4-3: Summary of the one way ANOVA (linear model) between depth and biomass, including also the Shapiro-Wilk test for normality, the Breusch-Pagan test for homoscedasticity and the Moran test of spatial autocorrelation performed on the residuals. Tests performed at different spatial resolutions, from 100 m to 2000 m are reported in different rows.

Depth vs. Biomass	Coefficient	p-value	Adj. R^2	Normality	Homoscedasticity	Autocorrelation
100 m (d.f. = 143)	0.0017318	**< 0.05**	0.03	> 0.5	> 0.05	> 0.5
200 m (d.f. = 98)	2.534e-03	**< 0.01**	0.06	> 0.5	**< 0.05**	> 0.5
300 m (d.f. =74)	0.002773	**< 0.05**	0.07	> 0.5	**< 0.05**	> 0.1
400 m (d.f. = 60)	0.002421	> 0.05	0.03	> 0.1	> 0.1	> 0.5
500 m (d.f. = 57)	0.002181	> 0.05	0.04	> 0.5	> 0.1	> 0.1
1000 m (d.f. = 37)	0.002480	> 0.1	0.03	> 0.1	> 0.1	
2000 m (d.f. = 17)	0.001920	> 0.1	-0.0002	< 0.05	0.5	

Table 4-4: Summary of the one way ANOVA (linear model) between slope and biomass, including also the Shapiro-Wilk test for normality, the Breusch-Pagan test for homoscedasticity and the Moran test of spatial autocorrelation performed on the residuals. Tests

performed at different spatial resolutions, from 100 m to 2000 m are reported in different rows.

Slope vs. Biomass	Coefficient	p-value	Adj R^2	Normality	Homoscedasticity	Autocorrelation
100 m (d.f. = 143)	0.020404	**< 0.01**	0.04	> 0.5	> 0.05	< 0.05
200 m (d.f. = 98)	0.03342	**< 0.01**	0.06	> 0.1	> 0.05	> 0.1
300 m (d.f. =74)	0.03456	**< 0.05**	0.05	> 0.5	**< 0.05**	> 0.06
400 m (d.f. = 60)	0.02901	> 0.1	0.02	> 0.1	> 0.05	> 0.5
500 m (d.f. = 57)	0.02700	> 0.1	0.009	> 0.1	> 0.1	> 0.1
1000 m (d.f. = 37)	0.08067	> 0.05	0.07	> 0.1	> 0.1	
2000 m (d.f. = 17)	0.1540	> 0.1	-0.03	> 0.05	> 0.1	

Table 4-5: Summary of the one way ANOVA (linear model) between fine BPI and biomass, including also the Shapiro-Wilk test for normality, the Breusch-Pagan test for homoscedasticity and the Moran test of spatial autocorrelation performed on the residuals. Tests performed at different spatial resolutions, from 100 m to 2000 m are reported in different rows.

Fine BPI vs. Biomass	Coefficient	p-value	Adj. R^2	Normality	Homoscedasticity	Autocorrelation
100 m (d.f. = 143)	0.0002555	> 0.5	-0.007	> 0.1	> 0.1	< 0.005
200 m (d.f. = 98)	0.005569	> 0.1	0.01	> 0.05	> 0.5	0.02
300 m (d.f. =74)	0.003901	> 0.1	0.004	> 0.05	> 0.5	< 0.01
400 m (d.f. = 60)	0.004263	> 0.1	0.001	> 0.1	> 0.5	> 0.5
500 m (d.f. = 57)	0.003639	> 0.1	0.02	> 0.1	> 0.5	> 0.1
1000 m	0.001551	> 0.1	-0.01	> 0.1	> 0.1	

Fine BPI vs. Biomass	Coefficient	p-value	Adj. R^2	Normality	Homoscedasticity	Autocorrelation
(d.f. = 37)						
2000 m (d.f. = 17)	0.001570	> 0.4	-0.03	< 0.05	> 0.5	

Table 4-6: Summary of the one way ANOVA (linear model) between broad BPI and biomass, including also the Shapiro-Wilk test for normality, the Breusch-Pagan test for homoscedasticity and the Moran test of spatial autocorrelation performed on the residuals. Tests performed at different spatial resolutions, from 100 m to 2000 m are reported in different rows.

Broad BPI vs. Biomass	Coefficient	p-value	Adj. R^2	Normality	Homoscedasticity	Autocorrelation
100 m (d.f. = 143)	0.0015610	> 0.05	0.02	> 0.5	> 0.1	> 0.02
200 m (d.f. = 98)	0.002492	**< 0.05**	0.04	> 0.5	> 0.05	> 0.1
300 m (d.f. =74)	0.002635	**< 0.05**	0.05	> 0.1	**< 0.05**	> 0.05
400 m (d.f. = 60)	0.002534	> 0.1	0.03	> 0.1	> 0.1	> 0.5
500 m (d.f. = 57)	0.002018	> 0.1	0.02	> 0.1	> 0.1	> 0.1
1000 m (d.f. = 37)	0.002393	> 0.1	0.02	> 0.1	> 0.1	
2000 m (d.f. = 17)	0.001570	> 0.1	-0.03	**< 0.05**	> 0.5	

Table 4-7: Summary of the one way ANOVA (linear model) between aspect-current interaction (ACI) and biomass, including also the Moran's I test of spatial autocorrelation performed on the residuals. Tests performed at different spatial resolutions, from 100 m to 2000 m are reported in different rows.

ACI vs. Biomass	Coefficient	p-value	Adj. R^2	Normality	Homoscedasticity	Autocorrelation
100 m (d.f. = 143)	0.0003600	> 0.1	0.003	> 0.5	**< 0.05**	< 0.01

ACI vs. Biomass	Coefficient	p-value	Adj. R^2	Normality	Homoscedasticity	Autocorrelation
200 m (d.f. = 98)	7.159e-06	> 0.5	-0.01	> 0.05	> 0.1	< 0.05
300 m (d.f. =74)	0.0001128	> 0.5	-0.01	> 0.05	> 0.5	< 0.01
400 m (d.f. = 60)	0.0005039	> 0.1	0.008	> 0.5	**< 0.05**	> 0.5
500 m (d.f. = 57)	0.0001373	> 0.5	-0.01	> 0.1	**< 0.05**	> 0.1
1000 m (d.f. = 37)	0.0002124	> 0.5	-0.02	> 0.1	> 0.5	
2000 m (d.f. = 17)	0.0003513	> 0.5	-0.04	**< 0.05**	> 0.1	

4.3.3 Multiple regressions.

Among the multiple regressions at the different spatial resolutions, only the finest one (100 m) is statistically significant (F = 1.861, d.f. = 15-129, p = 0.03, R^2 = 0.08, Table 4-8). In this regression none of the coefficients are significant, while the assumptions of normality, homoscedasticity and spatial autocorrelation are met (Shapiro-Wilk's p-value = 0.9, Breusch-Pagan's p-value = 0.08, Moran's p-value = 0.8, Table 4-8).

None of the other multiple regressions is overall significant, while some coefficients are: at 1000 and 2000 m these are the interaction between broad BPI and aspect-current interaction, the one between fine BPI, broad BPI and aspect-current interaction, and the four-way interaction between slope, fine BPI broad BPI and aspect-current interaction. These regressions have low degrees of freedom, warranting caution in the interpretation of the trends (Table 4-8). Furthermore, interactions between fine and broad BPI should be disregarded, as the two variables are collinear, as highlighted by the Spearman rank correlation with $\rho > |0.7|$ (Dormann et al. 2013). (Continues at page 86)

Table 4-8: Summary table for the multi-way ANOVA performed on the model at 7 different spatial resolutions.

	100 m	**200 m**	**300 m**	**400 m**	**500 m**	**1000 m**	**2000 m**
Intercept	7.199e-01 ***	7.556e-01 ***	6.881e-01 ***	8.301e-01 ***	7.659e-01 ***	7.238e-01 ***	1.138 **
Fine slope	3.012e-02	2.699e-02	8.634e-02	4.830e-03	9.144e-02	4.868e-02	-1.728
Fine BPI	-2.013e-02 *	-1.125e-02	-6.818e-03	-2.458e-02	-7.070e-03	-7.330e-03	-9.543e-02
Broad BPI	2.805e-03	4.746e-03	2.461e-03	2.806e-03	1.182e-03	1.483e-02	
Aspect-current interaction	5.311e-04	-9.680e-04	1.617e-03	4.746e-04	8.269e-04	2.883e-03	3.019e-04
Fine slope : fine BPI	2.741e-03	1.342e-03	2.455e-03	3.074e-03	5.910e-03	-3.603e-03	2.200e-01 *
Fine slope : broad BPI	-4.932e-04	-6.287e-04	-9.803e-04	1.095e-03	-2.634e-03	7.321e-04	
Fine BPI : broad BPI	7.145e-05	-3.714e-04	3.075e-04	4.258e-04	5.079e-04	6.735e-04	6.308e-03
Fine slope : Aspect-current interaction	-1.083e-04	4.779e-04	-7.920e-04	-1.478e-04	-4.047e-04	-2.098e-03	-2.602e-03
Fine BPI : Aspect-current interaction	-3.078e-05	9.085e-05	-2.155e-04	2.255e-04	-1.951e-04	-4.447e-04	-1.312e-03 *

	100 m	200 m	300 m	400 m	500 m	1000 m	2000 m
Broad BPI : Aspect-current interaction	3.335e-05	-1.612e-05	2.901e-05	-1.795e-04	-5.981e-07	6.169e-04 *	
Fine slope : fine BPI : broad BPI	7.073e-06	4.088e-05	-3.235e-05	-8.607e-05	-8.541e-05	-2.338e-04	-9.516e-03
Fine slope : fine BPI : Aspect-current interaction	-2.150e-06	2.108e-05	3.000e-06	-8.170e-05	3.219e-05	3.216e-04	3.237e-03 *
Fine slope : broad BPI : Aspect-current interaction	-3.381e-06	-7.553e-07	1.530e-06	5.527e-05	-1.023e-06	-4.948e-04	
Fine BPI : broad BPI : Aspect-current interaction	-6.886e-07	5.069e-06	-8.121e-07	6.173e-06	3.878e-06	-1.317e-05 *	6.109e-05
Fine slope :	1.976e-07	-9.624e-07	4.560e-07	-1.162e-06	-5.300e-07	6.981e-06 *	-1.081e-04 *

	100 m	**200 m**	**300 m**	**400 m**	**500 m**	**1000 m**	**2000 m**
fine BPI : broad BPI : aspect current interaction							
P value	0.03303	0.2304	0.4612	0.3324	0.6546	0.4887	0.4113
Adj. R^2	0.08	0.04	0.001	0.04	-0.05	-0.0009	0.1165
F (D.F.)	1.861 (129)	1.284 (84)	1.006 (60)	1.164 (46)	0.8162 (43)	0.9977 (23)	1.216 (7)
Residual error	0.319	0.3188	0.3305	0.2989	0.2754	0.2634	0.2437
Normality	0.9	0.6	0.9	0.2	0.4	0.96	0.7
Homoscedasticity	0.08	0.2	0.2	0.5	0.5	0.7	0.4
Autocorrelation	0.8	0.7	0.5	0.9	0.8		

4.3.4 GAMs.

Slope, fine BPI, broad BPI and aspect-current interaction were included in a generalised additive model (GAM) for each of the 7 spatial resolutions (Table 4-9, Figure 4-3 and Figure 4-4). The degrees of freedom were not sufficient at 1000 and 2000 m resolutions to fit the GAM; the other GAMs have similar GCV scores (~0.1), and therefore similar quality. The model for the 400 m resolution has the highest adjusted R^2 (0.17) and highest deviance explained (35.3%), while the lowest are at 300 m resolution (R^2 = 0.07, deviance explained = 20%).

Table 4-9: GAM summary showing the five tested spatial resolutions along the rows. The first four columns show the F value (and the smoothing parameter between brackets); none of the predictors is significant. 'n' is the number of data points in each model. Adjusted R^2, deviance explained % and GCV (generalised cross-validation) score are measures of the goodness of fit: better models have high R^2 and dev. exp., and low GCV score. Moran's p-value is the statistical significance of spatial autocorrelation.

	F (smoothing parameter)				**n**	**adj. R^2**	**dev. exp. %**	**GCV score**	**Moran's p**
	Slope	**Fine BPI**	**Broad BPI**	**ACI**					
100 m	0.788 (100)	2.390 (20)	0.451 (100)	1.061 (50)	145	0.13	20	0.11	0.4
200 m	0.407 (5)	1.052 (10)	0.297 (50)	0.916 (20)	100	0.14	25.5	0.1	0.7
300 m	1.078 (10)	0.261 (50)	0.016 (100)	0.340 (50)	76	0.07	20	0.12	0.5
400 m	0.398 (10)	1.943 (5)	0.432 (20)	0.815 (10)	62	0.17	35.3	0.11	0.6
500 m	0.376 (20)	0.856 (5)	0.499 (5)	0.064 (100)	59	-0.02	19.6	0.09	0.8

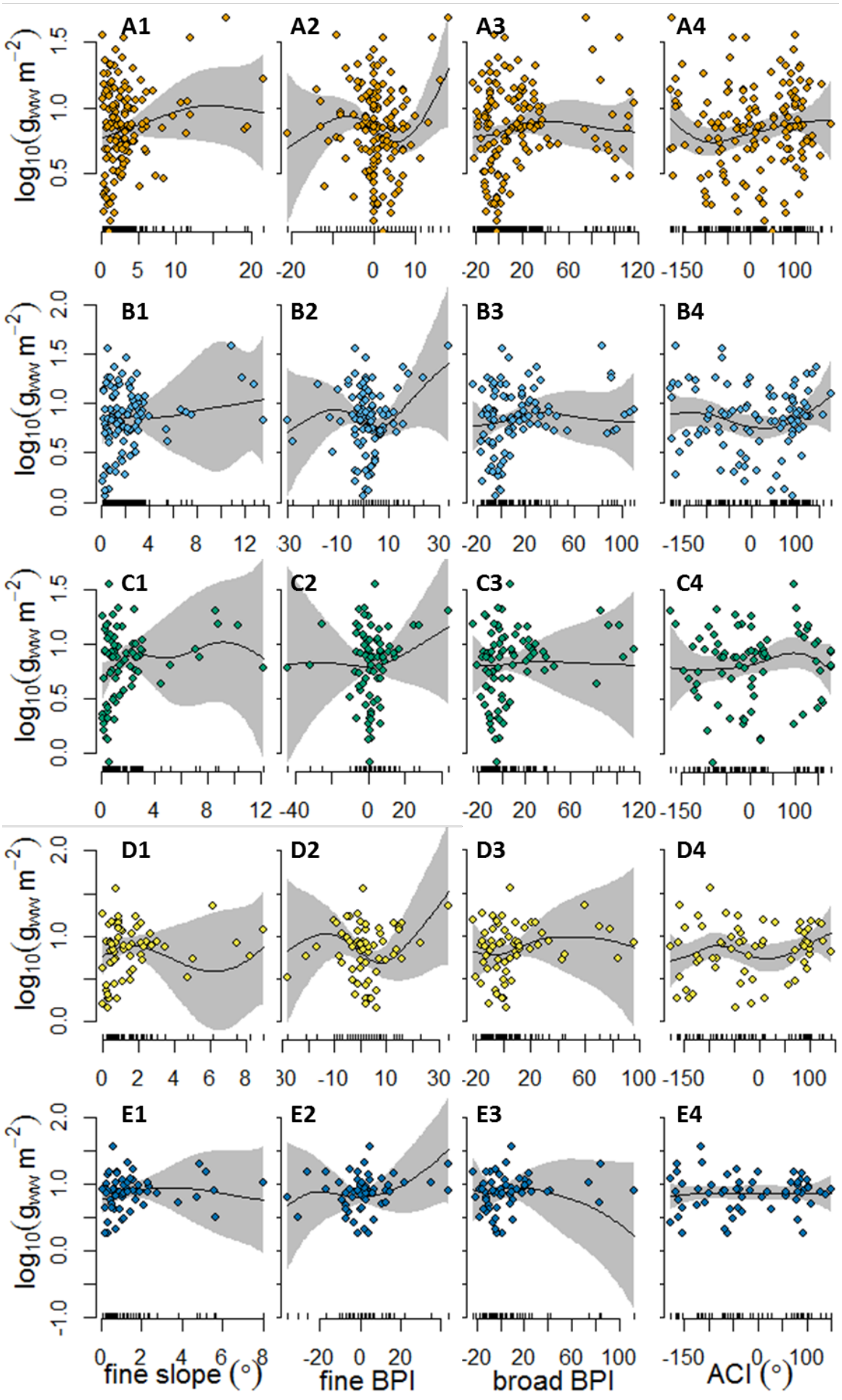
A1
A2
A3
A4
B1
B2
B3
B4
C1
C2
C3
C4
D1
D2
D3
D4
E1
E2
E3
E4
log10(gww m−2)
fine slope (°)
fine BPI
broad BPI
ACI (°)

Figure 4-3: Generalised Additive Model output for the abyssal hill dataset, obtained at 5 levels of spatial resolution, including 4 environmental predictors. The dots represent the images, grouped according to the resolution of the analysis (A = 100 m, B = 200 m, C = 300 m, D = 400 m, E = 500 m). On different columns are the four environmental variables (1 = slope (°), 2 = fine BPI, 3 = broad BPI, 4 = aspect-current interaction (°)). The black lines represent the predicted value, while the grey shaded areas are the 95% confidence intervals.

4.4 Discussion

The analysis of biomass distribution measured during photographic surveys around an abyssal hill in the northeast Atlantic has shown that seafloor morphology associated with small topographic features (~ 300 m of elevation over the surrounding abyssal plain) explains a small but significant portion of the observed variation in biomass. The statistical models employed in this study have highlighted the positive linear effects on biomass of slope and broad BPI at high resolution (100, 200 and 300 m), and the non-linear effects of fine BPI and aspect-current interaction. These trends suggest that, in the study area, elevated areas and steeper slopes might receive higher fluxes of organic carbon thanks to the exposure to currents (hydrodynamics dominated scenario). Similar distributions of megafauna had been previously recorded over larger seamounts (e.g. Genin et al. (1986) and McClain and Lundsten 2014), where increased density of suspension feeders were found at the top of the seamounts.

Given the limited steepness of the hill's slopes (maximum 22°), biomass is higher where the slopes are steeper. This is in contrast to what would be expected in a gravity-dominated scenario, when the steepness of the seafloor would result in removal of organic carbon towards deeper waters (Zeppilli et al. 2013). In addition, biomass is highest in areas with high broad BPI value, or areas, which are elevated over the surrounding terrain in a 4 km radius. This suggests that focussing of sinking POC takes place at the top of the hill, as suggested by the distribution of benthic communities over larger features (Genin et al. 1986, Thresher et al. 2011).

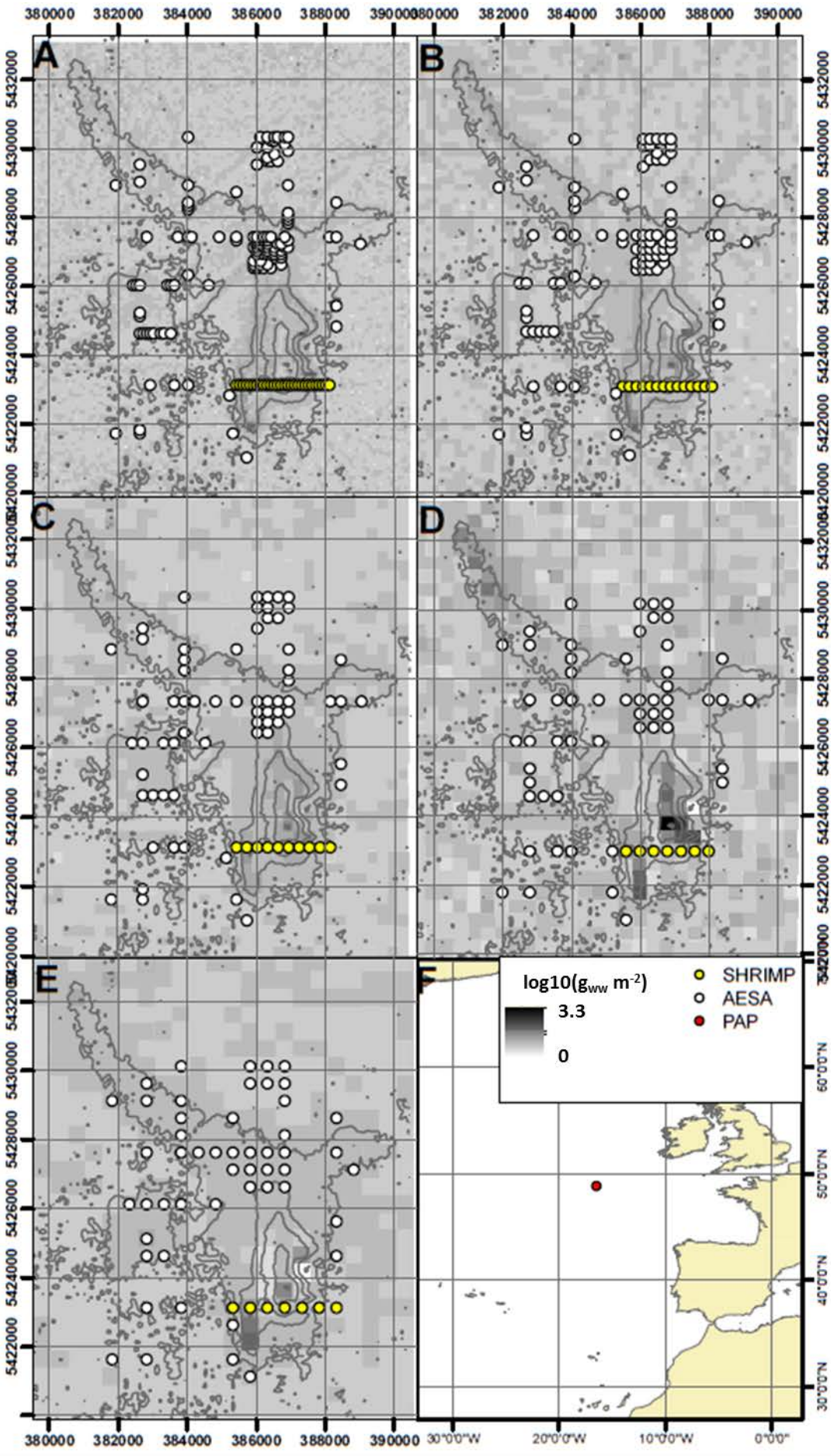
A
B
C
D
E
F
380000
382000
384000
386000
388000
390000
5432000
5430000
5428000
5426000
5424000
5422000
5420000
log10(g$_{ww}$ m^{-2})
3.3
0
SHRIMP
AESA
PAP
30°0'0"W
20°0'0"W
10°0'0"W
0°0'0"
60°0'0"N
50°0'0"N
40°0'0"N
30°0'0"N

Figure 4-4: Spatial interpolation of biomass predictions ($log_{10}(g_{ww}\ m^{-2})$) for the abyssal hill area from the GAM models at 5 resolutions: A = 100 m, B = 200 m, c = 300 m, D = 400 m, E = 500 m. The isobaths are spaced at 100 m intervals, from 4800 to 4500. The predicted biomass is represented in grey scale, going from white for 1 $g_{ww}\ m^{-2}$, to black for 2 $kg_{ww}\ m^{-2}$. The maps show how the small hill can introduce up to a three order of magnitudes increase of biomass in relation to the surrounding abyssal plain, which has low biomass level and inconsistent spatial distribution. Depth was not included in the GAMs. Coordinates are given in eastings and northings (UTM 28N projection), except for panel F which is in WGS84 projection.

Seven spatial resolutions have been tested, from 100 m to 2000 m, such that at the coarsest resolution the hill was reduced to a few pixels (Figure 4-1), and the range of values for the environmental predictors much reduced as a consequence of spatial averaging. As expected, at coarser spatial resolutions the linear trends between biomass and the metrics of morphology were not significant. This was caused by the reduction in the value range of the environmental predictors (i.e. the maximum slope at 100 m is 22° while at 2000 m it is 1°), by the averaging of biomass measurements from large and varied areas, and by the decrease in sample size (n) for the statistical tests. Nevertheless, the linear regressions of biomass with broad BPI at 200 m and 300 m resolution (measured over a 4000 m radius), and the relatively high R^2 obtained by the GAM at 400 m resolution (0.17, Table 4-9), suggest that the effect of seafloor morphology on biomass distribution could be detected also from metrics with broad resolution. At the two coarser resolutions (1000 m and 2000 m), it was not possible to test the GAMs, because of low degrees of freedom. The other GAMs, notwithstanding the reduction in the resolution of the prediction, result in similar patterns of biomass distribution when extrapolated to the whole hill area (Figure 4-4). Apart from the model at 400 m, which predicts an extremely high biomass for the summit of the hill ($10^3\ g_{ww}\ m^{-2}$), the other models suggest that the highest biomass is located on spurs on the eastern steep flanks, and on a spur on the southern flank. The values of biomass for these hotspots are intermediate in comparison to the maximum predicted by the GAM at 400 m. While not aiming at suggesting here the ideal spatial resolution for megafauna analysis over small abyssal hills, it can be stated that, where possible during planning and surveying, the finest spatial resolution of sampling should be aimed at. Nevertheless, as the resolution of the survey increases, spatial autocorrelation will be stronger and should be accounted for.

Furthermore, the same variable measured at different resolutions could be a proxy for different processes. For example, the small scale topographic depressions (negative values of fine BPI at 100 m resolution) seem to host intermediate levels of biomass, while most of it is concentrated on the large scale maxima of the bathymetry that have high broad BPI values. Therefore, a range of different spatial resolutions for different environmental variables can detect signals of processes happening at various scales. For this same reason, the present study improves previous analyses of biomass around the targeted hill (Morris et al. 2016) by using continuous explanatory

variables rather than bins, and by investigating the effect of varying the spatial scale of the analysis. This ultimately allows for the GAMs to be used to estimate values in un-sampled areas, albeit while explaining a small part of the variation.

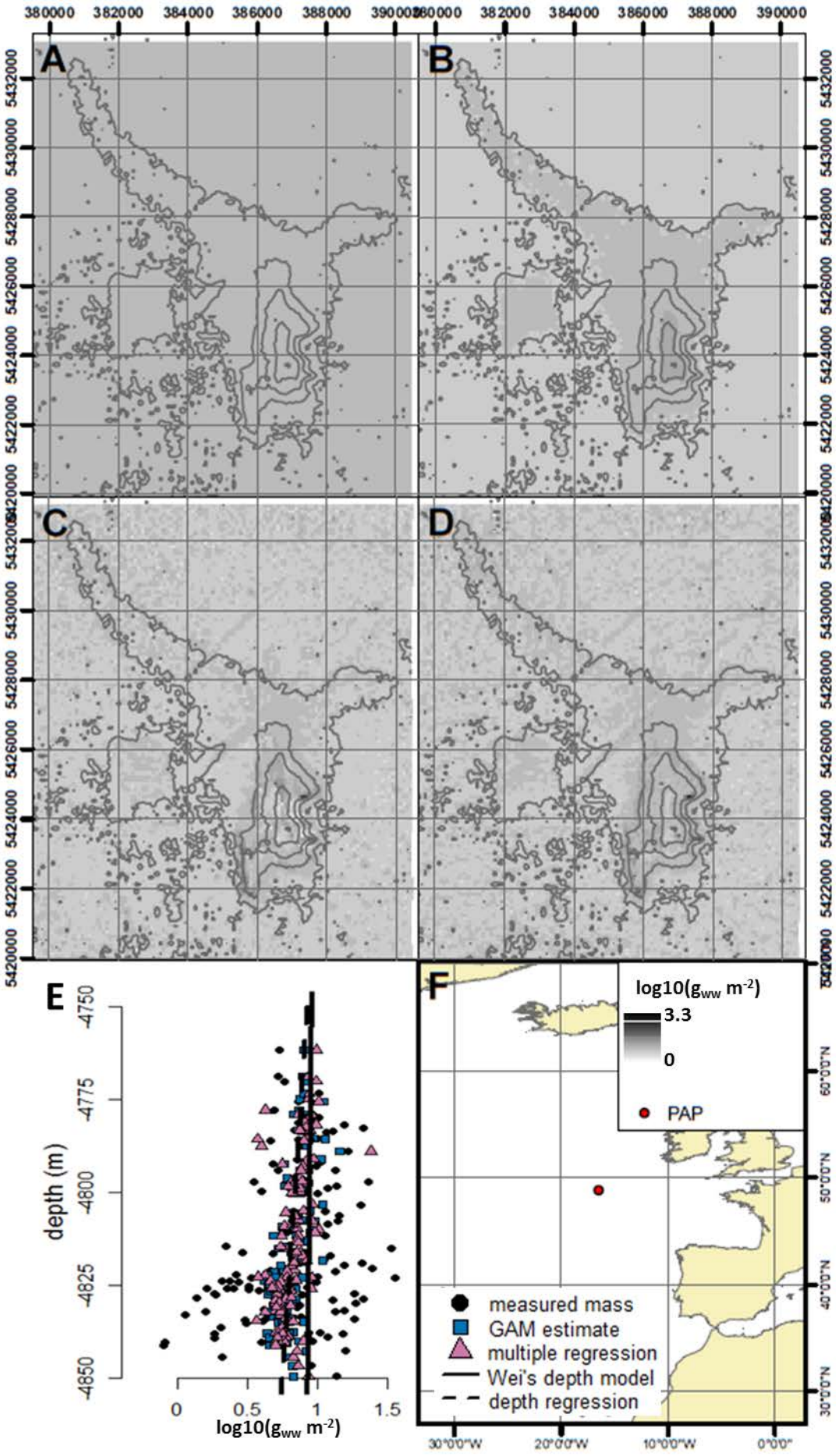
A
B
C
D
E
F
380000
382000
384000
386000
388000
390000
5432000
5430000
5428000
5426000
5424000
5422000
5420000
depth (m)
-4750
-4775
-4800
-4825
-4850
0
0.5
1
1.5
log10(g_ww m^-2)
log10(g_ww m^-2)
3.3
0
PAP
measured mass
GAM estimate
multiple regression
Wei's depth model
depth regression
30°0'0"W
20°0'0"W
10°0'0"W
0°0'0"
60°0'0"N
50°0'0"N
40°0'0"N
30°0'0"N

Figure 4-5: Spatial predictions of benthic biomass ($log_{10}(g_{ww}\ m^{-2})$) for the abyssal hill area with 4 different models at 100 m of spatial resolution. Isobaths are spaced at 100 m intervals, from 4800 m to 4500 m. A) Reduction of biomass with depth predicted by Wei et al. (2010). B) Reduction of biomass with depth detected at 100 m resolution. C) Biomass prediction using a multiple regression of slope, fine BPI, broad BPI and aspect-current interaction at 100 m resolution ($F = 1.861$, d.f. = 129, $R^2 = 0.08$, p-value < 0.05, Table 4-8). D) Biomass prediction using a Generalised Additive Model (GAM) including the effects of slope, fine BPI, broad BPI, and aspect-current interaction at 100 m resolution (n = 145, $R^2 = 0.13$, deviance explained = 20 %, GCV score = 0.11, Table 4-9). E) Scatterplot of biomass (x axis) along the depth gradient (y axis). Black dots are the biomass measured in the Autosub6000 and SHRIMP surveys across the abyssal hill area, blue squares are the biomass estimates from the GAM at 100 m resolution (Table 4-9), pink triangles are the biomass estimates from the multiple regression at 100 m resolution (Table 4-8), the black continuous line is the linear regression of biomass against depth predicted by Wei et al (2010), and the dashed line is the reduction of biomass along the depth gradient recorded at the abyssal hill.

The tested seafloor morphology variables improve the biomass prediction with respect to other existing seafloor biomass models (Figure 4-5). Given the small difference in depth between the top and the bottom of the abyssal hill, only a ~ 3% difference in biomass could have been expected if reduction of biomass with depth alone was accounted for (Martin et al. 1987, Lutz et al. 2007, Wei et al. 2010). In Figure 4-5a it can be seen that, according to a regression used to estimate the reduction of biomass with depth (Wei et al. 2010), the megafauna biomass distribution would be predicted to be invariable across the hill area. The reduction of biomass with depth in this study is 10-fold stronger than what would be expected for such a small depth gradient (10^{-4} in Wei et al 2010, Figure 4-5a, and 10^{-3} in this study, Figure 4-5b). By disregarding the effect of depth, and looking at the effect of seafloor morphology instead, two predictive models that perform better than the regression of biomass with depth have been obtained. Both the multiple regression (Figure 4-5c, p-value < 0.05, $R^2 = 0.08$) and the GAM (Figure 4-5d, GCV score 0.11, $R^2 = 0.13$) at 100 m resolution predict peaks of biomass on two protruding parts of the relatively steep eastern flanks of the hill, probably determined by the seafloor steepness, high fine BPI and positive aspect-current interaction in these areas. Furthermore, the models predict peaks of biomass at the hill summit, and on two parts of a southern spur of the hill. These latter two peaks could be determined by an interaction of the positive effect of BPI, together with the positive effect of the aspect-current interaction. Apart from the few hotspots, the top of the hill is predicted to have slightly less mass than the northern flanks. Furthermore, intermediate levels of biomass are predicted for the small rise to the west of the hill.

4.5 Conclusions

In this chapter, the interaction between hydrodynamic and gravitational transport in determining the distribution of standing stocks has been investigated, in relation to a small topographic feature: an abyssal hill of ~ 300 m elevation. The small size feature acted here as a natural experiment: the effect of depth change was virtually insignificant and therefore the effect of other metrics related to topography could be addressed. At fine resolution levels, linear regressions of biomass with slope and broad scale BPI have highlighted that biomass is higher in steeper and more elevated areas. In this hill case, the more complex multiple regression and GAM models investigating non-linear effects and interactions, nevertheless, did not provide more conclusive results. However, the results suggest that some process, potentially linked to hydrodynamics, results in increase fluxes of particulate organic matter in elevated and steeper areas.

Chapter 5: A global predictive model for biomass distribution, based on the effect of seafloor morphology.

5.1 Introduction

The world oceans cover > 70% of the Earth's surface (Watling et al. 2013) and, thanks to remote sensing, we now have some spatially and temporally continuous knowledge of many of its physical characteristics (temperature (Sarangi 2016), cloud coverage, wave and wind state over the ocean (Fu and Le Traon 2006, Hasager 2014)) and biological characteristics (i.e. seasonality of phytoplankton blooms (Messie and Chavez 2015) and their spatial variability (Behrenfeld and Falkowski 1997, Laws et al. 2011, Sarangi 2016)). Nevertheless, remote sensing does not allow investigating below the surface ocean, and therefore our knowledge of the ocean interior is limited to the areas that have been investigated directly, and to the inferences that can be made from those observations. The deep seafloor is often regarded as a long term sink of organic carbon, and therefore an important part of the global carbon cycle (Smith et al. 2008, Smith et al. 2008, Smith et al. 2009, Smith et al. 2013). Knowing its physics, chemistry and biology will greatly improve our understanding of the earth energetic and climatic systems; furthermore, investigating the magnitude and kinetics of its processes will improve the way that it is managed, not only for local conservation purposes, but also for global long term resources management.

From an ecological prospective, a first step to better understand the oceanic ecosystem under a 'carbon cycle' point of view is to quantify the organic carbon stock present on the seafloor, of which a part is constituted by the amount of benthic living animals, or biomass. These are the recipients of the atmospheric carbon sequestrated in the ocean interior through the biological carbon pump (Giering et al. 2014). Therefore, these fauna play a part in determining what proportion of the carbon is permanently stored in the sediment, and what proportion remains in the water as dissolved inorganic carbon, to then reach the atmosphere on a relatively short timescale (350 years, residence time of carbon in the oceans).

5.1.1 At coarse resolution and large scales, vertical flux processes control the input of food to the deep sea.

Global predictions of benthic standing stocks are made using our understanding of biomass trends in relation to depth, surface primary productivity and temperature (Rex et al. 2006, Wei et al.

2010, Jones et al. 2014). These factors are used as proxies for the vertical input of organic material (nutrients) from the surface ocean, through the water column and to the benthos (Lutz et al. 2002). Food availability and temperature are the main factors that determine the metabolism of individuals and, as a consequence, the standing stock of communities (Brown et al. 2004).

Surface primary production varies temporally and at basin scales, through the seasonal cycle (Lutz et al. 2007, Henson et al. 2011). At a regional spatial scale, the upwelling of deep sea water masses along eastern boundary currents creates hotspots for phytoplankton blooms, where the seasonal component is still quite strong (Messie and Chavez 2015). At smaller spatial scales and temporal resolution, surface primary productivity is influenced by eddies and fronts (Lima et al. 2002, Strass et al. 2002, Martin 2003, McGillicuddy et al. 2003, Prasanna Kumar et al. 2007).

When transferred to the benthos, the complex pattern of carbon fixation at the ocean surface is averaged over large spatial scales, resulting in patterns of benthic biomass distribution over latitudinal and productivity gradients (Thurston et al. 1994, Johnson et al. 2007). Furthermore, the flux of Particulate Organic Carbon (POC) decreases exponentially with depth (Martin et al. 1987, Lutz et al. 2002) resulting in well-documented trends of decreasing biomass with depth (Rex et al. 2006). Body size and *in-situ* temperature are key factors for the metabolic rates of ectotherms (Brown et al. 2004, Hughes et al. 2011). This mostly affects the benthos in the shallower parts of the ocean, where temperature changes with seasons, and has an effect on the vertical zonation of communities. Furthermore, it can have a strong effect in deep marginal seas, which generally represent end points of the thermal range either near 0 °C (Weddell Sea Linse et al. 2007) or near 14 °C (Mediterranean Sea Tecchio et al. 2011), and therefore present extreme thermodynamic conditions (Clarke and Fraser 2004). Finally, low oxygen concentration is a strong limiting factor for benthic communities in some areas (Levin et al. 2000, Quiroga et al. 2005); nevertheless, the global understanding of the biological response to oxygen minimum zones is low and therefore it is hard to include such factor in a global model.

5.1.2 At fine resolution, hotspots of benthic biomass could be distributed in relation to lateral advection of nutrients.

The large scale, coarse resolution patterns of biomass distribution just described have allowed inferring benthic biomass at global scale (Wei et al. 2010), and predicting its reduction in response to likely scenarios of climate change (IPCC 2014, Jones et al. 2014). Nevertheless, these predictions miss the biomass variability introduced by sub-degree environmental patterns. The ocean seafloor is not a monotonous landscape: the continental slopes are indented by large

canyon systems (Harris and Whiteway 2011), the mid ocean ridges are crossed by fracture zones (Alt 2012, Alt et al. 2013, Bell et al. 2016), and even the abyssal plains are covered by many topographic features such as seamounts (> 1000 m of elevation) and millions of hills (<1000 m of elevation) (Harris et al. 2014). Topographic features are generally associated with biomass measurements that are somewhat discordant with what would otherwise be expected as a consequence of the local depth and vertical food input alone (Rex et al. 2006). Biomass can be extremely high at the top of seamounts, possibly as a consequence of local hydrodynamic patterns (Genin et al. 1986, Genin 2004, Genin and Dower 2007), but also at the bottom of seamount flanks and on the axis of trenches (Danovaro et al. 2003, Glud et al. 2013, Zeppilli et al. 2013), seemingly as a consequence of lateral sediment transport caused by (or approximated by) gravity (Ichino et al. 2015) and by particular-matter dynamics induced by internal tides (Turnewitsch et al. 2014).

The previous chapters have focussed on three topographic features to detect the trends of biomass distribution associated with seafloor morphology. Chapter 2 showed how gravitational transport of organic sediments, controlled by slope steepness and direction, could result in food focussing along the axis and in the depressions of a hadal trench (Chapter 2 and Ichino et al. (2015)). Chapter 3 investigated the distribution of megafauna at two seamount locations in the northeast Pacific. This has shown that seamount shape could result in variable patterns of biomass distribution around the features, even if the trends between biomass and the topographic metrics were not conclusive. Chapter 4 showed that the effect of seafloor morphology is not only limited to large topographic features like seamounts, as it can be detected in the biomass distribution around a small abyssal hill (~ 300 m of elevation). In such small features, slopes are not steep enough to efficiently transfer the organic carbon, and therefore biomass is concentrated at the local maxima of the bathymetry, and in the areas that could be affected by current dynamics (Figure 3-4).

In this chapter, global benthic biomass trends are investigated along gradients of depth, vertical input of nutrients, temperature, seafloor slope steepness, local relative elevation, current direction variability and interaction between topography and current direction. The aim is to detect, in a global dataset, trends of biomass distribution in relation of seafloor morphology similar to those detected in local case studies. Statistical models based on these trends would provide global biomass predictions at the finest resolution yet available, 30 arc-seconds, 120 times higher than previous estimates (1° resolution, Wei et al. 2010).

5.2 Materials and methods

A total of 2199 records of whole-assemblage biomass for three generally accepted size classes of marine fauna (430 samples of meiofauna, 1182 of macrofauna and 511 of megafauna invertebrates) and for fish assemblage (76 samples), have been used to study the global distribution of benthic biomass in relation to seafloor topographic features (Figure 5-1). Meiofauna is defined here as the fraction of metazoan retained in sieves from 20 µm to 74 µm, and macrofauna as that retained in sieves from 250 µm to 520 µm. Sampling was conducted by different investigators from multiple institutions and over a period of more than 40 years. Megafauna is generally defined as the group of metazoans visible in photographs of the seafloor (typically ≥ 1 cm in size, Grassle 1975). Traditionally these are collected with trawling gear and observed with photographic techniques (see section below on statistical corrections applied in relation to the gear type); here, invertebrate megafauna has been kept separate from vertebrate megafauna (fish) as not all the surveys from which data were obtained included both assemblages.

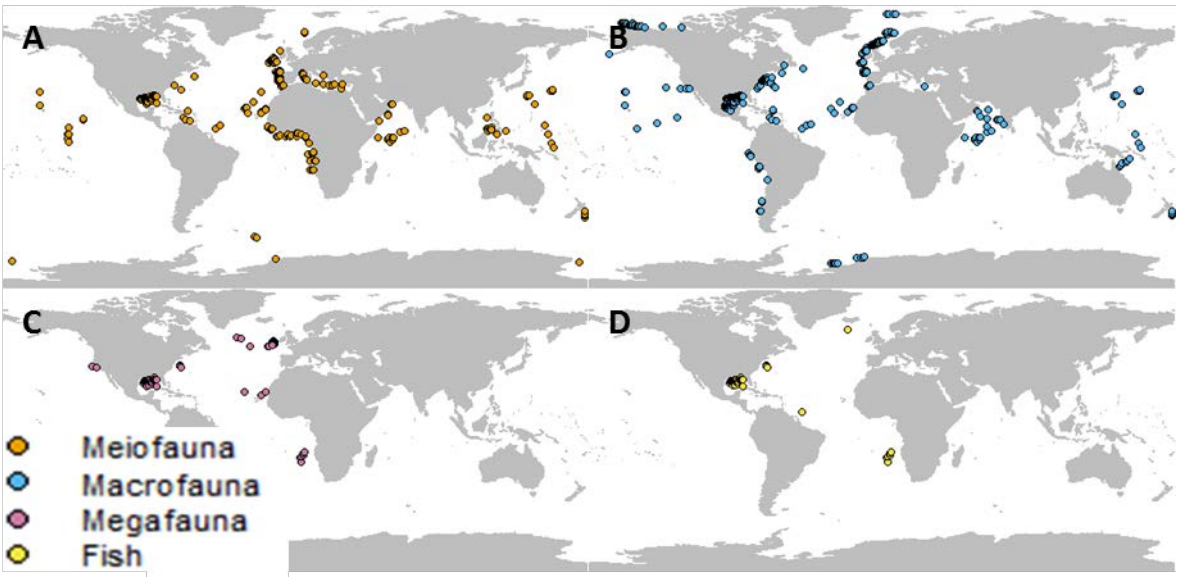

Figure 5-1: Sampling locations for the 4 size classes. Total samples = 2199, A) meiofauna samples = 430, B) macrofauna samples = 1182, C) megafauna invertebrates samples = 511, D) fish samples = 76.

Most of the records come from a previous collection of data during the Census of Marine Life (CoML, Wei et al. 2010). Only samples collected deeper than 500 m have been included in this study, to avoid the influence of mixed layer and shelf processes. Other smaller datasets have been added, including ROV dives over Davidson and Taney seamounts (Lundsten et al. 2009a, McClain et al. 2010, McClain and Lundsten 2014, and Chapter 3), the Autosub6000 and SHRIMP datasets collected in the Porcupine abyssal plain (Morris et al. (2014), Morris et al. (2016) and Chapter 4), trawl samples collected at three bathyal locations in the north part of the Mid-Atlantic Ridge (Alt

et al. 2013), and 12 macrofauna records collected with boxcores in the Goban Spur area (Flach and Heip 1996).

5.2.1 Environmental predictors for vertical input of food.

The main driver of benthic biomass distribution is food availability that, in the deep seafloor, is mainly controlled by surface productivity and water depth. Export flux from the mixed layer (mgC m^{-2} y^{-1}), is a measure of the quantity of organic matter that leaves the surface ocean and it mostly follows latitudinal gradients. In this study a log_{10} transformed global export flux estimated by Henson et al. (2011) at 1°of spatial resolution was used as a proxy for the vertical input of organic matter (Table 5-1). The POC exported from the surface is believed to sink vertically to the seafloor, gradually being remineralised (Martin et al. 1987). As a consequence, food availability is generally expected to decrease with depth, causing a reduction in biomass (Rex et al. 2006). Here the depth measurements provided by GEBCO (BODC 2003) at 30 arc-seconds resolution were used (Table 5-1). In all the analyses, depth has been log_{10} transformed, to better respect the assumption of homoscedasticity of the residuals in the linear models. Lastly, temperature (°C) for the bottom 100 m of water column at 1/4° resolution was obtained from the World Ocean Atlas (National Geophysical Data Center, 2009)(Table 5-1). As suggested by the MTE, temperature has a positive effect on the metabolic rate of individual organisms: as temperature increases, a higher proportion of the individual's energy budget is used for the basal metabolism. Therefore, higher temperatures have a negative effect on whole-ecosystem standing stock, as less energy will be available for growth and reproduction (Brown et al. 2004).

Table 5-1: List of the environmental predictors used in the global models, including their range of values, their source and their spatial resolution

	Minimum	**Mean (SD)**	**Maximum**	**Notes**
Depth (m)	-9624	-2489 (34.1)	-502	Global depth, obtained from GEBCO 08 (BODC 2013) at 30 arc-seconds resolution. The resolution in meters changes with latitude, from ~900 m at the equator to 0 at the poles. Depth has been log_{10} transformed in the analyses.
POC export (mgC $m^{-2}y^{-1}$)	707.5	13070 (183.4)	80950	Export of particulate organic carbon below 100 m depth (Henson et al. 2011). 1° resolution

	Minimum	Mean (SD)	Maximum	Notes
Temperature (°C)	-1.8	4.1 (0.7)	20.4	Temperature estimate for the seafloor, from the World Ocean Atlas (National Geophysical Data Center and Commerce 2009). This is used only in the multiple regression. 100 m of vertical resolution, 1/4° horizontal resolution
Slope steepness (°)	0	1.8 (0.6)	28	Slope calculated via the ArcGIS tool "Slope" in the "Spatial analyst" toolbox, from the global depth. 30 arc-seconds resolution.
Bathymetric position index (BPI)	-733	2 (0.9)	509	Relative elevation with respect to the surrounding features. Calculated using the Benthic Terrain Modeller plugin for ArcGIS 10.2 on the depth layer, within a 1 cell radius on the global depth (Wright, Pendleton et al. 2012). 30 arc-seconds resolution
Aspect-current interaction (°)	-180	-	180	Interaction between aspect (Spatial analyst, ArcGIS 10.2) and current direction (NEMO 1/12), a continuous variable defining the direction from which the current hits the slope. Current direction is at 1/12° resolution, while the aspect is at 30 arc-seconds resolution.
Standard deviation of current direction (°)	1.47	1.79 (0.001)	1.8	Calculated with the Yamartino method (Yamartino 1984) on a one-year current estimate obtained from NEMO. 1/12° resolution.

5.2.2 Environmental predictors for fine scale biomass distribution.

The main focus of this study was to look at the effect of seafloor morphology on the benthic community, as opposed to the effect of other factors related to water column processes only (i.e. salinity, oxygen concentration, seasonality of food particle fluxes as in Wei et al. (2010)). Here the seafloor morphology features examined included slope steepness, BPI and the aspect-current interaction. Slope (°) was measured in R (R core team 2014) from the GEBCO bathymetry with a conformal projection (Mercator for the latitudes within 37° north and south, and a stereographic projection for the polar regions, to reduce deformation, Keller (1988)). Slope is expected to have an effect on the deposition of organic food particles on the seafloor, where steep slopes might lose sinking particulate organic matter to deeper depths, therefore playing a role in the distribution of benthic communities (Table 5-1).

The BPI is a measure of relative elevation: areas with positive BPI are higher than the surroundings, as could happen for the top of seamounts, while areas with negative BPI, such as the axis of trenches, are lower (Figure 3-3)(Wilson et al. 2007).The BPI has been calculated for the global ocean using the Benthic Terrain Modeller plugin for ArcGIS 10.2 (Wright et al. 2012) (Table 5-1).

The aspect-current interaction (°) provides a qualitative proxy for the exposure of the slope to the current. This could help recording potential asymmetric distribution of standing stocks around features, which could arise when there is asymmetric sediment distribution because of the interaction between the current and the topography (Table 5-1, Figure 3-4 for a schematic representation). The mean background current direction at this global scale, used for calculating the aspect-current interaction, was estimated from the NEMO global circulation model (Madec 2008). From the NEMO model the yearly standard deviation of current direction (°) has been estimated, and has been used as a proxy for local variability of water column conditions (Table 5-1).

5.2.3 Spatial distribution and spatial weights.

The spatial distribution of the samples was irregular, as they were mostly collected from the northern hemisphere, and from the Atlantic Ocean, especially in proximity to continental margins (Figure 5-1). Therefore, spatial weights were applied to all the statistical models, to reduce the effect of intensely sampled areas (i.e. northeast Atlantic) on the overall pattern. The spatial weight of a sample equalled the reciprocal of the number of samples found in a 30 arc-seconds radius from it (the spatial resolution of the analysis), with 1 being the spatial weight for a sample with no neighbours, and 0.009 being the weight for the sample with most neighbours (a

megafauna sample with 109 neighbours, from the AESA dataset (Morris et al. 2014, Morris et al. 2016) and Chapter 4).

5.2.4 Gear.

Samples used in this study were collected over more than forty years, and by many different institutions; therefore, a large variety of gear types were used. Different gear types are known to have different sampling efficiencies because of the bow wave effect, for coring tools, and of the difficulty of assessing actual trawling time and efficiency, for trawls and sledges. To account for this, the gears have been grouped in five major types: the box corers (BC_GR, including, the USNEL (United States Naval Electronic Laboratory) box corer, the NIOZ (Netherlands Institute for Sea Research) box corer, the spade box corer and all the grab-like samplers, used for meiofauna and macrofauna), the multiple corers (MC, including megacorers and multicorers, used for meiofauna and macrofauna), fish trawls and sledges (FT_SL, including Agassiz trawls, beam trawls and epibenthic sledge, used for fish and megafauna), otter trawls (OT, including semiballon and shrimp trawls, used for fish and megafauna) and photographic records (PH, including both photo and videos, used for fish and megafauna). The 'gear' factor has been preliminarily included in the regressions; gear type had a significant effect only on the macrofauna biomass models, whereby BC_GR gear collected more biomass than the MC gear at comparable levels of the predictors. Gear type was removed from the models for the other size classes, as it did not have a significant effect on the results.

Because of the reduction of abundance with depth, it is often necessary to increase the trawled area when sampling in deeper parts of the ocean. Preliminary data exploration showed a positive trend between trawled area and depth, for fish and megafauna. A first regression of $\log_{10}$-transformed biomass against gear and sampled area was calculated; the residuals of this regression have then been used as a dependent variable for all the subsequent models. This does not apply to other gear types: in fact, these tools have fixed sampling area that constitutes the sampling unit.

5.2.5 Statistical analysis.

The relationship between biomass standing stock and environmental predictors was investigated with statistical models. All the statistical analyses were performed using R (R core team 2014). Pairwise Spearman rank correlations ('corr.test' routine from the package 'psych' (Ravelle 2015)) between biomass measurements and independent environmental variables were used as a test to highlight the cases of covariance between the model predictor variables, and as a first test of the

hypotheses. Linear models between biomass and each predictor were tested using 'lm' and 'anova' routines.

Shapiro-Wilk tests were performed on the residuals of each regression to test the assumption of normality; a $\log_{10}$ transformation of the biomass measurements was used in the linear models and in all the subsequent analyses, to meet the assumption of normality of the residuals. Heteroscedasticity of the residuals was tested with the Breusch-Pagan test ('bptest' routine in the 'lmtest' package (Zeileis and Hothorn 2002)); therefore, a $\log_{10}$ transformation of depth and export flux values was used in all the models to meet the assumption of normality of the residuals. Finally, Moran's test of spatial autocorrelation was used to test for the independence of the residuals (Paradis et al. 2004). These were performed separately for each of the five major ocean basins (Atlantic, Indian, Pacific, Southern and Arctic Ocean) to better constrain the mismatch between geographic distance and the actual distance across the ocean, which can differ significantly in some areas (e.g. between the equatorial Pacific and the Gulf of Mexico).

The cumulative effect of the predictors was then investigated using multiple regressions ('lm') and generalised additive models GAMs, which allow for non-linear relationships between the predictors and biomass, with the aim of obtaining a predictive model ('gam' routine from the R package 'gam' (Hastie 2015)). The modelled patterns of biomass in relation to topography were extrapolated globally, and analysed in relation to existing biomass models based on depth alone, and on water column processes (Wei et al. 2010).

5.3 Results

For all the four assemblages, the multiple regression is significant, and the deviance explained by the GAMs is 45.9%, 58.9 %, 42.4% and 60.9% for meio-, macro-, megafauna and fish, respectively (Table 5-2). The multiple regression for macrofauna has the highest predictive power (F 65.57, d.f. = 864, p-value < 2.2x10-16, R^2 = 0.63, Shapiro-Wilk p-value < 2.2x10-16, Breusch–Pagan p-value < 0.001), while it is lowest for megafauna (F 10.59, d.f. = 384, p-value < 2.2x10-16, R^2 = 0.34, Shapiro-Wilk p >0.1, Breusch–Pagan p <0.001) (Table 5-3). All the multiple regressions, apart from the one for the fish assemblage, fail the test for the homoscedasticity of the residuals, while only the regression for macrofauna fails the Shapiro-Wilk test for normality. The residuals of the regressions present a high degree of spatial autocorrelation: the meiofauna residuals are independent only in the Arctic and Southern oceans, those of the macrofauna regressions are independent in the Pacific, Arctic and Southern oceans, while the residuals of the regression for the fish assemblage are never spatially autocorrelated (Table 5-3). (continues at 130).

Table 5-2: Summary table for Generalised Additive Models (GAM) of meiofauna, macrofauna, megafauna invertebrates and fish (on the rows) built with 7 environmental predictors: log_{10}(depth) = D, log_{10}(export flux) = EF, temperature = T, Bathymetric Position Index = BPI, slope = S, standard deviation of current direction = dSD, and aspect-current interaction = ACI. For each predictor the smooth parameter is reported within parentheses, then the F statistic and the significance. For each model is reported the number of data points included in the training set (n, 75% of the whole dataset), the adjusted R^2, the deviance explained, the GCV score, and the significance of the Moran test for spatial autocorrelation performed on the residuals of the GAM at global scale (G), in the Atlantic (Atl), Pacific (Pac), Indian (In), Southern (Sou) and Arctic ocean (Arc).

	(smooth parameter) F and significance							n	adj. R^2	dev. exp. %	GCV score	Spatial autocorrelation					
	D	**EF**	**T**	**BPI**	**S**	**dSD**	**ACI**					**G**	**Atl**	**Pac**	**In**	**Sou**	**Arc**
Meio.	(5)	(20)	(5)	(1)	(10)	(10)	(250)	344	0.41	45.9%	0.25	< 0.001	< 0.001	< 0.01	< 0.01	> 0.5	> 0.1
	9.845 ***	8.713 ***	6.478 ***	1.818	2.276 *	2.113	0.324										
Macro.	(0.5)	(500)	(20)	(5)	(0.5)	(10)	(200)	784	0.57	58.9%	0.16	< 0.001	< 0.001	< 0.001	< 0.001	> 0.5	> 0.1
	37.673 ***	2.090	51.646 ***	0.209	12.806 ***	1.241	0.312										
Mega.	(2000)	(10)	(1)	(5)	(5)	(10)	(10)	431	0.39	42.4%	0.09	< 0.001	< 0.001	< 0.001			
	0.640	9.865	2.192	3.298	0.707	2.548	3.886										

	(smooth parameter) F and significance							n	adj. R^2	dev. exp. %	GCV score	Spatial autocorrelation					
	D	EF	T	BPI	S	dSD	ACI					G	Atl	Pac	In	Sou	Arc
		***	*	**		*	**										
Fish	(1)	(5)	(2)	(10)	(12)	(20)	(10)	67	0.38	60.9%	0.45	< 0.001					
	1.021	0.783	0.217	0.514	1.177	0.258	.944										

Table 5-3: Multiple linear regressions of log_{10} transformed meio-, macro-, megafauna invertebrates and fish against 7 environmental predictors and their interactions. In the table are reported the coefficient and significance of a scaled and a non-scaled version of each regression, the overall p-value of each regression, the R^2, the F statistic with the degrees of freedom (d.f.) and the residual standard error. Finally are reported the significance for the Shapiro-Wilk test of normality, the one for the Breusch–Pagan test of homoscedasticity, and the one for the Moran's test for spatial autocorrelation at global scale and in the 5 major ocean basins. All the tests are performed on the residuals of the linear regressions.

	Meiofauna		**Macrofauna**		**Megafauna**		**Fish**	
	Not scaled	**Scaled**	**Not scaled**	**Scaled**	**Not scaled**	**Scaled**	**Not scaled**	**Scaled**
Intercept	26	26.40	-1.14	-1.14	-3.40	-3.40	88.75	88.75
log_{10}(Depth)	-1.48e+01 ***	-4.24 ***	0.66	0.18	5.62	1.42	-30.90	-9.59
log_{10}(Export flux)	-1.15e+01 ***	-2.89 ***	1.26	0.39	6.74	1.15	-25.48	-3.65
Temperature	-2.27	-10.87	8.77 ***	27.70 ***	2.65	4.46	-0.62	-1.39
Direction SD	1.29e+01	0.27	1.37	0.06	-10.07	-0.06	7.50	0.09

	Meiofauna		Macrofauna		Megafauna		Fish	
	Not scaled	**Scaled**	**Not scaled**	**Scaled**	**Not scaled**	**Scaled**	**Not scaled**	**Scaled**
	***	***	*	*	*	*		
BPI	7.24e-01	19.65	0.11	3.59	-37.23	-19.82	-2.14	-66.93
Slope	6.49	18.74	1.05	2.22	10.46	39.67	23.75	52.33
	***	***	**	**	*	*		
AC Interaction	-8.12e-02	-8.01	0.01	0.53	5.87e-02	5.99	-0.27	-28.55
MC			0.33	0.12				
			***	***				
log_{10}(Depth) :	3.55	4.37	-0.49	-0.63	-1.84	-2.32	7.74	8.34
log_{10}(Export flux)	***	***						
log_{10}(Depth) :	5.56e-01	8.79	-3.17	-29.52	-9.99e-01	-4.52	-0.52	-2.90
Temperature			***	***				

	Meiofauna		Macrofauna		Megafauna		Fish	
	Not scaled	**Scaled**	**Not scaled**	**Scaled**	**Not scaled**	**Scaled**	**Not scaled**	**Scaled**
log_{10}(Export flux) :	5.78e-01	11.02	-2.19	-27.81	-9.33e-01	-6.24	0.14	1.30
Temperature			***	***				
SD Direction :	-4.03e-01	-19.66	-0.06	-3.75	2.04e-01	19.71	1.19	67.34
BPI								
SD Direction :	-3.59	-18.62	-0.55	-2.07	-5.74	-39.42	-13.20	-52.47
Slope	***	***	***	**	*	*		
BPI :	-1.20e-01	-60.82	-0.02	-6.02	2.03e-01	111.54	0.60	178.69
Slope					***	***		
SD Direction :	4.51e-02	8.03	-0.003	-0.58	-3.27e-02	-6.02	0.15	28.19
AC Interaction								
BPI :	7.80e-03	20.65	-0.002	-5.06	3.47e-04	1.78	0.006	15.66
AC Interaction								

	Meiofauna		Macrofauna		Megafauna		Fish	
	Not scaled	**Scaled**	**Not scaled**	**Scaled**	**Not scaled**	**Scaled**	**Not scaled**	**Scaled**
Slope :	-5.76e-03	-1.83	0.003	0.79	4.84e-02	15.93	0.35	89.51
AC Interaction								
log_{10}(Depth) :	-1.44e-01	-9.03	0.79	29.35	3.40e-01	6.08	0.13	2.99
log_{10}(Export flux) :			***	***				
Temperature								
SD Direction :	6.66e-02	60.80	0.01	6.10	-1.12e-01	-111.51	-0.34	-181.43
BPI :					***	***		
Slope								
SD Direction :	-4.30e-03	-20.47	0.001	5.28	-1.76e-04	-1.64	-0.003	-15.71
BPI :								
AC Interaction								
SD Direction :	3.13e-03	1.786	-0.001	-0.70	-2.67e-02	-15.92	-0.19	-89.08

	Meiofauna		Macrofauna		Megafauna		Fish	
	Not scaled	Scaled	Not scaled	Scaled	Not scaled	Scaled	Not scaled	Scaled
Slope : AC Interaction								
BPI : Slope : AC Interaction	-1.80e-03	-100.33	0.0002	5.26	-1.15e-05	-0.51	-0.004	-113.17
SD Direction : BPI : Slope : AC Interaction	9.97e-04	100.10	-0.0001	-5.45	4.92e-06	0.40	0.002	115.50
p-value	< 2.2e-16		< 2.2e-16		< 2.2e-16		< 0.001	
Adjusted R^2	0.38		0.63		0.34		0.42	

		Meiofauna		Macrofauna		Megafauna		Fish	
		Not scaled	Scaled	Not scaled	Scaled	Not scaled	Scaled	Not scaled	Scaled
F-statistic (d.f.)		9.91 (301)		65.57 (864)		10.59 (384)		3.182 (44)	
Residual standard error		0.4949		0.3906		0.3047		0.5059	
Normality test		>0.05		< 2.2e-16		> 0.1		> 0.1	
Homoscedasticity test		< 0.001		< 0.001		< 0.001		> 0.1	
	Global	< 0.001		< 0.001		< 0.001		> 0.5	
	Atlantic	< 0.001		< 0.001		< 0.001		> 0.05	
	Pacific	< 0.001		> 0.5		< 0.01			
	Indian	< 0.01		< 0.001					
	Arctic	> 0.1		> 0.1					
	Southern	> 0.5		> 0.5					

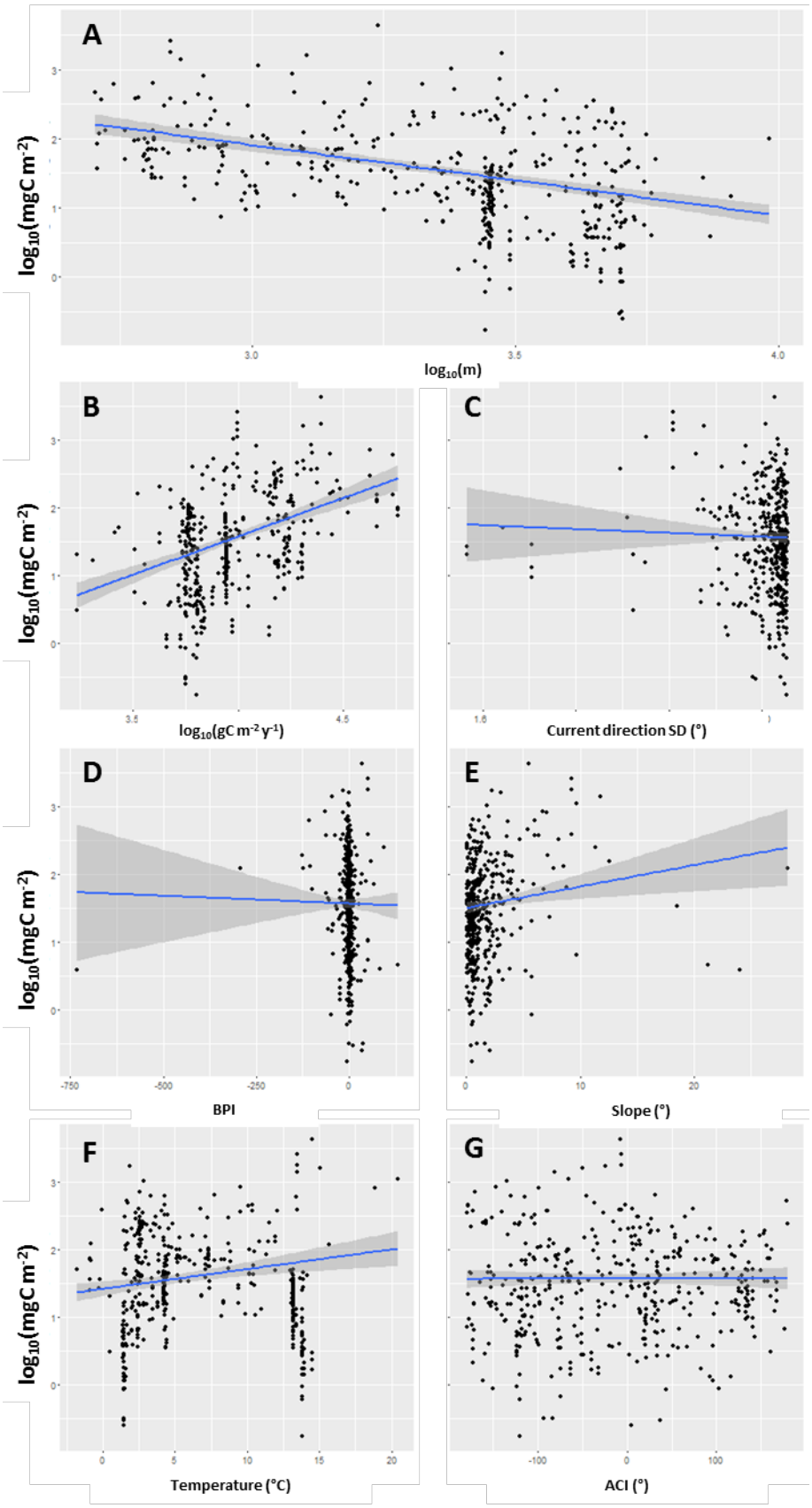

Figure 5-2: The result of 7 linear models (y = I + mx) of meiofauna biomass (y, measured as $\log_{10}$(mgC m^{-2})) against 7 environmental variables (x). A) Biomass decreases significantly with depth ($\log_{10}$(m), I = 4.96, m = -1.02, F = 100.5, d.f. = 428, p-value < 2.2e-16). B) Biomass increases significantly with export flux ($\log_{10}$(gC m^{-2} y^{-1}), I = -2.96, m = 1.15, F = 91.61, d.f. = 428, p-value < 2.2e-16). C) The standard deviation of

current direction (°) does not have an effect on biomass. D) The Bathymetric Position Index (BPI) does not affect biomass significantly. E) Biomass increases significantly as slope (°) increases (I = 1.5, m = 0.03, F = 8.351, d.f. 428, p-value < 0.01). F) Biomass increases significantly as temperature (°C) increases (I = 1.42, m = 0.03, F = 12.29, d.f. = 428, p-value < 0.001). G) Aspect-current interaction (°) does not have a significant effect on meiofauna biomass.

Table 5-4: Simple linear regressions (y = I+mx) between log_{10} transformed meiofauna biomass (y) and 7 environmental predictors (x). For each regression are reported the strength and significance of the Spearman rank correlation, the intercept (I) and slope (m) of the linear regression, together with their significance, the overall p-value of the linear regression, the R^2, F value, and residual error. Finally, are reported the significance for the Shapiro-Wilk test of normality, the one for the Breusch–Pagan test of homoscedasticity, and the one for the Moran's test for spatial autocorrelation at global scale, and in the 5 major oceans. All the tests are performed on the residuals of the linear regression.

	Spearman ρ	**Coefficients**	**p-value**	**Adj. R^2**	**F (d.f. =428)**	**Residual error**	**Normality test**	**Homoscedasticity test**	**Spatial autocorrelation**	
									Global	< 0.001
									Atlantic	< 0.001
									Pacific	< 0.001
									Indian	< 0.01
									Arctic	> 0.1
									Southern	> 0.1
									Global	< 0.001
									Atlantic	< 0.001
									Pacific	< 0.001
									Indian	< 0.01
									Arctic	> 0.1
									Southern	> 0.1
									Global	< 0.001
									Atlantic	< 0.001
									Pacific	< 0.001

	Spearman ρ	Coefficients	p-value	Adj. R^2	F (d.f. =428)	Residual error	Normality test	Homoscedasticity test	Spatial autocorrelation	
									Indian	< 0.01
									Arctic	> 0.1
									Southern	> 0.1
									Global	< 0.001
									Atlantic	< 0.001
									Pacific	< 0.001
									Indian	< 0.01
									Arctic	> 0.1
									Southern	> 0.1
									Global	< 0.001
									Atlantic	< 0.001
									Pacific	< 0.001
									Indian	< 0.01
									Arctic	> 0.1
									Southern	> 0.1
									Global	< 0.001
									Atlantic	< 0.001
									Pacific	< 0.001

	Spearman ρ	Coefficients	p-value	Adj. R^2	F (d.f. =428)	Residual error	Normality test	Homoscedasticity test	Spatial autocorrelation	
		***							Indian	< 0.01
									Arctic	> 0.1
									Southern	> 0.1
									Global	< 0.001
									Atlantic	< 0.001
									Pacific	< 0.001
									Indian	< 0.01
									Arctic	> 0.1
									Southern	> 0.1

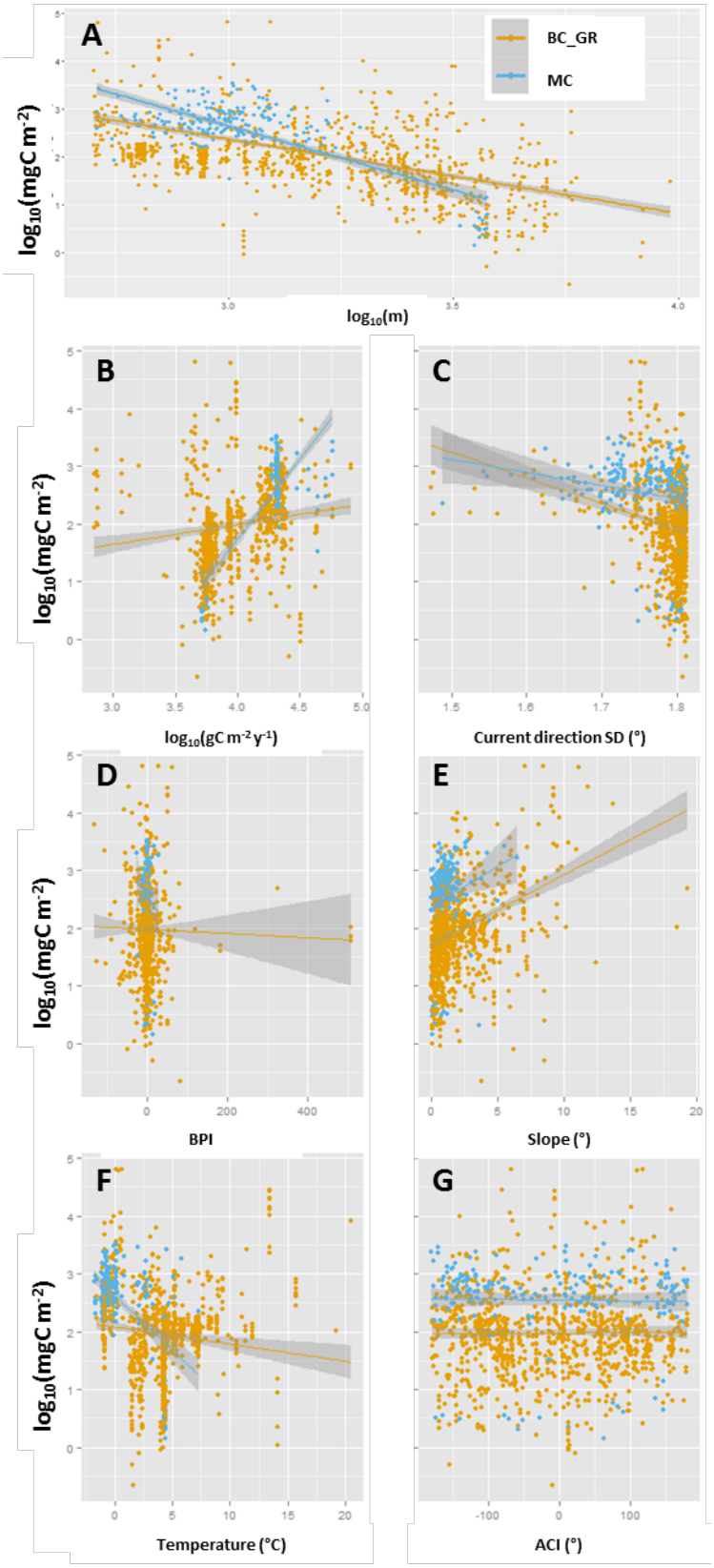

Figure 5-3: The result of 7 linear models (y = I + mx) of macrofauna biomass (y, measured as $\log_{10}$(mgC m^{-2})) against 7 environmental variables (x), and type of gear used for collection (MC = multiple corers, BC_GR = box corers and grabs. A) Biomass decreases significantly with depth ($\log_{10}$(m), I = 7.54, m = -1.71, F = 378.7, d.f. = 1179, p-value < 2.2e-16). B) Biomass increases significantly with export flux ($\log_{10}$(gC m^{-2} y^{-1}), I = -0.38, m = 0.59, F = 98.6, d.f. = 1179, p-value < 2.2e-16). C) The standard deviation of current direction (°) causes a significant decrease in macrofauna biomass (I = 8.47, m = -3.64, F = 93.9, d.f. = 1179, p-value < 2.2e-16). D) The Bathymetric

Position Index (BPI) has a negative effect on biomass (I = 1.98, m = -0.0005, F = 60.94, d.f. = 1179, p-value < 2.2e-16). E) Biomass increases significantly as slope (°) increases (I = 1.7, m = 0.12, F = 143.1, d.f. 1179, p-value < 0.01). F) Biomass decreases significantly as temperature (°C) increases (I = 2.16, m = -0.05, F = 82.99, d.f. = 1179, p-value < 0.001). G) Aspect-current interaction (°) does not have a significant effect on macrofauna biomass. The gear-type effect is always significant.

Table 5-5: Simple linear regressions (y = I+mx) between log_{10} transformed macrofauna biomass (y) and 7 environmental predictors (x). For each regression are reported the strength and significance of the Spearman rank correlation, the intercept (I) , slope (m), and gear term (MC) of the linear regression, together with their significance, the overall p-value of the linear regression, the R^2, F value, and residual error. Finally, are reported the significance for the Shapiro-Wilk test of normality, the one for the Breusch–Pagan test of homoscedasticity, and the one for the Moran's test for spatial autocorrelation at global scale, and in the 5 major oceans. All the tests are performed on the residuals of the linear regression.

	Spearman ρ	**Coefficients**		**p-value**	**Adj. R^2**	**F (d.f.=1179)**	**Residual error**	**Normality test**	**Homoscedasticity test**	**Spatial autocorrelation**	
										Global	< 0.001
										Atlantic	< 0.001
		m	-1.71 ***							Pacific	> 0.5
										Indian	< 0.001
										Arctic	> 0.1
										Southern	> 0.5
										Global	< 0.001
										Atlantic	< 0.001
		m	0.59 ***							Pacific	> 0.5
										Indian	< 0.001
										Arctic	> 0.1
										Southern	> 0.5
										Global	< 0.001

	Spearman ρ	Coefficients		p-value	Adj. R^2	F (d.f.=1179)	Residual error	Normality test	Homoscedasticity test	Spatial autocorrelation	
			***							Atlantic	< 0.001
		m	-3.64							Pacific	> 0.5
			***								
										Indian	< 0.001
										Arctic	> 0.1
										Southern	> 0.5
										Global	< 0.001
										Atlantic	< 0.001
		m	-0.0005							Pacific	> 0.5
										Indian	< 0.001
										Arctic	> 0.1
										Southern	> 0.5
										Global	< 0.001
										Atlantic	< 0.001
		m	0.12							Pacific	> 0.5
			***								
										Indian	< 0.001
										Arctic	> 0.1

	Spearman ρ	Coefficients	p-value	Adj. R^2	F (d.f.=1179)	Residual error	Normality test	Homoscedasticity test	Spatial autocorrelation	
									Southern	> 0.5
									Global	< 0.001
									Atlantic	< 0.001
		m	-0.05 ***						Pacific	> 0.5
									Indian	< 0.001
									Arctic	> 0.1
									Southern	> 0.5
									Global	< 0.001
									Atlantic	< 0.001
		m	4.8e-06						Pacific	> 0.5
									Indian	< 0.001
									Arctic	> 0.1
									Southern	> 0.1

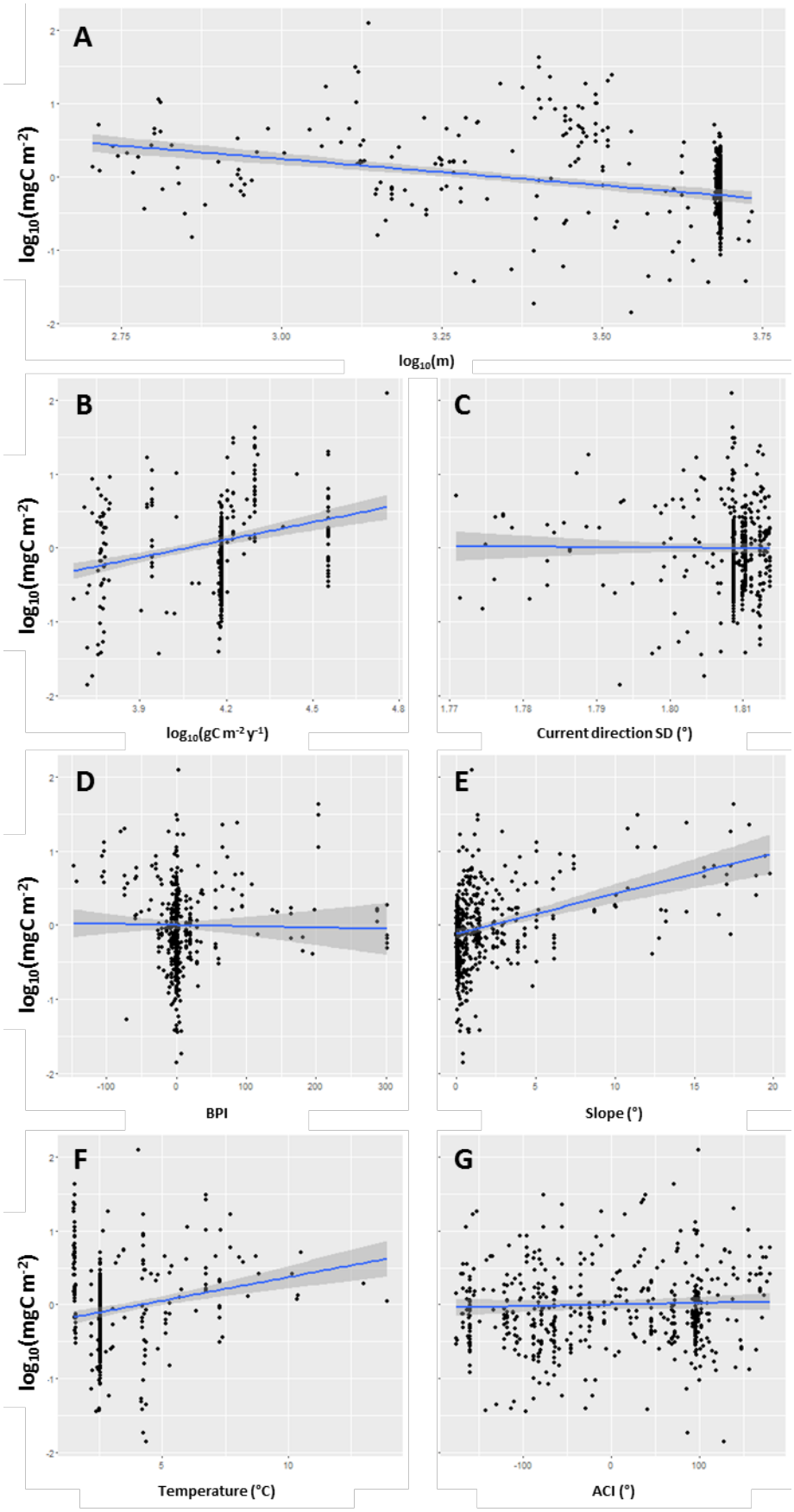

Figure 5-4: The result of 7 linear models (y = I + mx) of megafauna biomass (y, measured as $\log_{10}$(mgC m^{-2})) against 7 environmental variables (x). A) Biomass decreases significantly with depth ($\log_{10}$(m), I = 2.41, m = -0.72, F = 66.68, d.f. = 537, p-value = 2.3e-15). B) Biomass increases significantly with export flux ($\log_{10}$(gC m^{-2} y^{-1}), I = -3.23, m = 0.79, F = 45.79, d.f. = 537, p-value = 3.5e-11). C) The standard deviation of

current direction (°) does not significantly affect megafauna biomass. D) The Bathymetric Position Index (BPI) does not have a significant effect on biomass. E) Biomass increases significantly as slope (°) increases (I = -0.12, m = 0.05, F = 52.03, d.f. 537, p-value = 1.9e-12). F) Biomass increases significantly as temperature (°C) increases (I = -0.26, m = 0.06, F = 26.31, d.f. = 537, p-value = 4.1e-7). G) Aspect-current interaction (°) does not have a significant effect on megafauna biomass.

Table 5-6: Simple linear regressions (y = I+mx) between log_{10} transformed megafauna biomass (y), corrected by sampled area, and 7 environmental predictors (x). For each regression are reported the strength and significance of the Spearman rank correlation, the intercept (I) and slope (m) of the linear regression, together with their significance, the overall p-value of the linear regression, the R^2, F value, and residual error. Finally, are reported the significance for the Shapiro-Wilk test of normality, the one for the Breusch–Pagan test of homoscedasticity, and the one for the Moran's test for spatial autocorrelation at global scale, in the Atlantic and in the Pacific oceans. All the tests are performed on the residuals of the linear regression.

Spearman ρ	Coefficients		p-value	Adj. R^2	F (d.f.=537)	Residual error	Normality test	Homoscedasticity test	Spatial autocorrelation	
	I	2.41183 ***							Global	< 0.001
									Atlantic	< 0.001
									Pacific	< 0.01
	I	-3.2265 ***							Global	< 0.001
									Atlantic	< 0.001
									Pacific	< 0.01
	I	1.2012							Global	< 0.001
									Atlantic	< 0.001
									Pacific	< 0.01
	I	0.0010							Global	< 0.001
									Atlantic	< 0.001
									Pacific	< 0.01

	Spearman ρ	Coefficients		p-value	Adj. R^2	F (d.f.=537)	Residual error	Normality test	Homoscedasticity test	Spatial autocorrelation	
Slope	0.38 ***	I	-0.11716 ***	< 0.001	0.09	52.03	0.36	< 0.001	> 0.5	Global	< 0.001
										Atlantic	< 0.001
										Pacific	< 0.01
		I	-0.2645 ***							Global	< 0.001
										Atlantic	< 0.001
										Pacific	< 0.01
		I	-0.0001							Global	< 0.001
										Atlantic	< 0.001
										Pacific	< 0.01

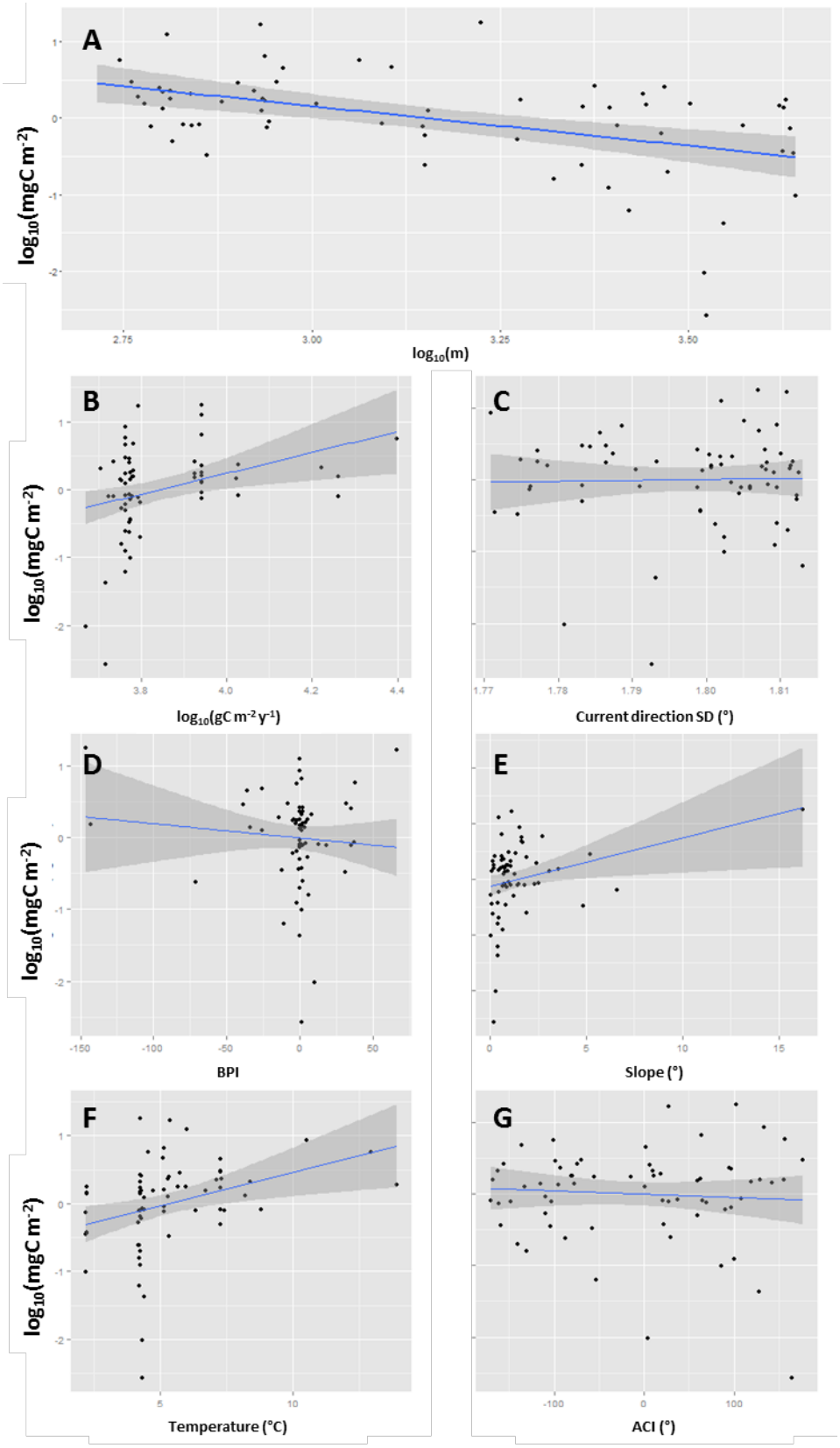

Figure 5-5: The result of 7 linear models (y = I + mx) of fish biomass (y, measured as log_{10}(mgC m^{-2})) against 7 environmental variables (x). A) Biomass decreases significantly with depth (log_{10}(m), I = 3.26, m = -1.04, F = 19.77, d.f. = 65, p-value < 0.001). B) Biomass increases significantly with export flux (log_{10}(gC m^{-2} y^{-1}), I = -5.91, m = 1.54, F = 8.01, d.f. = 65, p-value <0.01). C) The standard deviation of current direction (°) does not significantly affect megafauna biomass. D) The Bathymetric Position Index (BPI) does not have a significant effect on biomass. E) Biomass increases significantly as slope (°) increases (I = -0.12, m = 0.09, F = 5.89, d.f. 65, p-value <0.05). F) Biomass increases

significantly as temperature (°C) increases (I = -0.52, m = 0.10, F = 8.19, d.f. = 65, p-value < 0.01). G) Aspect-current interaction (°) does not have a significant effect on macrofauna biomass.

Table 5-7: Simple linear regressions (y = I+mx) between log_{10} transformed fish biomass (y), corrected by sampled area, and 7 environmental predictors (x). For each regression are reported the strength and significance of the Spearman rank correlation, the intercept (I) and slope (m) of the linear regression, together with their significance, the overall p-value of the linear regression, the R^2, F value, and residual error. Finally, are reported the significance for the Shapiro-Wilk test of normality, the one for the Breusch–Pagan test of homoscedasticity, and the one for the Moran's test for spatial autocorrelation at global scale and in the Atlantic ocean. All the tests are performed on the residuals of the linear regression.

	Spearman ρ	**Coefficients**		**p-value**	**Adj. R^2**	**F (d.f.=65)**	**Residual error**	**Normality test**	**Homoscedasticity test**	**Spatial autocorrelation**	
		I	3.2648 ***							Global	> 0.5
		m	-1.0352 ***							Atlantic	> 0.5
		I	-5.9107 **							Global	> 0.1
		m	1.5372 **							Atlantic	> 0.5
		I	-2.289							Global	> 0.1

	Spearman ρ	Coefficients		p-value	Adj. R^2	F (d.f.=65)	Residual error	Normality test	Homoscedasticity test	Spatial autocorrelation	
		m	1.273							Atlantic	> 0.5
		I	-0.0066							Global	> 0.1
		m	-0.0020							Atlantic	> 0.5
		I	-0.1229							Global	> 0.5
		m	0.0870 *							Atlantic	> 0.5
		I	-0.5226 *							Global	> 0.5
		m	0.0986 **							Atlantic	> 0.5
		I	-0.005							Global	> 0.1
		m	-0.0005							Atlantic	0.9

5.3.1 Vertical input of food determines biomass reduction with depth and towards oligotrophic areas.

As expected, an increase in depth causes a reduction in the biomass: this is significant in the linear regressions for all the assemblages (Table 5-3, Table 5-4, Table 5-5, Table 5-6 and Table 5-7, Figure 5-2, Figure 5-3, Figure 5-4 and Figure 5-5), and in the GAMs of meio and macrofauna.(Table 5-2, Figure 5-6). The GAM suggests that this effect is weakest for the meiofauna. An increase in food availability (export flux) has a positive effect on standing stock, but this is not significant for macrofauna and fish assemblage according to the GAMs. The effect of water temperature is negative for macrofauna and positive for the other three assemblages. While this is quite likely an effect of the collinearity between depth and temperature, which is generally warmer at shallower sites, the Spearman rank correlation between these two predictors is above 0.7 only for fish (ρ = 0.9). In addition, the GAMs suggest that the strongest decrease of biomass with temperature takes place at a different temperature range for the different assemblages: ~10 °C for meiofauna, 3-7 °C for macrofauna and below 5 °C for megafauna invertebrates and fish. This could reflect the effect of different metabolic rates for different mean body sizes and temperatures, as suggested by the MTE.

When considering all the predictors together (multiple regressions, Table 5-3), some interactions between the predictors are significant. A positive interaction between depth and export flux highlights that an increase in surface export reduces the negative effect of depth on meiofauna biomass (Table 5-3). Conversely, macrofauna biomass is significantly affected by a negative interaction of water temperature with both export flux and depth; this latter interaction is also the strongest factor in the macrofauna scaled regression (coefficient = -29.52). The interaction between temperature and depth, and temperature and export flux, means that as temperature increases the effect of depth and input of nutrients become more negative. Furthermore, depth, export flux and temperature together affect the macrofauna biomass with a significant positive interaction, suggesting that by increasing one of these three predictors the effects of the others increase as well.

5.3.2 At fine scale, biomass is focussed on steeper slopes and local maxima of the bathymetry.

The biomass of all four assemblages increases significantly as slope increases (significant simple linear regressions for all assemblages, significant slope terms for meio macro and megafauna invertebrates in the multiple regressions, and significant effect of slope in the GAM for meio and macrofauna assemblages). Slope is also the strongest predictor affecting the meiofauna standing

stock, as shown by a coefficient of 18.74 in the scaled multiple regression. Macrofauna standing stocks decrease as current direction becomes more variable. The GAM highlights a significant effect of current direction variability also for the megafauna biomass, nevertheless it was not possible to detect the trend of this effect even when testing simple linear models on smaller ranges of the direction SD predictor. The GAM also highlights significant non-linear effects of BPI and aspect-current interaction on the megafauna standing stock, which decreases from the local minima of the bathymetry towards the flat areas (negative BPI, coeff. : -0.006, p-value <0.001), while it then increases towards the local maxima of the bathymetry (coeff.: 0.002, p-value <0.05); megafauna also decreases when the interaction of current with slope direction is negative (from -180 to -80, coeff. : -0.004, p-value <0.05), while it is constant for the rest of the predictor's range.

All the assemblages, apart from fish, are affected by a negative interaction between slope and current direction variability, suggesting that at steeper slopes the variability of current direction plays a stronger negative effect than on flat areas. Furthermore the strongest effect on megafauna biomass is played by the interaction between BPI and slope (scaled coefficient = 111.54), suggesting that, in steep areas, the effect of relative elevation also becomes more positive. Finally, a negative interaction between BPI, slope and current direction variability is significant for megafauna, and it also plays the strongest effect, although not significant, in the fish regression (scaled coefficient = -181.43).

The effect of the gear type was significant only for macrofauna, therefore the other assemblages have not been corrected for this effect. MC samples have significantly higher biomass than BC_GR ones at shallow depths, and less at deeper depths. This results in steeper regression slopes against depth, export flux and temperature, while the regression slopes are similar for the regression with aspect-current interaction, current direction SD and slope steepness.

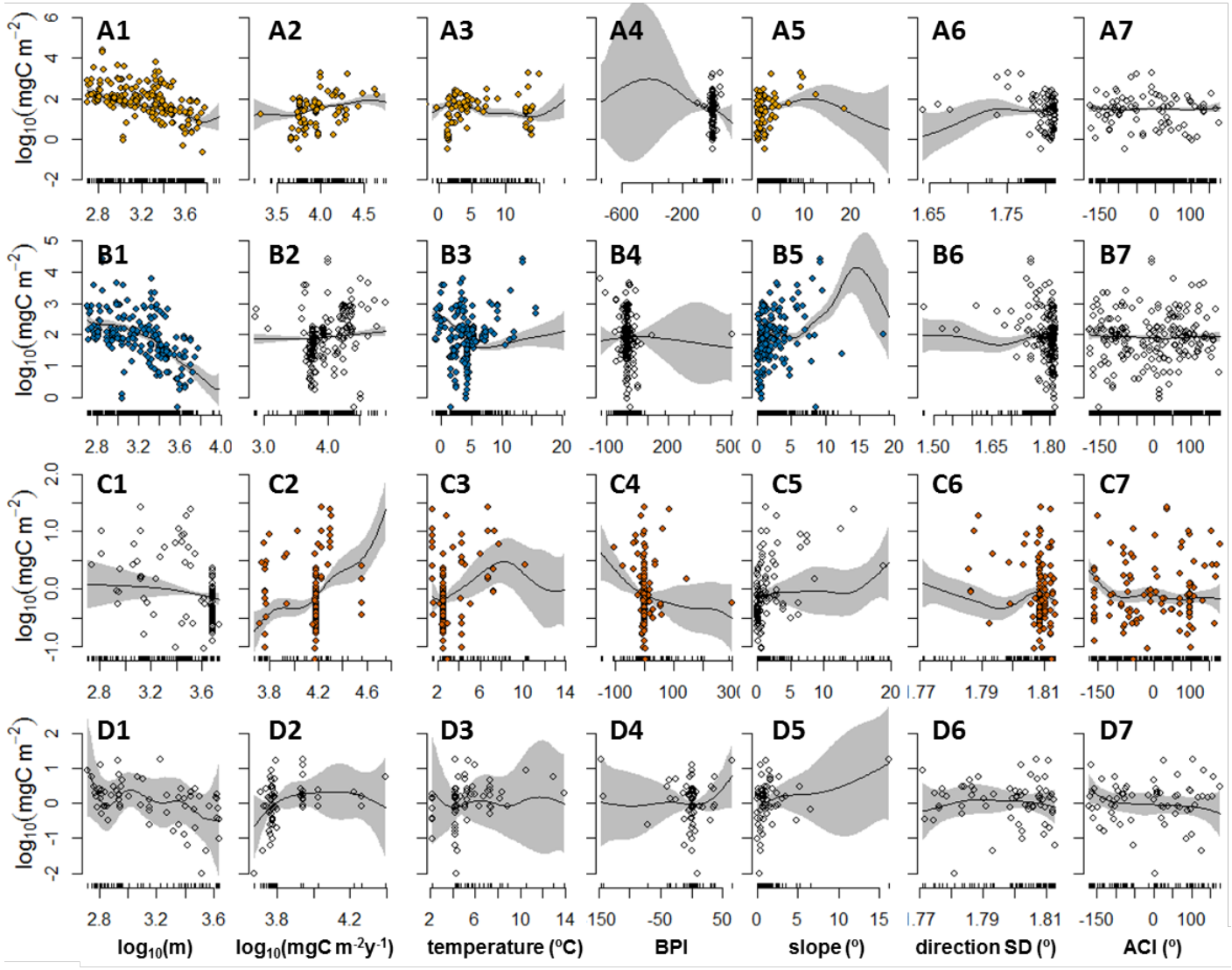
A1
A2
A3
A4
A5
A6
A7
B1
B2
B3
B4
B5
B6
B7
C1
C2
C3
C4
C5
C6
C7
D1
D2
D3
D4
D5
D6
D7
log10(mgC m-2)
log10(m)
log10(mgC m-2y-1)
temperature (°C)
BPI
slope (°)
direction SD (°)
ACI (°)

Figure 5-6: results of the Generalised Additive Models (GAMs) for meiofauna (A), macrofauna (B) megafauna (C) and fish (D) biomass measured as $log_{10}(mgC\ m^{-2})$. The GAMs include 7 explanatory variables: depth (column 1, measured in $log_{10}(m)$), export flux from the surface (column 2, measured in $log_{10}(gC\ m^{-2}\ y^{-1})$), temperature (column 3, measured in °C), Bathymetric Position Index (BPI, no dimensions, column 4), slope steepness (column 5, measured in °), standard deviation of current direction (column 6, measured in °), aspect-current interaction (column 7, measured in °). The GAMs were performed on a training set of data including 75% of the records, while the remaining 25% was used for testing. In each panel, the black line represents the predicted biomass value, the grey area represents the 95% confidence interval, the circles are the datapoints from the testing dataset, not used for the creation of the GAMs. Coloured circles identify significant relationships.

Table 5-8: Spearman rank correlations for meiofauna and macrofauna. The strength of the correlations (ρ) is reported, and significant correlations are in bold.

Meio \ Macro	Mass	Depth	Export flux	Direction SD	BPI	Slope	Temperature	AC interaction
Mass		**0.541**	**0.499**	**-0.346**	-0.024	**0.248**	**-0.279**	-0.02
Depth	**0.432**		**0.33**	**-0.358**	0.04	**0.201**	**0.249**	0.043
Export flux	**0.389**	**0.312**		**-0.226**	0.031	0.028	**-0.261**	-0.02
Direction SD	-0.083	**-0.105**	0.046		0.029	**-0.22**	**0.157**	0.039
BPI	**-0.149**	-0.018	-0.026	0.026		-0.042	-0.037	**0.141**
Slope	**0.221**	**0.245**	0.039	**-0.129**	**-0.134**		**0.062**	**-0.065**
Temperature	0.013	**0.449**	**0.13**	**0.298**	0.079	-0.03		0.023
AC interaction	0.037	0.067	-0.052	-0.062	**0.256**	-0.057	-0.001	

Table 5-9: Spearman rank correlations for megafauna and fish. The strength of the correlations (ρ) is reported, and significant correlations are in bold.

Mega \ Fish	Mass	Depth	Export flux	Direction SD	BPI	Slope	Temperature	AC interaction
Mass		**0.529**	**0.294**	**-0.259**	-0.059	**0.237**	**0.38**	0.008
Depth	**-0.224**		0.073	-0.195	0.047	**0.536**	**0.901**	0.071
Export flux	**0.527**	**0.122**		0.121	-0.025	-0.126	0.044	-0.04

Mega \ Fish	Mass	Depth	Export flux	Direction SD	BPI	Slope	Temperature	AC interaction
Direction SD	**0.324**	-0.004	**0.259**		0.046	-0.089	**-0.278**	-0.006
BPI	0.012	**0.311**	**0.153**	0.073		-0.104	0.003	0.153
Slope	**0.131**	**0.641**	**0.262**	**0.382**	**0.139**		**0.534**	0.145
Temperature	**-0.513**	**0.286**	**-0.374**	**-0.222**	**-0.089**	**-0.09**		0.078
AC interaction	0.003	**0.091**	**0.087**	-0.041	0.054	0.021	**0.116**	

5.4 Discussion

Models for the distribution of four benthic assemblages along gradients of 7 environmental variables have been provided: three predictors were linked to the regional effects related to the vertical sinking POC flux food supplies, and four were linked to the focussing of benthic biomass on sub-degree topographic features. These are the highest spatially resolved estimates for the global seafloor to date, and provide a useful tool for assessment, planning and model development, both for biologists and earth system modellers.

5.4.1 At global scale, benthic biomass is controlled by food supply and temperature.

The biomass of all the assemblages decreased significantly with depth when tested in one way linear models, a common trend in benthic biomass distribution (Rex et al. 2006). A biomass reduction with depth was detected also in the multiple regressions (but significant only for meiofauna) and in the GAMs (significant for meio- and macrofauna). Such a trend, nevertheless, does not imply a causal relationship between biomass and depth, in fact depth is widely considered as a proxy for vertical POC input (Lutz et al. 2002, Lutz et al. 2007). This sinking food supply is produced in the euphotic layer of the ocean and, in the models, is included as 'export flux' or the amount of organic carbon that leaves the surface ocean (Henson et al. 2011). Here the effect of food availability and biomass is captured in the interaction term between depth and export flux in the multiple linear regressions. This is positive and significant for the meiofauna multiple regression, suggesting that the negative effect of depth on biomass becomes weaker in areas of higher export flux. Strongly seasonal areas, such as the northeast Atlantic or the Southern ocean (240 g C m^{-2} y^{-1} and 398 g C m^{-2} y^{-1} respectively) can therefore be expected to have a standing stock reduction with depth than oligotrophic areas such as the sub-tropical gyres (~100 g C m^{-2} y^{-1})(values from Longhurst et al. 1995).

Seafloor temperature is a covariate of depth as it is higher at the surface where the ocean is heated by the sun (Spearman rank correlation coefficient (ρ) is 0.449 for locations with meiofauna data (Table 5-8), 0.249 for macrofauna (Table 5-8), 0.286 for megafauna (Table 5-9), and 0.901 for fish (Table 5-9)). As a consequence the negative effect of temperature on biomass could be masked by the effect of depth, especially in the megafauna and fish regressions for which the number of observations is lower (n = 511 and 76 respectively). It should be noted that, in the multiple regression for the macrofauna, depth and temperature have a significant positive interaction which shows that the decrease of biomass with depth gets stronger when bottom water temperatures are higher. This agrees with the drastic decrease of benthic biomass with

depth recorded in the warm waters of the eastern Mediterranean Sea (Tselepides and Lampadariou, 2004), included in the macrofauna dataset used here. Temperature also negatively interacts with export flux; this suggests that as temperatures get warmer the positive effect of export flux on macrofauna biomass gets weaker as well, further supporting the finding of low deep sea biomass in the Mediterranean, which has warm waters and low primary production (~200 g C m^{-2} y^{-1}, Longhurst et al. 1995).

In addition, temperature is known to have a causal relationship with biomass: as temperature increases, metabolic rates increase and therefore a smaller fraction of the available energy can be used for growth and reproduction, with a negative effect on whole community standing stocks (Brown et al. 2004, Clarke and Fraser 2004). The significance of the temperature factor results from the simple and multiple linear regressions is weak, and as only macrofauna biomass decreases significantly as temperature increases (Table 5-4, Table 5-5, Table 5-6 and Table 5-7, Figure 5-2, Figure 5-3, Figure 5-4 and Figure 5-5), while a significant effect of temperature on biomass is picked up by the GAMs of meio-, macro and megafauna.

The close interaction between the effects of depth, temperature and food input have led to predictions of up to 5% of benthic biomass reduction globally under likely scenarios of climate change (Jones et al. 2014). In fact, a likely increase in surface primary production, being localised in the shelf seas and in the Arctic Ocean, would not be enough to counteract the increase in remineralisation in the water column (Yool et al. 2017), caused by the higher water temperatures, and the consequent reduction of POC flux. In such a scenario, general reductions of mean body sizes are also likely (Gardner et al. 2011, Jones et al. 2014), as well as localised reductions in diversity or range shifts, as more marine species will be exposed to temperature ranges outside their thermal optimum (Yasuhara and Danovaro 2016).

5.4.2 Some signals of local biomass focussing at topographic features detected in a global dataset.

The models here were aimed at improving existing benthic biomass standing stock estimates by introducing the effect of seafloor morphology. The results of simple linear regressions show that biomass of all the targeted assemblages increases with slope, as suggested also by the biomass distribution around small abyssal hills (Morris et al. 20016, and Chapter 4), and the density of deposit feeders at offshore Pacific seamounts (McClain and Lundsten 2014). While this effect is likely a consequence of the higher exposure of slopes to current-mediated lateral inputs of sediments, there are also reasons to suggest that organic carbon is removed from the steepest slopes in favour of the deeper flatter areas (Chapter 2, Chapter 3 and Zeppilli et al. 2014).

The range of slopes sampled in the available dataset was small (0°-22°), therefore, the global scale models here are currently missing the tendencies of biomass in steeper areas. Extending the range of slopes from which the samples are collected could be challenging, as a consequence of limitations related to the sampling gear. Coring for meio- and macrofauna collection in rough terrains or on very steep slopes can be challenging for traditional corers or grabs, and similarly, trawling for megafauna and fish collection is limited by terrain morphology, as suggested by the maximum slope of only 15° in the fish dataset used here.

Remotely operated vehicles (ROVs) and hover class autonomous underwater vehicles (AUVs) are a good alternative sampling platform. They have been used to sample slopes steeper than 30°, and cliffs (Bell et al. 2016), and can collect sediment cores targeting very specific types of seafloor morphology and substrate type. Furthermore, flight class AUVs are effective for surveying very large areas at fine resolution, to investigate the megafauna distribution, as demonstrated by the AESA project (Morris et al. (2014), Morris et al. (2016) and in Chapter 4). Additionally, photographic surveys allow recording the effect of substrate type, which was not included in this exercise. Indeed most of the sampling here was necessarily limited to soft sediments by the gear types. Meio- and macrofauna, which mostly live in the sediments, are likely to have less biomass in areas where rocky substrates are predominant, while sessile megafauna and suspension feeders are likely to be favoured in such habitats (Jones et al. 2013). Both the trends of biomass with slope and BPI recorded were likely affected by substrate type, nevertheless substrate type could not be accounted for in the statistical modelling.

The effect of sediment removal from steep slopes can potentially result in higher biomass at the bottom of such slopes, as suggested by the high nematode biomass recorded at the bottom of Condor seamount (Zeppilli et al. 2014).

It should be noted that, since the global slopes layer used here has a 30 arc-seconds resolution, which at the equator equals a resolution of about 1000 m, the slope value does not directly relate to the inclination of the seafloor in the sampling location, but rather to whether the area around it at the scale of the grid cell is flat or not. As a consequence, the slope value here could be considered as the amount of sediment transport generally happening through the area, in which case a steeper slope could be linked to a more frequent lateral transport of the organic carbon and/or increased nutrient flux.

Only megafauna biomass followed a significant non-linear trend with the BPI while the other assemblages showed no effect from this variable. An increase in BPI had previously been linked to an increase in phytodetritus coverage and megafauna biomass around small abyssal hills (Morris et al. 2016) and to megafauna biomass in northeast Pacific seamounts, being more dominant than

any negative effect of slope (Chapter 3). The notion that elevated areas are more exposed to hydrodynamic activity, and therefore to elevated particle fluxes, is well established thanks to observations of megafauna (Genin et al. 1986, Thresher et al. 2011) and some observations of macrofauna (Chivers et al. 2013). Nevertheless, the phenomenon was only rarely addressed in a quantitative way.

Similarly, to slopes, there are also discrete examples of how BPI can affect local particulate organic matter distribution and biomass distribution of all assemblages. Three surveys which specifically targeted the megafauna distribution around topographic features where added in the global dataset (Alt 2012, Alt et al. 2013, Chapter 3 and Chapter 4), while the same was not done for the other assemblages, which is possibly why most models here have not detected links between BPI and biomass. The effect of abrupt topography on water circulation and sediment deposition patterns has been examined, and in particular the formation of asymmetric current flow fields which result in food focussing on the downstream side of the seamounts (Turnewitsch et al. 2004, Bashmachnikov et al. 2013). These processes are believed to be a consequence of the obstruction posed by seamounts to low and high frequency movements of water masses, and therefore to be globally widespread (Turnewitsch et al. 2013). Furthermore, seamounts with shallow summits could also interact with the physics and biology of the surface layers of the ocean, having a positive effect on primary production and export that would affect also the area surrounding the seamount itself (Turnewitsch et al. 2016). The models did not detect a signal of these processes in the meio-, macrofauna and fish assemblages, therefore a specific sampling design could be devised to detect the effects of specific current movements on these groups of benthic fauna, and to clarify the effect on megafauna.

5.4.3 Caveats to the performance of the statistical models.

The residuals of the macrofauna multiple regression had a non-normal distribution, and only the residuals of the fish multiple regression were homoscedastic. This is likely a consequence of the mix of datasets analysed. The varied type of collection methods results in non-random patterns in the biomass measurements that, nevertheless, are not well understood and therefore cannot be corrected for. Furthermore, all the residuals, both from the multiple regressions and from the GAMs, showed a high degree of spatial autocorrelation. This suggests that, even if metrics for the morphology of the seafloor at fine scale (30 arc-seconds) are introduced the models are not able to explain fully the variability in the biomass distribution. A possible way to avoid these issues would be to design a more standardised method of biomass collection, in which environmental variables that have an effect at sub-kilometre scale such as substrate type are accounted for in a

stratified design. Overall, the level of spatial autocorrelation still present in the residuals after having applied the models means that the model predictions should be interpreted with care.

5.4.4 Spatial analysis.

For a comparison between the different models, biomass has been predicted for the area between 30°-40° N, and 130°-120° W, in the northeast Pacific, and between 40°-50° N and 20°-10° W in the northeast Atlantic. In the Pacific sector, the biomass predicted with a model based on water characteristics (Wei et al. 2010) is 1.8 $\log_{10}$(mgC m^{-2}) for meiofauna, 1.4 $\log_{10}$(mg C m^{-2}) for macrofauna, 1.1 $\log_{10}$(mg C m^{-2}) for megafauna and 0.6 $\log_{10}$(mg C m^{-2}) for fish (Table 5-10a). While the multiple regression presented here predicts a mean biomass that is many orders of magnitude higher, the prediction from the GAMs are similar for the meiofauna and macrofauna (1.9 and 2.1 $\log_{10}$(mg C m^{-2}) respectively) (Table 5-10a). The mean difference across the Pacific sector between Wei et al. (2010) predictions and new fine predictions (30 arc-seconds resolution, calculated as the averaged pixel-by-pixel difference among the two maps) is always < |0.2| orders of magnitude, apart from the multiple regression for macrofauna which is on average 0.9 $\log_{10}$(mg C m^{-2}) lower according to the multiple regression, and for the megafauna which is 1.2 $\log_{10}$(m gC m^{-2}) higher in the multiple regression, and 1.1 $\log_{10}$(mgC m^{-2}) higher in the GAM.

In the northeast Atlantic previous biomass predictions at 1° resolution were of 1.6, 1.8, 1.2 and 0.6 $\log_{10}$ (mg C m^{-2}) for meio-, macro-, megafauna and fish respectively. The predictions with the multiple regression presented here are extremely high, while the GAM models for meio- and macrofauna are of 1.7 and 1.9 $\log_{10}$(mg C m^{-2}) respectively, and the total biomass predictions for the area are similar as well (Table 5-10b). The mean difference between existent and new predictions of meiofauna, macrofauna and fish across the Atlantic sector is low both for the multiple regressions and for the GAMs (< |0.52| $\log_{10}$(mg C m^{-2})), while for megafauna it is a bit higher (1.4 and 1.6 $\log_{10}$(mg C m^{-2}) in the multiple regression and in the GAM respectively).

At global scale, Wei et al. (2010) predicted a total of 110 Mt C (all the assemblages included). Predictions presented here are orders of magnitude higher, probably because of the small range of slopes and BPI included in the dataset, and of the small number of observations especially in the megafauna and fish models. The dataset used here included only the samples collected in waters deeper than 500 m, and the model predicts 55 Mt C in meio- and macrofauna together in this area, against 33 Mt C predicted by Wei et al. (2010) for the same depth range. The similarity between these two predictions suggests that , within the range of environmental variables included in the model, the results are relatively accurate, also considering that, for the above

mentioned Pacific and Atlantic sectors, the coefficient of variation of Wei et al. (2010) predictions are between 2 and 10%.

The models presented here have a much higher spatial resolution and thus variability than the model of Wei et al. (2010). In fact, the multiple regressions predict extremely low and high minimum and maximum values, possibly because linear models are not robust towards extrapolations outside the range of the predictors. The GAMs' predictions are more constrained, but still higher than the ranges predicted by Wei et al. (2010) (Table 5-10).

The model spatial extrapolations have 120 times more resolution (30 arc-seconds) than previous ones (1 degree in Wei et al. 2010). The ht-index, a measure of the scaling structure of the features in a map (Jiang and Yin 2014), is used to define the orders of complexity (fractal dimension) of the biomass spatial extrapolations: this is a measure of the complexity of the patterns of a map. In the northeast Pacific the outputs have generally a higher ht-index than previous predictions apart from fish, for which it is lower both in the multiple regression and in the GAM; the difference is also small for the megafauna GAM, which has an ht index of 3 while it was 2 in the previous prediction (Table 5-10). For meio- and macrofauna, instead, the ht-index is much higher in the new predictions. In the northeast Atlantic the previous predictions had low scaling structure (max ht-index = 4 for the meiofauna), while the predictions presented here have very high ht-index (> 10). These results show that the introduction of seafloor morphology metrics has produced the desired result of increasing the variability in the spatial predictions.

While the improved estimation of biomass at higher spatial resolution was an aim of this modelling exercise, the predictions obtained are promising, but clearly have extreme values. The likely reason for this is that the dataset used did not cover well enough the range of topographic features that are found globally. In particular, the range of slopes in the dataset is small (0°-22°, and most samples are from below 5° of slope) in comparison to the global slopes predictions used for the spatial extrapolations of the models (0°-87°). On the other hand the advantage of using multiple regressions and GAMs in predictive modelling, rather than Random Forests (Wei et al. 2010), is that these are not black boxes: the mechanistic understanding of the ecology of benthic communities can be used to inform model selection and interpretation. The models presented here provide a first step in the direction of a full resolution global model of benthic biomass distribution in relation to topographic features, nevertheless more targeted sampling designs will be needed to improve their predictive power.

5.5 Conclusions

The benthic biomass of meio-, macro-, megafauna and fish assemblages was investigated globally in relation to the morphology of the seafloor. While most data used here was not originally collected with an interest in investigating the relationship between biomass and topographic features, some of the trends detected in the local case studies (chapters 3 and 4) arise also at global scale, such as the positive effects on biomass of slope. Overall, depth, export flux and temperature remain the most important factors in determining biomass distribution globally; nevertheless, the fact that weak trends of biomass with topography metrics can be detected in a dataset that was not collected for this purpose suggests that great improvements can be made in this field, to better understand standing stock distributions in the deep sea.

Table 5-10: Summary of the model's spatial extrapolations in the area between 30°-40° N, and 130°-120° W in the northeast Pacific (A), and between 40°-50° N and 20°-10° W in the northeast Atlantic (B). For each model are reported the minimum, 1st quartile, mean (standard deviation), median, 3rd quartile and maximum value, together with the total mass (log_{10}(mgC m^{-2}) predicted for the area. The comparison between the proposed models and published ones (Wei et al. 2010) is made by using the ht-index, a measure of the scaling structure of the features in a map (Jiang and Yin 2014), and the mean difference between the existing models (Wei et al. 2010) and the new ones for the same assemblages.

	Min	1st quartile	Mean	(SD)	Median	3rd quartile	Maximum	Total mass	ht-index	Mean difference	(SD)
A)											
Meiofauna (Wei et al. 2010)	0.8	1.0	1.8	(0.0004)	1.6	1.8	2.7	13.7	0		
Macrofauna (Wei et al. 2010)	0.6	0.8	1.4	(0.0004)	0.9	1	2.5	13.4	NA		
Megafauna (Wei et al. 2010)	0.4	0.6	1.1	(0.0005)	0.8	1.1	2	13.1	2		
Fish (Wei et al. 2010)	-0.3	-0.1	0.6	(0.0004)	0.2	0.7	1.5	12.6	1		
Meiofauna – multiple regression	-92.7	1.3	113.5	(0.0004)	1.6	1.9	119.6	125.4	10	-0.08	(0.0003)
Macrofauna – multiple regression	-647.5	2.2	Inf	(0.003)	2.3	2.4	1725	Inf	9	-0.89	(0.003)
Megafauna – multiple regression	-107	-0.6	105.1	(0.0005)	-0.4	-0.2	111.2	117.1	11	1.24	(0.0005)
Fish – multiple regression	-2831	-0.1	Inf	(0.004)	0.5	1.2	609.2	Inf	0	-0.19	(0.004)

	Min	1st quartile	Mean	(SD)	Median	3rd quartile	Maximum	Total mass	ht-index	Mean difference	(SD)
Meiofauna – GAM	-21.7	1.2	1.7	(0.0003)	1.5	1.7	4.2	13.6	13	0.03	(0.0003)
Macrofauna – GAM	-17.8	1.4	2.1	(0.0003)	1.5	1.7	5.0	14.1	15	-0.04	(0.0004)
Megafauna – GAM	-7.3	-0.5	5	(0.0004)	-0.4	-0.004	11.1	16.9	3	1.13	(0.0003)
Fish – GAM	-3.6	0.06	75.6	(0.0005)	0.3	0.5	81.7	87.6	0	0.07	(0.0008)
B)											
Meiofauna (Wei et al. 2010)											
Macrofauna (Wei et al. 2010)	1.2	1.5	1.8	(0.0002)	1.8	1.9	2.4	13.7	0		
Megafauna (Wei et al. 2010)	1.1	1.2	1.3	$(7{\cdot}10^{-5})$	1.2	1.3	1.5	13.2	NA		
Fish (Wei et al. 2010)	0.2	0.4	0.6	(0.0002)	0.5	0.7	1.4	12.6	4		
Meiofauna – multiple regression	-42.6	1.6	20.8	(0.0002)	1.7	1.8	26.9	32.7	0	-0.09	(0.0002)
Macrofauna – multiple regression	-373.8	1.9	Inf	(0.002)	2.1	2.2	636.7	Inf	10	-0.51	(0.001)
Megafauna – multiple regression	-16.1	-0.3	98.4	(0.0004)	-0.2	-0.02	104.5	110.3	11	1.35	(0.0003)

	Min	1st quartile	Mean	(SD)	Median	3rd quartile	Maximum	Total mass	ht-index	Mean difference	(SD)
Fish – multiple regression	-1110	0.6	Inf	(0.003)	0.9	1.2	1258	Inf	0	-0.17	(0.003)
Meiofauna – GAM	-9.9	1.4	1.6	(0.0002)	1.5	1.7	3.8	13.6	14	0.06	(0.0003)
Macrofauna – GAM	-19.1	1.1	1.8	(0.0003)	1.3	1.4	4.5	13.8	14	0.31	(0.0004)
Megafauna – GAM	-2.1	-0.5	6	(0.0002)	-0.3	-0.2	12	17.9	12	1.57	(0.0002)
Fish – GAM	-1.5	-0.2	31.7	(0.0004)	0.01	0.2	37.8	43.6	12	0.49	(0.0004)

Chapter 6: Thesis conclusions

6.1 Results summary.

The primary goal of this thesis was to investigate the distribution of deep benthic biomass in relation to seafloor morphology. The information gained from this approach increases our understanding of seafloor ecology, and therefore can be used towards a series of applications such as the creation of tools for survey planning and management of seafloor resources, as well as developing further benthic ecological models, also in relation to global carbon cycling models.

Throughout the chapters, topographic features of different type and size have been investigated to highlight the effects of topography on benthic biomass distribution at different scales. In Chapter 2, evidence for the validity of the gravitational lateral sediment transport theory in hadal trenches has been provided through the development of a computer model. Depending on the efficiency of lateral transport, biomass in hadal trenches can be expected to be up to two orders of magnitude higher than if lateral transport was not taken into account. Since the publication of this piece of research (Ichino et al. 2015) some evidence has been collected, suggesting that ΔS (the measure of 'slope budget' used in Chapter 2 as a metric to explain biomass focussing) is the best explanatory variable to explain infauna biomass distribution at six sites in two trenches (Leduc and Rowden, 2017).

In Chapter 3 and Chapter 4 the theory of gravitational sediment transport has been tested in three locations, where currents are also believed to have an effect. The results show that gravity and currents interact with different strengths, depending on different environmental conditions. In particular, slope steepness appears to be a factor in determining whether organic sediments are mostly transported downslope, or with currents towards more exposed areas. When the slopes are gentle, such as in a small abyssal hill (Chapter 4), more biomass is found at the top of the feature. When the slopes are steep, nevertheless, the pattern of food deposition can change and more organic particles could flow gravitationally towards the deeper parts of the feature (as suggested by some tests in Chapter 3). Therefore, introducing seafloor morphology metrics such as slope and BPI can improve the accuracy of benthic biomass distribution predictions, and increase their spatial resolution. In the future, efforts could be directed towards better estimating the biomass and towards finer characterization the seafloor morphology, especially targeting potential spatial mismatches between the environmental predictors.

Finally, in Chapter 5 topographic metrics have been used to investigate the distribution of four benthic assemblages at global scale. The correlations that have been found, while weak, suggest

that the effect of topography on biomass can be significant at global scale; therefore, introducing topography in predictive models for biomass distribution can improve their spatial resolution. Also, the extremely high values of biomass predicted, mostly, by the multiple regression approach suggested that non-linear statistical models are better suited at predicting values outside the investigated areas and outside the value range covered by the independent variables (slope and BPI in this case).

6.2 Dataset limitations.

The case studies at the Pacific seamounts and at the Atlantic abyssal hill demonstrated the applicability of the methodology, and gave a new insight into the effect of seafloor morphology when tested on individual topographic features. The datasets used in those chapters, and especially the one collected with Autosub6000 (Chapter 4) were collected with the aim of investigating the effects of the topography on the seafloor community. On the contrary, the dataset used for the global study (Chapter 5) was not originally collected with such a study in mind. The main consequence of this is that the samples are not representative of the full range of topographic features that can be found across the ocean seafloor. While canyons are totally absent from the dataset, and therefore have not been addressed in the thesis, some data from slopes, seamounts and (non-hadal) trenches were present. Others have been added, including the ones used in Chapter 3 and Chapter 4. Nevertheless the resulting dataset covered only a small range of slope and BPI values, and within the small ranges sampled, the extreme values were under-represented. While it was still possible to detect some effects of seafloor morphology, such as the positive correlation between slope and biomass, the errors in the predictions are very high because of this limitation, reducing the predictive power of the models at global scale. The predictive power (R^2) of meio- and macrofauna models is higher than for the other assemblages, potentially because of the higher number of data points. This results in biomass predictions more similar to those presented by Wei et al. (2010).

All the datasets could be improved by including more samples, which specifically target topographic feature gradients. These are common in the literature nevertheless, since the interest is generally directed towards investigating diversity and community structure, biomass is generally either not measured or not reported. Including biomass measurements in benthic surveys, which target meio and macrofauna, would greatly help towards improving our understanding of benthic ecology, without greatly increasing the costs of the investigation. While megafauna biomass measurements had been limited by technical constraints for a long time, it is now becoming more precise and easier to obtain, thanks to the advent of automated photographic surveys and the improvements made in estimating individuals' biomass from their

size (Durden et al. 2010). Furthermore, the advancements made in machine-learning techniques and image recognition allow processing very large picture datasets at a fraction of the cost (both in terms of time and money), allowing to extend the spatial scale and resolution of the surveys.

To simplify even further both the sample collection and the modelling, the Metabolic Theory of Ecology could be included explicitly in the models. The scaling of metabolic processes such as respiration, growth and mortality with temperature and body size has suggested that standing stocks of the whole assemblage could be inferred by the measurement of just a small portion of it Brown et al. 2004). The bulk of the biomass is generally constituted by the larger organisms; a good estimate of the megafauna biomass, together with accurate measurement of *in-situ* temperature and total POC flux (lateral and vertical inputs) would potentially allow for inferring the biomass of smaller size classes (meio- and macrofauna).

6.3 Recommendations for future research

Overall, further improvements to the estimation of global benthic biomass can be achieved through new targeted sampling. This additional data from remote and invisible parts of the planet's biome, increase our understanding of benthic processes not only in relation to ecosystem conservation but also to climate modelling (Yool et al. 2017). The present work has highlighted various significant trends of biomass with topography, at local and global scales, which are considered as proxy of local lateral redistribution of organic sediments. These effects are weaker than the large scale effects of export flux and depth, nevertheless they appear to be relevant at a local scale, when specific topographic features of different size have been investigated. The Generalized Additive Models presented in this thesis have suggested the presence of some non-linear correlations between biomass and topography. Future investigations should aim at mechanistically determining the types of non-linear correlation and, in particular, they should investigate more in depth the presence of thresholds, such as the one in the slope-biomass correlation that appeared in this study, and the current speed that causes sediment resuspension of phytodetritus. Furthermore, the multiple linear regressions presented here, have highlighted the presence of numerous significant interactions among topographic metrics. In the future, non-linear trends and interactions should be addressed together by using General Linear Models instead. For these to be effective, targeted surveys are required.

Firstly, the trend of biomass with slope steepness should be investigated. Biomass seems to increase as slope gets steeper (as seen in chapters 3, 4 and 5), nevertheless some evidence suggests that biomass decreases at steeper slopes (Figure 3-6c). This trend could change among different size classes and feeding types, and it could be affected by the type of substrate (hard or

soft). In addition, the interaction of slope with BPI and currents should be further investigated. In order to target areas with different current regimes, global NEMO current estimates could be used, together with non-hydrostatic modelling at sub-km scale in areas with complex topography. Accurate, prolonged, measurements of current direction and intensity should then be included in the surveys.

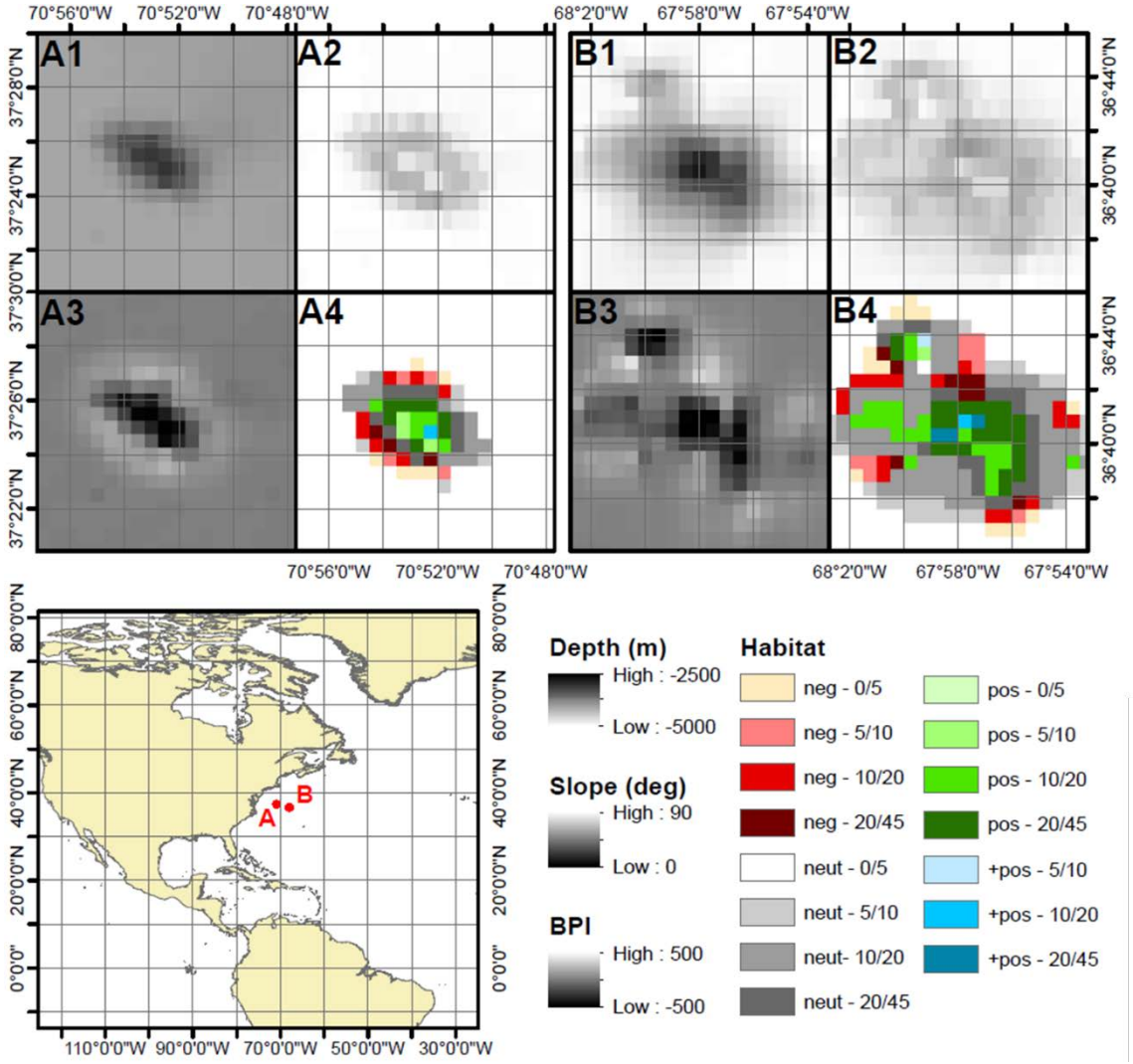

Figure 6-1: Example of survey design, aimed at investigating the effect of depth, slope, BPI, and vertical input of organic carbon on the distribution of benthic fauna around seamounts. Knauss (A) and Caryn (B) seamounts are located ~200 and ~350 nautical miles off the US east coast respectively. They both have a conical shape, and their summit is at a depth of 2500 meters, while the base of Caryn seamount lays deeper (~5000 m, panel B1)) than Knauss's (~4000 m, panel A1). Furthermore, slope (panels A2 and B2) and BPI (panels A3 and B3) have similar ranges between the two locations. This allows identifying at least 12 distinct habitat types that can be found at both locations (panels A4 and B4): the habitats are defined by the BPI (negative, neutral and positive) and by the slope steepness (0°/5°, 5°/10°, 10°/20°, 20°/45°). Furthermore, there are some areas with extremely high BPI (> 500, shades of blue), which are present at both locations at least in the 10°/20° slope range. Considering also that Knauss seamount is likely to receive more input of organic carbon from the coast and the productive waters of the Gulf Stream, the two locations are suitable for

a comparative study on the distribution of benthic biomass around seamounts, in relation to food input.

A nested sampling design including depth, slope, BPI, substrate type, current direction and intensity, should be used to investigate biomass distribution at few selected locations. For the purpose of global extrapolations, these local surveys should be done at a resolution comparable to the best available global bathymetric maps. Figure 6-1 gives an example of how a survey could be carried out by focussing the investigation on two seamounts, with similar shape and topographic characteristics, but with different size and input of organic carbon from the ocean surface. In such a survey, the predictors that would be investigated are input of food from the surface (high or low), water temperature at the seafloor, BPI (negative, neutral, or positive) and slope (0°/5°, 5°/10°, 10°/20°, and 20°/45°).

These predictors allow identifying habitat types that are common across different locations (coloured pixels in Figure 6-1). Replicated samples (video transects for megafauna or sediment cores for meio- and macrofauna) should be taken for each habitat type, across the two locations, on all sides of the seamounts and across a range of depths. Furthermore, current meters could be deployed at the survey locations for extended periods (months) to investigate the short and long term patterns of current mean and variability.

This approach, when applied across several such case studies covering a broad range of conditions, should allow moving towards new global biomass estimates, which would be based on mechanistic understanding of the effect of topography on biomass, instead of the simple statistic correlations used here. Such global predictions would highlight the variability of biomass distribution at local scale, which introduces a further layer of complexity on the existing global estimates based vertical fluxes predictions alone. Furthermore, the predictions could be used to inform policy makers and stakeholders regarding the productivity of the oceans, as well as helping to identify the potential impact of industries working in the deep sea (i.e. oil, gas and minerals).

List of references

Alt, C. H. S. (2012). On the benthic invertebrate megafauna at the Mid-Atlantic Ridge, in the vicinity of the Charlie-Gibbs Fracture Zone. Faculty of Natural and Environmental Sciences, School of Ocean and Earth Science, University of Southampton. PhD: 280.

Alt, C. H. S., A. Rogacheva, B. Boorman, J. A. Hughes, D. S. M. Billett, A. J. Gooday and D. O. B. Jones (2013). "Trawled megafaunal invertebrate assemblages from bathyal depth of the Mid-Atlantic Ridge (48 degrees-54 degrees N)." Deep Sea Research II 98: 326-340.

Bashmachnikov, I., C. M. Loureiro and A. Martins (2013). "Topographically induced circulation patterns and mixing over Condor seamount." Deep Sea Research II 98: 38-51.

Behrenfeld, M. J. and P. G. Falkowski (1997). "Photosynthetic rates derived from satellite-based chlorophyll concentration." Limnology and Oceanography 42(1): 1-20.

Bell, J., C. H. S. Alt and D. O. B. Jones (2016). "Benthic megafauna on steep slopes at the Northern Mid-Atlantic Ridge." Marine Ecology 37(6). Belyaev, G. M. (1989). Deep-Sea Ocean trenches and their fauna. Moscow, Nauka Publishing House.

Bendtsen, J., C. Lundsgaard, M. Middelboe and D. Archer (2002). "Influence of bacterial uptake on deep-ocean dissolved organic carbon." Global Biogeochemical Cycles 16(4).

Bernhardt, M. and K. Schultz (2010). "SnowSlide: A simple routine for calculating gravitational snow transport." Geophysical Research Letters 37.

Bernhardt, M., K. Schulz, G. E. Liston and G. Zangl (2012). "The influence of lateral snow redistribution processes on snow melt and sublimation in alpine regions." Journal of Hydrology 424: 196-206.

Billett, D. S. M. and A. L. Rice (2001). "The BENGAL programme: introduction and overview." Progress In Oceanography 50(1-4): 13-25.

Blankenship, L. E., A. A. Yayanos, D. B. Cadien and L. A. Levin (2006). "Vertical zonation patterns of scavenging amphipods from the Hadal zone of the Tonga and Kermadec Trenches." Deep Sea Research I 53(1): 48-61.

BODC (2003). Centenary Edition of the GEBCO Digital Atlas. General Bathymetric Chart of the Oceans. British Oceanographic Data Centre, Liverpool, U.K, Intergovernmental Oceanographic Commission and the International Hydrographic Organization.

Brown, J. H., J. F. Gillooly, A. P. Allen, V. M. Savage and G. B. West (2004). "Toward a metabolic theory of ecology." Ecology 85(7): 1771-1789.

Chivers, A. J., B. E. Narayanaswamy, P. A. Lamont, A. Dale and R. Turnewitsch (2013). "Changes in polychaete standing stock and diversity on the northern side of Senghor Seamount (NE Atlantic)." Biogeosciences 10(6): 3535-3546.

Clark, M. R., A. A. Rowden, T. Schlacher, A. Williams, M. Consalvey, K. I. Stocks, A. D. Rogers, T. D. O'Hara, M. White, T. M. Shank and J. M. Hall-Spencer (2010). The Ecology of Seamounts: Structure, Function, and Human Impacts. Annual Review of Marine Science. 2: 253-278.

Clarke, A. and K. P. P. Fraser (2004). "Why does metabolism scale with temperature?" Functional Ecology 18(2): 243-251.

Danovaro, R., N. Della Croce, A. Dell'Anno and A. Pusceddu (2003). "A depocenter of organic matter at 7800 m depth in the SE Pacific Ocean." Deep Sea Research II 50(12): 1411-1420.

Danovaro, R., C. Gambi and N. Della Croce (2002). "Meiofauna hotspot in the Atacama Trench, eastern South Pacific Ocean." Deep Sea Research I 49(5): 843-857.

Dansereau, D. G., S. B. Williams (2011). Seabed modeling and distractor extraction for mobile AUVs using light field filtering. 2011 IEEE International Conference on Robotics and Automation: 1634-1639.

Dormann, C. F., J. Elith, S. Bacher, C. Buchmann, G. Carl, G. Carre, J. R. G. Marquez, B. Gruber, B. Lafourcade, P. J. Leitao, T. Munkemuller, C. McClean, P. E. Osborne, B. Reineking, B. Schroder, A. K. Skidmore, D. Zurell and S. Lautenbach (2013). "Collinearity: a review of methods to deal with it and a simulation study evaluating their performance." Ecography 36(1): 27-46.

Duffy, G. A., L. Lundsten, L. A. Kuhnz and C. K. Paull (2014). "A comparison of megafaunal communities in five submarine canyons off Southern California, USA." Deep Sea Research II 104: 259-266.

Duineveld, G. C. A., M. S. S. Lavaleye and E. M. Berghuis (2004). "Particle flux and food supply to a seamount cold-water coral community (Galicia Bank, NW Spain)." Marine Ecology Progress Series 277: 13-23.

Durden, J. M., B. J. Bett, T. Horton, A. Serpell-Stevens, K. J. Morris, D. S. M. Billett and H. A. Ruhl (2016). "Improving the estimation of deep-sea megabenthos biomass: dimension to wet weight conversions for abyssal invertebrates." Marine Ecology Progress Series 552: 71-79.

Durden, J. M., B. J. Bett, D. O. B. Jones, V. A. I. Huvenne and H. A. Ruhl (2015). "Abyssal hills - hidden source of increased habitat heterogeneity, benthic megafaunal biomass and diversity in the deep sea." Progress In Oceanography 137: 209-218.

ESRI (2010). ArcGIS. E. E. S. R. Institute). Redlands, California.

Fabiano, M., A. Pusceddu, A. Dell'Anno, M. Armeni, S. Vanucci, R. S. Lampitt, G. A. Wolff and R. Danovaro (2001). "Fluxes of phytopigments and labile organic matter to the deep ocean in the NE Atlantic Ocean." Progress In Oceanography 50(1-4): 89-104.

Falkowski, P. G., R. T. Barber and V. Smetacek (1998). "Biogeochemical controls and feedbacks on ocean primary production." Science 281(5374): 200-206.

Flach, E. and C. Heip (1996). "Vertical distribution of macrozoobenthos within the sediment on the continental slope of the Goban Spur area (NE Atlantic)." Marine Ecology Progress Series 141(1-3): 55-66.

Fu, L. L. and P. Y. Le Traon (2006). "Satellite altimetry and ocean dynamics." Comptes Rendus Geoscience 338(14-15): 1063-1076.

Gage, J. D. and B. J. Bett (2005). Deep-sea benthic sampling. Methods for the study of marine benthos. Third edition. A. Eleftheriou and A. McIntyre: 273-325.

Galeron, J., M. Sibuet, M. L. Mahaut and A. Dinet (2000). "Variation in structure and biomass of the benthic communities at three contrasting sites in the tropical Northeast Atlantic." Marine Ecology Progress Series 197: 121-137.

Gallo, N. D., J. Cameron, K. Hardy, P. Fryer, D. H. Bartlett and L. A. Levin (2015). "Submersible and lander-observed community patterns in the Mariana and New Britain Trenches: Influence of productivity and depth on epibenthic community structure." Deep Sea Research I 99: 119-133.

Gardner, J. L., A. Peters, M. R. Kearney, L. Joseph and R. Heinsohn (2011). "Declining body size: a third universal response to warming?" Trends in Ecology & Evolution 26(6): 285-291.

Gardner, J. V., A. A. Armstrong, B. R. Calder and J. Beaudoin (2014). "So, how deep is the Mariana Trench?" Geology 37(1): 1-13.

Genin, A. (2004). "Bio-physical coupling in the formation of zooplankton and fish aggregations over abrupt topographies." Journal of Marine Systems 50(1-2): 3-20.

Genin, A., P. K. Dayton, P. F. Lonsdale and F. N. Spiess (1986). "Corals on seamount peaks provide evidence of current acceleration over deep-sea topography." Nature 322(6074): 59-61.

Genin, A. and J. F. Dower (2007). Seamount plankton dynamics. Seamounts: Ecology, Conservation and Management. T. J. Pitcher, T. Morato, P. J. B. Hart et al.: 85-100.

George, R. Y. and R. P. Higgins (1979). "Eutrophic hadal benthic community in the Puerto Rico Trench." Ambio Special Report 6: 51-58.

Giering, S. L. C., R. Sanders, R. S. Lampitt, T. R. Anderson, C. Tamburini, M. Boutrif, M. V. Zubkov, C. M. Marsay, S. A. Henson, K. Saw, K. Cook and D. J. Mayor (2014). "Reconciliation of the carbon budget in the ocean's twilight zone." Nature 507(7493): 480-+.

Glud, R. N., F. Wenzhöfer, M. Middelboe, K. Oguri, R. Turnewitsch, D. E. Canfield and H. Kitazato (2013). "High rates of microbial carbon turnover in sediments in the deepest oceanic trench on Earth." Nature Geoscience 6(4): 284-288.

Griesbach, S., R. H. Peters and S. Youakim (1982). "An allometric model for pesticide bioaccumulation." Canadian Journal of Fisheries and Aquatic Sciences 39(5): 727-735.

Harris, P. T., M. Macmillan-Lawler, J. Rupp and E. K. Baker (2014). "Geomorphology of the oceans." Marine Geology 352: 4-24.

Harris, P. T. and T. Whiteway (2011). "Global distribution of large submarine canyons: Geomorphic differences between active and passive continental margins." Marine Geology 285(1-4): 69-86.

Hasager, C. B. (2014). "Offshore winds mapped from satellite remote sensing." Wiley Interdisciplinary Reviews-Energy and Environment 3(6): 594-603.

Hastie, T. (2015). gam: Generalized Additive Models.

Henson, S. A., R. Sanders, E. Madsen, P. J. Morris, F. Le Moigne and G. D. Quartly (2011). "A reduced estimate of the strength of the ocean's biological carbon pump." Geophysical Research Letters 38.

Higgs, N. D., A. R. Gates and D. O. B. Jones (2014). "Fish food in the Deep Sea: revisiting the role of large food-falls." Plos One 9(5).

Honjo, S., S. J. Manganini, R. A. Krishfield and R. Francois (2008). "Particulate organic carbon fluxes to the ocean interior and factors controlling the biological pump: A synthesis of global sediment trap programs since 1983." Progress In Oceanography 76(3): 217-285.

Hudson, I. R., B. D. Wigham, D. S. M. Billett and P. A. Tyler (2003). "Seasonality and selectivity in the feeding ecology and reproductive biology of deep-sea bathyal holothurians." Progress In Oceanography 59(4): 381-407.

Hughes, S. J. M., H. A. Ruhl, L. E. Hawkins, C. Hauton, B. Boorman and D. S. M. Billett (2011). "Deep-sea echinoderm oxygen consumption rates and an interclass comparison of metabolic rates in Asteroidea, Crinoidea, Echinoidea, Holothuroidea and Ophiuroidea." Journal of Experimental Biology 214(15): 2512-2521.

Ichino, M. C., M. R. Clark, J. C. Drazen, A. Jamieson, D. O. B. Jones, A. P. Martin, A. A. Rowden, T. M. Shank, P. H. Yancey and H. A. Ruhl (2015). "The distribution of benthic biomass in hadal trenches: A modelling approach to investigate the effect of vertical and lateral organic matter transport to the seafloor." Deep Sea Research I 100: 21-33.

Ilicak, M., S. Legg, A. Adcroft and R. Hallberg (2011). "Dynamics of a dense gravity current flowing over a corrugation." Ocean Modelling 38(1-2): 71-84.

IMCS, O. M. G. (2013). "https://www.myroms.org/index.php."

Inman, D. L., C. E. Nordstrom and R. E. Flick (1976). "Currents in submarine canyons - air-sea-land interaction." Annual review of Fluid Mechanics 8: 275-310.

IPCC (2014). IPCC, 2014: Climate Change 2014: Synthesis Report. Contribution of Working Groups I, II and III to the Fifth Assessment Report of the Intergovernmental Panel on Climate Change Core Writing Team. Geneva, Switzerland, IPCC: 151.

Itoh, M., K. Kawamura, T. Kitahashi, S. Kojima, H. Katagiri and M. Shimanaga (2011). "Bathymetric patterns of meiofaunal abundance and biomass associated with the Kuril and Ryukyu trenches, western North Pacific Ocean." Deep Sea Research I 58(1): 86-97.

Itou, M., I. Matsumura and S. Noriki (2000). "A large flux of particulate matter in the deep Japan Trench observed just after the 1994 Sanriku-Oki earthquake." Deep Sea Research I 47(10): 1987-1998.

Ivanov, V. V., G. I. Shapiro, J. M. Huthnance, D. L. Aleynik and P. N. Golovin (2004). "Cascades of dense water around the world ocean." Progress In Oceanography 60(1): 47-98.

Jamieson, A. J., T. Fujii, D. J. Mayor, M. Solan and I. G. Priede (2010). "Hadal trenches: the ecology of the deepest places on Earth." Trends in Ecology & Evolution 25(3): 190-197.

Jamieson, A. J., T. Fujii, M. Solan, A. K. Matsumoto, P. M. Bagley and I. G. Priede (2009). "First findings of decapod crustacea in the hadal zone." Deep Sea Research I 56(4): 641-647.

Jamieson, A. J., N. M. Kilgallen, A. A. Rowden, T. Fujii, T. Horton, A. N. Loerz, K. Kitazawa and I. G. Priede (2011). "Bait-attending fauna of the Kermadec Trench, SW Pacific Ocean: Evidence for an ecotone across the abyssal-hadal transition zone." Deep Sea Research II 58(1): 49-62.

Jamieson, A. J., N. C. Lace, A.-N. Lörz, A. A. Rowden and S. B. Piertney (2013). "The supergiant amphipod *Alicella gigantea* (Crustacea: Alicellidae) from hadal depths in the Kermadec Trench, SW Pacific Ocean." Deep Sea Research II 92: 107-113.

Jamieson, A. J. and P. H. Yancey (2012). "On the validity of the Trieste flatfish: dispelling the myth." Biological Bulletin 222(3): 171-175.

Jiang, B. and J. J. Yin (2014). "Ht-Index for quantifying the fractal or scaling structure of geographic Features." Annals of the Association of American Geographers 104(3): 530-541.

Johnson, N. A., J. W. Campbell, T. S. Moorre, M. A. Rex, R. J. Etter, C. R. McClain and M. D. Dowell (2007). "The relationship between the standing stock of deep-sea macrobenthos and surface production in the western North Atlantic." Deep Sea Research I 54(8): 1350-1360.

Jones, D. O. B., B. J. Bett, R. B. Wynn and D. G. Masson (2009). "The use of towed camera platforms in deep-water science." Underwater Technology 28(2): 41-50.

Jones, D. O. B., C. O. Mrabure and A. R. Gates (2013). "Changes in deep-water epibenthic megafaunal assemblages in relation to seabed slope on the Nigerian margin." Deep Sea Research I 78: 49-57.

Jones, D. O. B., A. Yool, C.-L. Wei, S. A. Henson, H. A. Ruhl, A. R. Watson and M. Gehlen (2014). "Global reductions in seafloor biomass in response to climate change." Global Change Biology 20(6).

Keller, C. P. (1988). "Map projections – A working manual – Snyder, JP." American Cartographer 15(4): 415-416.

Kelly-Gerreyn, B. A., A. P. Martin, B. J. Bett, T. R. Anderson, J. I. Kaariainen, C. E. Main, C. J. Marcinko and A. Yool (2014). "Benthic biomass size spectra in shelf and deep-sea sediments." Biogeosciences 11(22): 6401-6416.

Kelly, R. H. and P. H. Yancey (1999). "High contents of trimethylamine oxide correlating with depth in deep-sea teleost fishes, skates, and decapod crustaceans." Biological Bulletin 196(1): 18-25.

Kunze, E., L. K. Rosenfeld, G. S. Carter and M. C. Gregg (2002). "Internal waves in Monterey Submarine Canyon." Journal of Physical Oceanography 32(6): 1890-1913.

Lampitt, R. S. (1985). "Evidence for the seasonal deposition of detritus to the deep-sea floor and its subsequent resuspension." Deep Sea Research Part A 32(8): 885-897.

Lampitt, R. S. and M. P. Burnham (1983). "A free-fall time-lapse camera and current-meter system “Bathysnap” with notes on the foraging behaviour of a bathyal decapod shrimp." Deep Sea Research Part A 30(9): 1009-1017.

Laws, E. A., E. D'Sa and P. Naik (2011). "Simple equations to estimate ratios of new or export production to total production from satellite-derived estimates of sea surface temperature and primary production." Limnology and Oceanography-Methods 9: 593-601.

Laxson, C. J., N. E. Condon, J. C. Drazen and P. H. Yancey (2011). "Decreasing urea: trimethylamine N-oxide ratios with depth in chondrichthyes: a physiological depth limit?" Physiological and Biochemical Zoology 84(5): 494-505.

Lebrato, M., K. A. Pitt, A. K. Sweetman, D. O. B. Jones, J. E. Cartes, A. Oschlies, R. H. Condon, J. C. Molinero, L. Adler, C. Gaillard, D. Lloris and D. S. M. Billett (2012). "Jelly-falls historic and recent observations: a review to drive future research directions." Hydrobiologia 690(1): 227-245.

Leduc, D. and A. A. Rowden (2017). "Not to be sneezed at: does pollen from forests of exotic pine affect deep oceanic trench ecosystems?" Ecosystems: 1-11.

Levin, L. A., J. D. Gage, C. Martin and P. A. Lamont (2000). "Macrobenthic community structure within and beneath the oxygen minimum zone, NW Arabian Sea." Deep Sea Research II 47(1-2): 189-226.

Levin, L. A. and C. Dibacco (1995). "Influence of sediment transport on short-term recolonization by seamount infauna." Marine Ecology Progress Series 123(1-3): 163-175.

Lima, I. D., D. B. Olson and S. C. Doney (2002). "Biological response to frontal dynamics and mesoscale variability in oligotrophic environments: Biological production and community structure." Journal of Geophysical Research 107: 1-21.

Linse, K., A. Brandt, J. M. Bohn, B. Danis, C. De Broyer, B. Ebbe, V. Heterier, D. Janussen, P. J. L. Gonzalez, M. Schueller, E. Schwabe and M. R. A. Thomson (2007). "Macro- and megabenthic assemblages in the bathyal and abyssal Weddell Sea (Southern Ocean)." Deep Sea Research II 54(16-17): 1848-1863.

Liu, J. T., Y.-H. Wang, R. J. Yang, R. T. Hsu, S.-J. Kao, H.-L. Lin and F. H. Kuo (2012). "Cyclone-induced hyperpycnal turbidity currents in a submarine canyon." Journal of Geophysical Research-Oceans 117.

Longhurst, A., S. Sathyendranath, T. Platt and C. Caverhill (1995). "An estimate of global primary production in the ocean from satellite radiometer data." Journal of Plankton Research 17(6): 1245-1271.

Lundsten, L., J. P. Barry, G. M. Cailliet, D. A. Clague, A. P. DeVogelaere and J. B. Geller (2009a). "Benthic invertebrate communities on three seamounts off southern and central California, USA." Marine Ecology Progress Series 374: 23-32.

Lundsten, L., C. R. McClain, J. P. Barry, G. M. Cailliet, D. A. Claguel and A. P. DeVogelaere (2009b). "Ichthyofauna on three seamounts off southern and central California, USA." Marine Ecology Progress Series 389: 223-232.

Lutz, M., R. Dunbar and K. Caldeira (2002). "Regional variability in the vertical flux of particulate organic carbon in the ocean interior." Global Biogeochemical Cycles 16(3).

Lutz, M. J., K. Caldeira, R. B. Dunbar and M. J. Behrenfeld (2007). "Seasonal rhythms of net primary production and particulate organic carbon flux to depth describe the efficiency of biological pump in the global ocean." Journal of Geophysical Research-Oceans 112(C10).

Madec, G. (2008). NEMO reference manual, oceanic dynamic component: NEMO-OPA. Note du Pole de modelisation. France, Instituir Pierre Simmon Laplace. 27.

Martin, A. P. (2003). "On estimates for the vertical nitrate flux due to eddy pumping." Journal of Geophysical Research 108(C11).

Martin, J. H., G. A. Knauer, D. M. Karl and W. W. Broenkow (1987). "VERTEX - Carbon cycling in the northeast Pacific." Deep Sea Research Part A 34(2): 267-285.

Mayor, D. J., B. Thornton, S. Hay, A. F. Zuur, G. W. Nicol, J. M. McWilliam and U. F. M. Witte (2012). "Resource quality affects carbon cycling in deep-sea sediments." Isme Journal 6(9): 1740-1748.

McClain, C. R. and L. Lundsten (2014). "Assemblage structure is related to slope and depth on a deep offshore Pacific seamount chain." Marine Ecology 36(2).

McClain, C. R., L. Lundsten, J. Barry and A. DeVogelaere (2010). "Assemblage structure, but not diversity or density, change with depth on a northeast Pacific seamount." Marine Ecology 31(Suppl. 1): 1-12.

McClain, C. R., L. Lundsten, M. Ream, J. Barry and A. DeVogelaere (2009). "Endemicity, biogeography, composition, and community structure on a Northeast Pacific seamount." Plos One 4(1).

McGillicuddy, D. J., L. A. Anderson, S. C. Doney and M. E. Maltrud (2003). "Eddy-driven sources and sinks of nutrients in the upper ocean: Results from a 0.1 degrees resolution model of the North Atlantic." Global Biogeochemical Cycles 17(2).

McGillicuddy, D. J., A. R. Robinson, D. A. Siegel, H. W. Jannasch, R. Johnson, T. D. Dickey, J. McNeil, A. Michaels and A. H. Knap (1998). "Influence of mesoscale eddies in new production in the Sargasso sea." Nature 394(6690): 263-266.

Meiburg, E. and B. Kneller (2010). Turbidity Currents and Their Deposits. Annual Review of Fluid Mechanics. 42: 135-156.

Messie, M. and F. P. Chavez (2015). "Seasonal regulation of primary production in eastern boundary upwelling systems." Progress In Oceanography 134: 1-18.

Middelburg, J. J. (2011). "Chemoautotrophy in the ocean." Geophysical Research Letters 38.

Mohn, C., S. Erofeeva, R. Turnewitsch, B. Christiansen and M. White (2013). "Tidal and residual currents over abrupt deep-sea topography based on shipboard ADCP data and tidal model solutions for three popular bathymetry grids." Ocean Dynamics 63(2-3): 195-208.

Morris, K. J., B. J. Bett, J. M. Durden, N. M. A. Benoist, V. A. I. Huvenne, D. O. B. Jones, K. Robert, M. C. Ichino, G. A. Wolff and H. A. Ruhl (2016). "Landscape-scale spatial heterogeneity in phytodetrital cover and megafauna biomass in the abyss links to modest topographic variation." Scientific Reports 6.

Morris, K. J., B. J. Bett, J. M. Durden, V. A. I. Huvenne, R. Milligan, D. O. B. Jones, S. McPhail, K. Robert, D. M. Bailey and H. A. Ruhl (2014). "A new method for ecological surveying of the abyss using autonomous underwater vehicle photography." Limnology and Oceanography-Methods 12: 795-809.

Olu, K., S. Lance, M. Sibuet, P. Henry, A. F. Medioni and A. Dinet (1997). "Cold seep communities as indicators of fluid expulsion patterns through mud volcanoes seaward of the Barbados accretionary prism." Deep Sea Research II 44(5): 811-841.

Paradis, E., J. Claude and K. Strimmer (2004). "APE: analyses of phylogenetics and evolution in R language." Bioinformatics 20: 289-290.

Paull, C. K., W. Ussler, H. G. Greene, R. Keaten, P. Mitts and J. Barry (2003). "Caught in the act: the 20 December 2001 gravity flow event in Monterey Canyon." Geo-Marine Letters 22(4): 227-232.

Peters, R. H. (1983). Cambridge studies in ecology: The ecological implications of body size. New York, N.Y., U.S.A., Cambridge University Press.

Portner, H. O. (2002). "Climate variations and the physiological basis of temperature dependent biogeography: systemic to molecular hierarchy of thermal tolerance in animals." Comparative Biochemistry and Physiology a-Molecular and Integrative Physiology 132(4): 739-761.

Prasanna Kumar, S., M. Nuncio, N. Ramaiah, S. Sardesai, J. Narvekar, V. Fernandes and J. T. Paul (2007). "Eddy-mediated biological productivity in the Bay of Bengal during fall and spring intermonsoons." Deep Sea Research I 54(9): 1619-1640.

Quiroga, E., R. Quinones, M. Palma, J. Sellanes, V. A. Gallardo, D. Gerdes and G. Rowe (2005). "Biomass size-spectra of macrobenthic communities in the oxygen minimum zone off Chile." Estuarine Coastal and Shelf Science 62(1-2): 217-231.

R core team (2014). R: A Language and Environment for Statistical Computing. Vienna, Austria, R Foundation for Statistical Computing.

Ravelle, W. (2015). psych: Procedures for Personality and Psychological Research. Northwestern University, Evanston, Illinois, USA.

Reimers, C. E., R. A. Jahnke and D. C. McCorkle (1992). "Carbon fluxes and burial rates over the continental slope and rise off central California with implications for the global carbon cycle." Global Biogeochemical Cycles 6(2): 199-224.

Rex, M. A. and R. J. Etter (2010). Deep-sea biodiversity: pattern and scale, Harvard University Press; Cambridge & London.

Rex, M. A., R. J. Etter, J. S. Morris, J. Crouse, C. R. McClain, N. A. Johnson, C. T. Stuart, J. W. Deming, R. Thies and R. Avery (2006). "Global bathymetric patterns of standing stock and body size in the deep-sea benthos." Marine Ecology Progress Series 317: 1-8.

Richardson, M. D., K. B. Briggs, F. A. Bowles and J. H. Tietjen (1995). "A depauperate benthic assemblage from the nutrient-poor sediments of the Puerto-Rico Trench." Deep Sea Research I 42(3): 351-364.

Roberts, S. and M. Hirshfield (2004). "Deep-sea corals: out of sight, but no longer out of mind." Frontiers in Ecology and the Environment 2(3): 123-130.

Rodgers, A. D. (1994). The biology of seamounts. Advances in Marine Biology. J. H. S. Blaxter and A. J. Southward. 30: 305-354.

Rowden, A. A., J. F. Dower, T. A. Schlacher, M. Consalvey and M. R. Clark (2010a). "Paradigms in seamount ecology: fact, fiction and future." Marine Ecology-an Evolutionary Perspective 31: 226-241.

Rowden, A. A., T. A. Schlacher, A. Williams, M. R. Clark, R. Stewart, F. Althaus, D. A. Bowden, M. Consalvey, W. Robinson and J. Dowdney (2010b). "A test of the seamount oasis hypothesis: seamounts support higher epibenthic megafaunal biomass than adjacent slopes." Marine Ecology-an Evolutionary Perspective 31: 95-106.

Ruhl, H. A., B. J. Bett, S. J. M. Hughes, C. H. S. Alt, E. J. Ross, R. S. Lampitt, C. A. Pebody, K. L. Smith and D. S. M. Billet (2014). "Links between deep-sea respiration and community dynamics." Ecology 95(6): 1651-1662.

Ruhl, H. A., J. A. Ellena and K. L. Smith, Jr. (2008). "Connections between climate, food limitation, and carbon cycling in abyssal sediment communities." Proceedings of the National Academy of Sciences of the United States of America 105(44): 17006-17011.

Ruhl, H. A. and K. L. Smith (2004). "Shifts in deep-sea community structure linked to climate and food supply." Science 305(5683): 513-515.

Ryan, J. P., F. P. Chavez and J. G. Bellingham (2005). "Physical-biological coupling in Monterey Bay, California: topographic influences on phytoplankton ecology." Marine Ecology Progress Series 287: 23-32.

Samadi, S., L. Bottan, E. Macpherson, B. R. De Forges and M.-C. Boisselier (2006). "Seamount endemism questioned by the geographic distribution and population genetic structure of marine invertebrates." Marine Biology 149(6): 1463-1475.

Sarangi, R. K. (2016). "Remote sensing observations of ocean surface chlorophyll and temperature with the impact of cyclones and depressions over the Bay of Bengal water." Marine Geodesy 39(1): 53-76.

Schlacher, T. A., A. R. Baco, A. A. Rowden, T. D. O'Hara, M. R. Clark, C. Kelly and J. F. Dower (2014). "Seamount benthos in a cobalt-rich crust region of the central Pacific: conservation challenges for future seabed mining." Diversity and Distributions 20(5).

Schlining, B. M., N. J. Stout (2006). MBARI's video annotation and reference system. Oceans 2006, Vols 1-4: 1146-1150.

Schmidt, W. E. and E. Siegel (2011). "Free descent and on bottom ADCM measurements in the Puerto Rico Trench, 19.77 degrees N, 67.40 degrees W." Deep Sea Research I 58(9): 970-977.

Smith, C. R. and A. R. Baco (2003). "Ecology of whale falls at the deep-sea floor." Oceanography and Marine Biology 41: 311-354.

Smith, C. R., F. C. De Leo, A. F. Bernardino, A. K. Sweetman and P. M. Arbizu (2008). "Abyssal food limitation, ecosystem structure and climate change." Trends in Ecology & Evolution 23(9): 518-528.

Smith, K. L., Jr., H. A. Ruhl, B. J. Bett, D. S. M. Billett, R. S. Lampitt and R. S. Kaufmann (2009). "Climate, carbon cycling, and deep-ocean ecosystems." Proceedings of the National Academy of Sciences of the United States of America 106(46): 19211-19218.

Smith, K. L., Jr., H. A. Ruhl, R. S. Kaufmann and M. Kahru (2008). "Tracing abyssal food supply back to upper-ocean processes over a 17-year time series in the northeast Pacific." Limnology and Oceanography 53(6): 2655-2667.

Smith, K. L., H. A. Ruhl, M. Kahru, C. L. Huffard and A. D. Sherman (2013). "Deep ocean communities impacted by changing climate over 24 y in the abyssal northeast Pacific Ocean." Proceedings of the National Academy of Sciences of the United States of America 110(49): 19838-19841.

Stefanoudis, P. V. and A. J. Gooday (2015). "Basal monothalamous and pseudochambered benthic foraminifera associated with planktonic foraminiferal shells and mineral grains from the Porcupine Abyssal Plain, NE Atlantic." Marine Biodiversity 45(3): 357-369.

Stefanoudis, P. V., R. Schiebel, R. Mallet, J. M. Durden, B. J. Bett and A. J. Gooday (2016). "Agglutination of benthic foraminifera in relation to mesoscale bathymetric features in the abyssal NE Atlantic (Porcupine Abyssal Plain)." Marine Micropaleontology 123: 15-28.

Strass, V. H., A. C. Naveira Garbato, R. T. Pollard, H. I. Fischer, I. Hense, J. T. Allen, J. F. Read, H. Leach and V. Smetacek (2002). "Mesoscale frontal dynamics: shaping the environment of primary production in the Antarctic Circumpolar Current." Deep Sea Research II 49: 3735-3769.

Suess, E. (1980). "Particulate organic-carbon flux in the oceans - surface productivity and oxygen utilization." Nature 288(5788): 260-263.

Sweetman, A. K. and U. Witte (2008). "Response of an abyssal macrofaunal community to a phytodetrital pulse." Marine Ecology Progress Series 355: 73-84.

Taira, K., S. Kitagawa, T. Yamashiro and D. Yanagimoto (2004). "Deep and bottom currents in the Challenger Deep, Mariana Trench, measured with super-deep current meters." Journal of Oceanography 60(6): 919-926.

Tecchio, S., E. Ramirez-Llodra, F. Sarda, J. B. Company, I. Palomera, A. Mecho, R. Pedrosa-Pamies and A. Sanchez-Vidal (2011). "Drivers of deep Mediterranean megabenthos communities along longitudinal and bathymetric gradients." Marine Ecology Progress Series 439: 181-U219.

Tempera, F., E. Giacomella, N. C. Mitchell, A. S. Campos, A. B. Henriques, I. Bashmachnikov, A. Martins, A. Mendonca, T. Morato, A. Colaco, F. M. Porteiro, D. Catarino, J. Goncalves, M. R. Pinho, E. J. Isidro, R. S. Santos and G. Menezes (2012). "Mapping Condor Seamount seafloor environment and associated biological assemblages (Azores, NE Atlantic)." Seafloor Geomorphology as Benthic Habitat: Geohab Atlas of Seafloor Geomorphic Features and Benthic Habitats: 807-818.

Thresher, R. E., J. Adkins, S. J. Fallon, K. Gowlett-Holmes, F. Althaus and A. Williams (2011). "Extraordinarily high biomass benthic community on Southern Ocean seamounts." Scientific Reports 1.

Thurston, M. H., B. J. Bett, A. L. Rice and P. A. B. Jackson (1994). "Variations in the invertebrate abyssal megafauna in the North-Atlantic Ocean." Deep Sea Research I 41(9): 1321-1348.

Thurston, M. H., A. L. Rice and B. J. Bett (1998). "Latitudinal variation in invertebrate megafaunal abundance and biomass in the North Atlantic Ocean Abyss." Deep Sea Research II 45(1-3): 203-224.

Tietjen, J. H., J. W. Deming, G. T. Rowe, S. Macko and R. J. Wilke (1989). "Meiobenthos of the Hatteras abyssal-plain and Puerto-Rico trench - Abundance, biomass and association with bacteria and particulate fluxes." Deep Sea Research Part A 36(10): 1567-1577.

Tselepides, A. and N. Lampadariou (2004). "Deep-sea meiofaunal community structure in the Eastern Mediterranean: are trenches benthic hotspots?" Deep Sea Research I 51(6): 833-847.

Turnewitsch, R., M. Dumont, K. Kiriakoulakis, S. Legg, C. Mohn, F. Peine and G. Wolff (2016). "Tidal influence on particulate organic carbon export fluxes around a tall seamount." Progress In Oceanography 149: 189-213.

Turnewitsch, R., S. Falahat, J. Nycander, A. Dale, R. B. Scott and D. Furnival (2013). "Deep-sea fluid and sediment dynamics-Influence of hill- to seamount-scale seafloor topography." Earth-Science Reviews 127: 203-241.

Turnewitsch, R., S. Falahat, J. Stehlikova, K. Oguri, R. N. Glud, M. Middelboe, H. Kitazato, F. Wenzhöfer, K. Ando, S. Fujio and D. Yanagimoto (2014). "Recent sediment dynamics in hadal trenches: Evidence for the influence of higher-frequency (tidal, near-inertial) fluid dynamics." Deep Sea Research I 90: 125-138.

Turnewitsch, R., N. Lahajnar, M. Haeckel and B. Christiansen (2015). "An abyssal hill fractionates organic and inorganic matter in deep-sea surface sediments." Geophysical Research Letters 42(18): 7663-7672.

Turnewitsch, R., J. L. Reyss, D. C. Chapman, J. Thomson and R. S. Lampitt (2004). "Evidence for a sedimentary fingerprint of an asymmetric flow field surrounding a short seamount." Earth and Planetary Science Letters 222(3-4): 1023-1036.

Vandorpe, T., I. Martins, J. Vitorino, D. Hebbeln, M. Garcia and D. Van Rooij (2016). "Bottom currents and their influence on the sedimentation pattern in the El Arraiche mud volcano province, southern Gulf of Cadiz." Marine Geology 378: 114-126.

Venables, H. J., R. T. Pollard and E. E. Popova (2007). "Physical conditions controlling the development of a regular phytoplankton bloom north of the Crozet Plateau, Southern Ocean." Deep Sea Research II 54(18-20): 1949-1965.

Verfaillie, E., P. Doornenbal, A. Mitchell, J. White and V. Van Lancker (2007) “The bathymetric position index (BPI) as a support tool for habitat mapping. Worked example for the MESH Final Guidance.”

Vetter, E. W. and P. K. Dayton (1998). "Macrofaunal communities within and adjacent to a detritus-rich submarine canyon system." Deep Sea Research II 45(1-3): 25-54.

Vinogradova, N. G., A. Gebruk and V. N. Romanov (1993). “Some new data on the Orkney Trench ultra abyssal fauna.” The Second Polish-Soviet Antarctic Symposium, Institute of Ecology, Publishing Office.

Watling, L., J. Guinotte, M. R. Clark and C. R. Smith (2013). "A proposed biogeography of the deep ocean floor." Progress In Oceanography 111: 91-112.

Wei, C.-L., G. T. Rowe, E. Escobar-Briones, A. Boetius, T. Soltwedel, M. J. Caley, Y. Soliman, F. Huettmann, F. Qu, Z. Yu, C. R. Pitcher, R. L. Haedrich, M. K. Wicksten, M. A. Rex, J. G. Baguley, J.

Sharma, R. Danovaro, I. R. MacDonald, C. C. Nunnally, J. W. Deming, P. Montagna, M. Levesque, J. M. Weslawski, M. Wlodarska-Kowalczuk, B. S. Ingole, B. J. Bett, D. S. M. Billett, A. Yool, B. A. Bluhm, K. Iken and B. E. Narayanaswamy (2010). "Global patterns and predictions of seafloor biomass using Random Forests." Plos One 5(12).

White, M. and C. Mohn (2004). “Seamounts: a review of physical processes and their influence on the seamount ecosystem.” OASIS Report. Galway, Ireland.

Wilson, M. F. J., B. O'Connell, C. Brown, J. C. Guinan and A. J. Grehan (2007). "Multiscale terrain analysis of multibeam bathymetry data for habitat mapping on the continental slope." Marine Geodesy 30(1-2): 3-35.

Wolff, T. (1961). "The deepest recorded fishes." Nature 190((4772)): 283.

Wolff, T. (1970). "Concept of hadal or ultra-abyssal fauna." Deep Sea Research 17(6): 983-1003.

Woolley, S. N. C., D. P. Tittensor, P. K. Dunstan, G. Guillera-Arroita, J. J. Lahoz-Monfort, B. A. Wintle, B. Worm and T. D. O'Hara (2016). "Deep-sea diversity patterns are shaped by energy availability." Nature 533: 393-396.

Wright, D. J., M. Pendleton, J. Boulware, S. Walbridge, B. Gerlt, D. Eslinger, D. Sampson and E. Huntley (2012). ArcGIS Benthic Terrain Modeler (BTM), v. 3.0, Environmental Systems Research Institute, NOAA Coastal Services Center, Massachusetts Office of Coastal Zone Management.

Xu, J. P., M. Noble, S. L. Eittreim, L. K. Rosenfeld, F. B. Schwing and C. H. Pilskaln (2002). "Distribution and transport of suspended particulate matter in Monterey Canyon, California." Marine Geology 181(1-3): 215-234.

Yamartino, R. J. (1984). "A comparison of several single-pass estimators of the standard-deviation of wind direction." Journal of Climate and Applied Meteorology 23(9): 1362-1366.

Yancey, P. H., M. E. Gerringer, J. C. Drazen, A. A. Rowden and A. J. Jamieson (2014). "Marine fish may be biochemically constrained from inhabiting deepest ocean depths." Proceedings of the National Academy of Sciences USA 111: 4461-4465.

Yasuhara, M. and R. Danovaro (2016). "Temperature impacts on deep-sea biodiversity." Biological Reviews 91(2): 275-287.

Yesson, C., M. R. Clark, M. L. Taylor and A. D. Rogers (2011). "The global distribution of seamounts based on 30 arc seconds bathymetry data." Deep Sea Research I 58(4): 442-453.

Yool, A., A. P. Martin, T. R. Anderson, B. J. Bett, D. O. B. Jones and H. A. Ruhl (2017). "Big in the benthos: Future change of seafloor community biomass in a global, body size-resolved model." Global Change Biology Yool, A., E. E. Popova and T. R. Anderson (2013). "MEDUSA-2.0: an intermediate complexity biogeochemical model of the marine carbon cycle for climate change and ocean acidification studies." Geoscientific Model Development 6(5): 1767-1811.

Zeileis, A. and T. Hothorn (2002). "Diagnostic checking in regression relationships." R News 2(3): 7-10.

Zeppilli, D., L. Bongiorni, A. Cattaneo, R. Danovaro and R. S. Santos (2013). "Meiofauna assemblages of the Condor Seamount (North-East Atlantic Ocean) and adjacent deep-sea sediments." Deep Sea Research II 98: 87-100.

Zeppilli, D., L. Bongiorni, R. S. Santos and A. Vanreusel (2014). "Changes in nematode communities in different physiographic sites of the Condor Seamount (North-East Atlantic Ocean) and adjacent sediments." Plos One 9(12).